UC Berkeley
UC Berkeley Electronic Theses and Dissertations

Title

Highly Sensitive and Specific In-Gel Assays for Detection of Proteins and Nucleic Acids

Permalink

https://escholarship.org/uc/item/5kv3r0gw

Author

Moss, Alden

Publication Date

2022

Peer reviewed|Thesis/dissertation

eScholarship.org Powered by the California Digital Library
University of California

Highly Sensitive and Specific In-Gel Assays for Detection of Proteins and Nucleic Acids

by

Alden C Moss

A dissertation submitted in partial satisfaction of the

requirements for the degree of

Joint Doctor of Philosophy
with University of California, San Francisco

in

Bioengineering

in the

Graduate Division

of the

University of California, Berkeley

Committee in charge:

Professor Amy E. Herr, Chair
Professor Adam Abate
Associate Professor Markita P. Landry
Professor Gerard Marriott

Fall 2022

Highly Sensitive and Specific In-Gel Assays for Detection of Proteins and Nucleic Acids

Copyright 2022

by

Alden Moss

Abstract

Highly Sensitive and Specific In-Gel Assays for Detection of Proteins and Nucleic Acids

by

Alden C Moss

Joint Doctor of Philosophy
with University of California, San Francisco in Bioengineering

University of California, Berkeley

Professor Amy E. Herr, Chair

Nucleic acid measurements and protein measurements have transformed biological inquiry, providing key insight into biological processes and disease mechanisms. Specifically, single-cell multimodal -omics assays that measure proteins and nucleic acids are becoming increasingly important to elucidate cell-to-cell heterogeneity and explore the relationships between classes of biomolecules in complex biological signaling pathways. Despite tremendous progress over the last decade, many measurement gaps still exist due to the poor sensitivity and specificity of currently available -omics assays. For example, currently available single-cell multimodal measurement tools lack the sensitivity and specificity to detect nucleic acid point mutations and protein isoforms in the same cell. In-gel -omics assays exhibit great promise to overcome these limitations due to the advantageous properties of hydrogel matrices, which result in improved sensitivity, specificity, and resolution. However, fundamental characterization of in-gel assays is lacking. The work presented in this dissertation is aimed at bridging measurement gaps in single-cell in-gel assays by (1) evaluating and characterizing various approaches for improved multiplexing and sensitivity of in-gel assays, and (2) developing novel single-cell multimodal electrophoretic assays to measure co-expression of proteins and nucleic acids.

First, we evaluated in-gel quenching of fluorophores with H_2O_2 as a strategy aimed at improving the multiplexing capability of in-gel immunoassays that employ fluorescence-based readouts. Significant quenching of commonly used fluorophores was observed, leading us to conclude that H_2O_2-based fluorophore quenching is a promising strategy for multiplexing of in-gel immunoassays. We then characterized the reaction kinetics and transport limitations of an in-gel fluorescence-based DNA readout and evaluated DNA sequence design parameters for signal amplification to develop assay design rules. When fluorescently labeled nucleotides were incorporated into single-stranded DNA overhangs immobilized in polyacrylamide hydrogels, we observed that the time for reaction completion was much greater than predicted by simple diffusion and reaction models. We attributed this discrepancy to retarded diffusion of the DNA polymerase resulting from interactions between the diffusing polymerase and the immobilized DNA. We also investigated the effects of the number of labeled nucleotides incorporated per strand and the spacing between labeled nucleotides on signal amplification. Consistent with our

hypotheses, increasing the number of and spacing between incorporated labeled nucleotides resulted in increased fluorescence signal. Ultimately, our results that highlight retarded diffusion behavior of the DNA polymerase and the effects of DNA sequence design on the degree of signal amplification will inform assay design for future in-gel assays that depend on DNA polymerase elongation-based fluorescence readouts.

Next, we characterized hybridization chain reaction (HCR) in polyacrylamide gels of different densities, evaluating the degree of signal amplification achieved, the reaction kinetics, and the concentration-dependent fluorescence response. A high degree of signal amplification with a linear concentration-dependent response is crucial for improved sensitivity of in-gel assays. Our system scrutinized HCR in polyacrylamide gels that contained HCR initiator that was co-polymerized into the gels via a 5' acrydite group. HCR resulted in three orders of magnitude of signal amplification when compared to hybridizing a fluorescently labeled single-stranded DNA oligomer. We also observed that reaction completion was achieved in 24 h across all gel densities and that in-gel HCR followed pseudo first-order DNA hybridization kinetics. Our results demonstrate that HCR is a promising signal amplification strategy across different gel densities. We then explored immuno-HCR as a strategy for improving the sensitivity of in-gel immunoassays. Immuno-HCR relies on DNA-antibody conjugates to convert protein information to DNA information for signal amplification via HCR. We began by studying the binding affinity of DNA-antibody conjugates with optical biolayer interferometry (BLI) and the partitioning behavior of DNA-antibody conjugates in polyacrylamide gels with confocal microscopy. Both the binding affinity and the partition coefficient of antibodies decreased in response to DNA conjugation, consistent with the theory that DNA conjugation results in molecules with larger hydrodynamic radii. After characterizing the binding and partitioning behavior of DNA-antibody conjugates, we applied immuno-HCR to detect proteins immobilized in a polyacrylamide gel. The result was poorer performance than standard immunoprobing with fluorescently labeled antibodies, which we attribute to an insufficient degree of signal amplification from linear HCR. Branched HCR methods that result in additional signal amplification have the potential to overcome the limitations that we observed, leading us to posit that immuno-HCR is potentially a feasible strategy for improved sensitivity of in-gel immunoassays.

Finally, we presented the concept for two assays that seek to fill the measurement gap that precludes co-detection of protein isoforms and nucleic acid point mutations in single cells. We first developed Single-Cell Protein and RNA Electrophoresis (scPREP), a single-cell multimodal in-gel electrophoretic assay for co-detection of beta-actin mRNA and protein. Our approach involved incorporating mRNA detection via in situ hybridization with padlock probes (PLPs) and rolling circle amplification (RCA) into the single-cell western blotting platform, which enables highly sensitive and specific single-cell protein measurements. With scPREP, we detected beta-actin mRNA molecules as fluorescent puncta and beta-actin protein as gaussian bands in the gel. Our preliminary results are a first step toward co-detection of nucleic acid point mutations and protein isoforms from single cells, as our chosen mRNA detection modality exhibits single-nucleotide specificity, and our protein detection modality is capable of identifying protein isoforms. Future work to expand scPREP has the potential to make a significant contribution to the -omics field and to biology. We concluded by presenting the concept for an electrophoretic assay with a qPCR readout for detection of mRNA from lysed and electrophoresed single cells. Future work is needed to demonstrate application of the concept we

outlined. While the initial motivation for this assay was for use as a characterization tool to study mRNA electrophoresis and capture in polyacrylamide gel, there is potential for use as a standalone assay. Overall, both assays have the potential to introduce novel measurement capabilities.

In total, the work presented in this dissertation advances the field of single-cell -omics by providing unique insight into the behavior of chemical reactions in hydrogel-based systems and presenting novel assay concepts for co-detection of proteins and nucleic acids from single cells. We ultimately aim to be able to measure co-expression of protein isoforms and nucleic acid point mutations in single cells with the technologies introduced here. Future studies that build off the results we present in this dissertation have the potential to further enhance the knowledge of in-gel assays and solve complex problems that will unlock new fields of biological inquiry.

To my family, friends, and research mentors who have supported me on my journey

Table of Contents

List of Figures

List of Tables

Acknowledgements

My journey to completing a PhD has been long and would not have been possible without a village to support and mentor me. I would like to start by recognizing my parents for their continual love and guidance, and for always encouraging me to explore my interests. While neither of them has a science background, they made sure that I had the opportunity to pursue science by taking me to the Oregon Museum of Science and Industry (OMSI), getting me all kinds of STEM children's books, and arranging 'field trips' to everywhere from a water treatment plant to a silicon wafer fab. My middle school science teacher, Mr. Olekas, was another key mentor of mine who let me run all kinds of wild chemistry experiments for my science fair projects. I would also like to recognize a few other educators and mentors who believed in me and supported me immensely during my childhood: Gina, Dr. Edwards, Susie, Mrs. McAdams, Colleen, Mr. Morris, Mrs. Pannu, and Mr. Horton.

Prior to graduate school, I was fortunate to have many mentors who trained me and inspired me to pursue a career in research. I will be forever grateful to Dr. Jeff Tyner at OHSU for taking me on as an intern in the Druker Lab while I was a high school student. I would also like to express profound gratitude to Stephanie Willis, Rebecca Smith, and Marilynn Chow, my first research mentors who not only had the patience to train me but also made my experience in the Druker Lab fun and enjoyable. My experience in the Druker Lab ultimately gave me a foundation of skills and laboratory research experience that led to my next research position during my freshman year of college at Oregon State University, where Dr. Adam Higgins entrusted me with an independent research project. Adam's belief in me allowed me to publish early on and gave me the freedom to explore many areas of research, including microfluidics, which ultimately inspired me to pursue my current line of research. I certainly would not be where I am without Adam. Some other important research mentors who trained and inspired me at Oregon State include Dr. Kate Schilke and Dr. Skip Rochefort. Finally, I would like to recognize my mentors Dr. Dan Appella, Dr. Nicole Morgan, Dr. Kaylyn Oshaben, and Tom Pohida at NIH who further inspired me to purse microfluidics and assay development as subfields of bioengineering.

Moving on to graduate school, I would like to start by expressing my profound gratitude for having had the opportunity to work with my advisor Dr. Amy Herr. Amy's deep knowledge, strong work ethic and infectious enthusiasm have all been an inspiration to me as an early career researcher. She has always challenged me to perform at the highest level through the detailed feedback she has given me on manuscripts and presentations, alongside fostering a lab culture of scientific rigor that has transformed my approach to science. I am additionally immensely appreciative of Amy's encouragement to attend conferences and professional development events. This PhD also would not have been possible without the support of everyone in the Herr Lab. I would like to mention a few specific people who were pivotal to my experience in the Herr Lab. First, I would like to recognize Anjali for being my first mentor in the lab and a great person to bounce ideas off of, but above all an amazing friend to share a desk space (and some laughs) with. I owe profound gratitude to Hector and Yizhe who served as key mentors and were

always there for me when I needed guidance, helping me develop the scientific rigor that is characteristic of all Herr Lab members. I will never cease to be inspired by Julea's passion for science and genuine care for everyone in the lab, which led her to help me with late night poster revisions and qualifying exam prep during weekends. Ali's attention to detail and methodical approach to science has definitely rubbed off on me, making me a better researcher. Louise always kept the lab environment fun and lighthearted by sharing analogies and fun facts as we walked together on our PhD journeys—we did it! I would also like to recognize Sam, Shaheen, Elaine, John, Alisha, Andoni, Kristine, Gabi, Ana, Yaw, Yang, Hyekyung, Anna, Trinh, and Maya for all the fruitful research discussions we have had.

In addition to Amy, there were many other faculty members who provided inspiration and essential guidance in my research. I would like to give special thanks to my qualifying exam and dissertation committee members for their feedback and support. From my excellent rotation experience to the insightful high-level research feedback he has provided me, Dr. Adam Abate has been a fundamental part of my PhD experience. Dr. Markita Landry's detailed feedback during our meetings, during my qualifying exam, and on my dissertation committee has helped me improve the rigor of my research. My meetings with Dr. Gerard Marriott have inspired me to think big-picture and outside the box. Dr. Dorian Liepmann was a phenomenal qualifying exam chair who made the experience, dare I say, fun. I would also like to express my gratitude to Dr. Aaron Streets for all the thought-provoking research discussions we had and for having had the opportunity to GSI his BioMEMS course.

None of my research would have been possible without my funding sources and an army of behind-the-scenes staff who make all the facilities run smoothly. The research presented in this dissertation was funded by NIH grants, and I was personally funded as a Siebel Scholar (Tom & Stacey Siebel Foundation). I would like to acknowledge the Stanley Hall building staff (Dave Rogers, Thom Opal, Kris Thompson, Mike Bentley, Chris Harden, and Cherry Chung) for providing a great physical environment to work in. Next, I would like to thank the BNC staff (Paul Lum and Dr. Naima Azgui), the MIC staff (Holly Aaron and Feather Ives), and Dr. Mary West of CTAF for all their hard work to keep equipment essential to my research running smoothly. I am also grateful for the administrative staff (Catherine Dea, April Alexander, Rocío Sanchez, and Kristin Olson) for making sure that materials are getting ordered properly, I am getting paid, and I am on track with the program requirements.

My faith communities have been a major rock for me throughout my journey. I also met many amazing people and learned a great deal through my service on campus (Graduate Assembly and Graduate Council) and volunteering off campus (BASIS and Loaves & Fishes). Finally, I would like to acknowledge my family and friends who have supported me through all the ups and downs of getting a PhD. There is no way that I would have made it without them. Thanks to everyone who helped make this accomplishment possible!

Chapter 1: Introduction

1.1 Motivation for Single-Cell Multimodal -Omics Assays

The Central Dogma of Biology describes the flow of information that governs all cellular processes, stating that DNA is transcribed to mRNA, which is translated to proteins. Modifications to any of the major classes of biomolecules and/or dysregulation of any of the processes within this progression of information flow can lead to diseases, including cancer[1]. Therefore, the suite of fields focused on the study of biomolecules that govern cellular processes, termed -omics, has exploded over the last two decades[2]. Many fields studying specific biomolecules or biomolecule modifications are encompassed by -omics, including genomics (DNA), transcriptomics (mRNA), proteomics (proteins), metabolomics (metabolites), epigenomics (epigenome), and more[2].

A traditional -omics assay measures biomolecules derived from an entire bulk cell population. Key information, such as the presence of cell subpopulations that drive disease progression and/or drug resistance, is lost in bulk -omics measurements due to cell-to-cell heterogeneity[3,4]. Single-cell assays have been revolutionizing the field by uncovering cell-to-cell heterogeneity, enabling new insights into cancer progression and drug resistance, immunology, and developmental biology[3,4]. Single-cell -omics assays that measure each of the major biomolecule classes exist[5,6]. However, single-cell transcriptomics has become the dominant field of single-cell analysis[7] due to advanced high-throughput single-cell mRNA sequencing methods, which have been largely enabled by droplet microfluidics[8].

While transcriptomics is powerful, there are limitations to relying solely on transcriptomics for single-cell analysis. One major limitation of mRNA measurements is that proteins are the functional units of a cell that directly carry out most cellular processes, and studies have shown that mRNA and protein expression levels are not well-correlated[9,10]. Many proteins also contain post-translational modifications that cannot be detected at the mRNA level[11]. In addition to proteomic measurements, genomic and epigenomic measurements also provide unique information into the cell state[12]. The ideal single-cell -omics assay would measure multiple classes of biomolecules to provide a complete picture of the cell state. This is now becoming a reality in single-cell multimodal -omics, which was named the Nature Method of the Year in 2019[13]. Recent studies have demonstrated various combinations of genomic, transcriptomic, proteomic, and epigenomic measurements that provide more complete pictures of a cell's molecular identity[5,6]. Single-cell multimodal -omics assays have already enabled improved classification of immune cell phenotypes, including during immune cell differentiation[14,15], and have revealed new information about the response to drug treatment in leukemia[16]. Advancements in single-cell multimodal -omics assays in the upcoming years will greatly expand the ability to elucidate complex biological phenomena.

1.2 Need for Improved Single-Cell Multimodal -Omics Assays

Despite the recent advancements in single-cell multimodal assay development, there are still numerous limitations and challenges that need to be addressed. The weakest link in single-cell multimodal -omics assays is currently single-cell proteomics. While nucleic acid -omics modalities take advantage of the high sensitivity and specificity of PCR and sequencing-based readouts, protein measurements have largely been limited to fluorescence readouts with labeled antibodies or mass spectrometry readouts[10]. Thus, proteomics measurements suffer from low sensitivity, limited multiplexing, and low specificity, when compared to nucleic acid measurements.

The first major limitation of single-cell proteomic assays is low sensitivity. This is largely due to the lack of protein signal amplification strategies that offer comparable performance and robustness to that of PCR for amplification of nucleic acids[10]. Therefore, single-cell proteomic assays must be sensitive enough to directly detect the number of protein copies present in a single cell, where the median protein copy number of a mammalian cell is ~170,000[17]. Mass spectrometry (MS) is considered the workhorse of proteomics due to the capability for discovery without a priori knowledge of the protein targets, and for its ability to detect proteoforms[10]. However, there are many challenges with sample preparation and sample loss in single-cell MS that result in a lower limit of detection (LLOD) of $>10^5$ protein copies per cell at best[18], rendering over half the proteome inaccessible. Single-cell MS also requires highly specialized and costly equipment, and training on complicated protocols, limiting broad adoption. Single-cell immunoblotting (scIB), a set of highly specific proteomic assays that combine polyacrylamide gel electrophoretic separations with an immunoassay, is limited to a LLOD of ~170,000 protein copies per cell[19,20], also rendering half of the proteome inaccessible. There are examples of fluorescence-based immunoassays that offer very high sensitivity, down to a few hundred protein copies per cell[21], but these approaches require custom equipment and do not provide the level of specificity that MS or scIB does. One strategy that many immunoassays employ for improved sensitivity is the use of DNA-antibody conjugates coupled with DNA signal amplification strategies. The advantage of this approach is the ability to convert the protein information into DNA information to harness the power of DNA signal amplification technologies, such as PCR[22], rolling circle amplification (RCA)[23], and hybridization chain reaction (HCR)[24]. In this dissertation, we investigate the use of DNA-conjugated antibodies coupled with DNA signal amplification strategies for improved immunoassay sensitivity.

Another limitation of single-cell proteomic assays is limited multiplexing capability. Elucidating complex biological phenomena, including cell-cell interactions and signaling pathways, requires detection of multiple protein targets from the same cell[25]. While nucleic acid -omics assays are afforded virtually unlimited multiplexing capability due to the ability to identify unique sequences via sequencing, proteomic assays that depend on antibody-based fluorescence readouts are limited by spectral overlap of fluorophores[25]. Strategies to improve immunoassay multiplexing include (1) using DNA barcoded antibodies to convert the protein information to DNA for a sequencing readout[14,26], or (2) sequentially immunoprobing with fluorescently labeled antibodies and either stripping the antibodies from their protein targets with harsh detergent buffers[19,27] or quenching of the fluorophores with H_2O_2[28,29]. In this dissertation, we will be investigating sequential fluorophore quenching with H_2O_2 as a strategy toward improved multiplexing of in-gel immunoassays.

Finally, most single-cell proteomic assays lack the specificity to detect proteoforms. Proteoforms are alternative forms of a protein that consist of protein isoforms that arise from alternative splicing of mRNA or post-translational protein cleavage, and post-translation modifications, such as phosphorylation and glycosylation[11]. Estimates suggest that there are millions of human proteoforms, many of which crucially affect protein function[11]. Immunoassays are inherently limited by the availability and quality of specific antibodies, which do not exist in many cases[30]. Single-cell proteomic assays that either (1) do not rely on antibodies or (2) incorporate measures to improve immunoassay specificity are needed to identify proteoforms. Top-down MS is the gold standard for proteoform detection. Top-down MS is a subfield of MS where intact proteins are measured by MS, in contrast to bottom-up MS, where proteins are digested into peptide fragments prior to MS[31]. While top-down MS is powerful, the sensitivity is currently insufficient for meaningful single-cell analysis[31]. Alternatively, scIB achieves isoform-specific protein detection from single cells by introducing an electrophoretic separation step prior to immunoprobing with antibodies[32,33]. Two forms of scIB exist, both of which can detect protein isoforms: single-cell western blotting (scWB), which relies on a size-based protein separation[19], and single-cell isoelectric focusing (scIEF), which relies on a charge-based protein separation[33].

While scWB and scIEF are powerful single-cell proteomic assays, they are limited as single-mode assays that only measure proteins. There is a need for multimodal assays that combine the protein specificity afforded by scIB with nucleic acid measurements. Specifically, there is a measurement gap in the ability to detect protein isoforms and point mutations in the same single cell[6]. Our group introduced snapBlot, an assay that fractionally lyses the cytoplasm to enable a size-based electrophoretic protein separation coupled with a qPCR readout of nucleic acids extracted from the intact nuclei[34]. However, snapBlot is limited to detecting only nuclear mRNA, is not optimized for single cells, suffers from low throughput, and point mutation detection has not been demonstrated. In this dissertation, we seek to address these limitations through the development of a novel single-cell multimodal assay with the potential for isoform-specific protein detection and point mutation-specific nucleic acid detection.

1.3 Characteristics of In-Gel Assays

scWB and scIEF are examples of in-gel assays, where protein electrophoresis, capture, and detection are carried out within a polyacrylamide hydrogel matrix[19,33]. Over the last couple decades, in-gel assays have grown in popularity due to the advantageous physical, chemical, and optical properties of hydrogel substrates. Such assays include gel-enhanced tissue clearing[35], expansion microscopy[36,37], in-gel microarrays[38], and scIB[19,33]. Many of the benefits of in-gel assays can be attributed to the highly aqueous environment within a hydrogel since most of the volume of a hydrogel is occupied by water[39]. The result is that enzymatic reactions in hydrogels perform better than on surfaces or even in free solution in some cases[40]. However, there are crucial differences between in-gel assays and in-solution assays that are largely governed by the gel pore size and must be taken into account during assay design. In this dissertation, we will be focusing on polyacrylamide, one of the most common hydrogel materials. The primary strategy to modify the pore size of a polyacrylamide gel is to modulate the total acrylamide concentration (%T) and the concentration of the crosslinker relative to the total acrylamide concentration (% C), where increased %T and %C result in smaller pore size gels[41].

The first fundamental difference between in-gel and in-solution assays is hindered diffusion of solute molecules within the hydrogel matrix. While diffusion of solutes is unencumbered in free solution, collisions between the diffusing molecules and the polymer fiber chains that comprise the hydrogel matrix hinder diffusion within a hydrogel[39]. The degree of the hindered diffusion effect in a polyacrylamide gel is dependent on the hydrodynamic radius of the diffusing solute, the polymer volume fraction of the gel, and an empirically determined proportionality constant (Eqn. 1-1)[39].

$$D_{gel} = D_{soln} e^{-K_c R_h \varphi^{0.75}} \qquad \text{(Equation 1-1)}$$

where D_{gel} is the in-gel diffusion coefficient, D_{soln} is the diffusion coefficient of the solute in free solution, K_C is a proportionality constant, R_h is the hydrodynamic radius, and φ is the polymer volume fraction, which is related to the %T of the polyacrylamide gel. It is apparent from the exponential relationship that an increase in either the hydrodynamic radius of the diffusing solute or the gel pore size results in a drastic reduction in the diffusivity in gel compared to in free solution. The implication for assay design is that many assays that are reaction limited in solution will be transport limited in a hydrogel, thus requiring a longer reaction time.

Thermodynamic partitioning in hydrogels presents another fundamental difference between in-gel and in-solution assays. Due to unfavorable thermodynamic interactions of molecules confined in a hydrogel matrix, the solute concentration in a hydrogel is lower than in the surrounding free solution at equilibrium[42,43]. Partitioning behavior is typically reported as a partition coefficient (K), which is defined as the ratio of the solute concentration in the gel to the concentration in free solution at equilibrium (Eqn. 1-2). Thermodynamic partitioning can be influenced by several factors, including size-based interactions, hydrophobic interactions, electrostatic interactions, and affinity-based interactions. Studies have shown that uncharged polyacrylamide gels follow purely size exclusion partitioning according to the Ogston model (Eqn. 1-3)[42,43].

$$K = \frac{[solute]_{gel}}{[solute]_{soln}} \qquad \text{(Equation 1-2)}$$

$$K = \exp\left[-\phi\left(1 + \frac{R_h}{a_f}\right)^2\right] \qquad \text{(Equation 1-3)}$$

where $[solute]_{gel}$ is the solute concentration in the gel phase, $[solute]_{soln}$ is the solute concentration in the solution phase that is in equilibrium with the gel, Φ is the polymer volume fraction, R_h is the solute hydrodynamic radius, and a_f is the polymer chain radius. As with hindered diffusion, it is apparent from the exponential relationship that the partition coefficient drastically decreases with an increasing polymer volume fraction or solute hydrodynamic radius. The implication for assay design is that the in-gel concentration of large molecules is much lower than in solution, resulting in the need to use higher reagent concentrations or otherwise modify the assay to adapt to lower reagent concentrations.

Due to the differences between in-gel and in-solution assays outlined above, new in-gel formats of existing assays require additional characterization. While in-gel assays have been growing in popularity, there is still a lack of fundamental characterization studies of the diffusion and partitioning properties of various molecules in hydrogels. Additionally, there is a general lack of studies that compare the performance of in-gel and in-solution versions of an assay. A major

focus of this dissertation is to characterize key properties that govern the performance of in-gel assays.

1.4 Dissertation Overview

In this dissertation, we seek to address some of the major limitations of current single-cell assays. The first portion of this dissertation (Chapters 2-5) is focused on developing techniques and characterizing systems aimed at improving the target multiplexing and analytical sensitivity of in-gel protein assays. The second portion of this dissertation (Chapters 6 and 7) is focused on the development of single-cell multimodal electrophoretic assays to enable co-detection of nucleic acid point mutations and protein isoforms.

In Chapter 2, we evaluate H_2O_2-based quenching of fluorophores, motivated by a need to improve target multiplexing of in-gel immunoassays. We characterize the quenching behavior of various common fluorophores both in solution and in polyacrylamide hydrogels, demonstrating complete quenching of two fluorophores that are commonly used in scIB.

In Chapter 3, we develop an in-gel polymerase elongation method for fluorescence signal readout and amplification in hydrogel-based assays. We study the how the interplay of reaction and transport limitations govern the timescale of in-gel polymerase elongation, positing a novel retarded diffusion phenomenon. Additionally, we develop DNA sequence design rules for signal amplification by incorporation of multiple fluorophore-labeled nucleotides per strand.

In Chapter 4, we study how reaction time, gel density, and buffer composition influence hybridization chain reaction (HCR) signal amplification in dense polyacrylamide hydrogels to develop assay design rules. We fit the in-gel HCR fluorescence vs time data to a pseudo first-order DNA hybridization kinetics model, observing a good fit.

In Chapter 5, we investigate immuno-HCR as a signal amplification strategy for in-gel protein detection aimed at improving the analytical sensitivity of scIB. We characterize the properties of the DNA-antibody conjugates that enable immuno-HCR, including the degree of labeling, binding affinity, and the thermodynamic partitioning behavior. Furthermore, we compare the performance of immuno-HCR to standard immunoprobing with fluorophore-labeled antibodies in the detection of immobilized proteins in dense polyacrylamide gels.

In Chapter 6, we work toward developing a single-cell multimodal electrophoretic assay that integrates point mutation-specific in-gel mRNA measurements with isoform-specific protein measurements. In our design, protein and mRNA from single cells are electrophoresed together into a polyacrylamide gel, followed by mRNA detection via in situ hybridization and protein detection via immunoprobing with fluorophore-labeled antibodies.

In Chapter 7, we introduce the concept of a single-cell electrophoretic assay with a qPCR readout for absolute quantification of mRNA. Starting with an assay previously developed by our group (snapBlot), we describe several design and fabrication innovations that will enable analysis of whole-cell mRNA from electrophoresed single cells. We also generate qPCR standard curves for absolute quantification of beta-actin mRNA.

In Chapter 8, we provide some concluding remarks and present future research directions that build on the advancements outlined in this dissertation. Finally, the included appendices contain analysis scripts.

1.5 Bibliography

(1) Alberts, B.; Bray, D.; Hopkins, K.; Johnson, A.; Lewis, J.; Raff, M.; Roberts, K.; Walter, P. *Essential Cell Biology*, 4th ed.; Garland Science, 2014.

(2) D'Adamo, G. L.; Widdop, J. T.; Giles, E. M. The Future Is Now? Clinical and Translational Aspects of "Omics" Technologies. *Immunol. Cell Biol.* **2021**, *99* (2), 168–176. https://doi.org/10.1111/imcb.12404.

(3) Svahn, H. A.; Van Den Berg, A. Single Cells or Large Populations? *Lab Chip* **2007**, *7* (5), 544–546. https://doi.org/10.1039/b704632b.

(4) Wang, D.; Bodovitz, S. Single Cell Analysis: The New Frontier in "Omics." *Trends Biotechnol.* **2010**, *28* (6), 281–290. https://doi.org/10.1016/j.tibtech.2010.03.002.

(5) Macaulay, I. C.; Ponting, C. P.; Voet, T. Single-Cell Multiomics: Multiple Measurements from Single Cells. *Trends Genet.* **2017**, *33* (2), 155–168. https://doi.org/10.1016/j.tig.2016.12.003.

(6) Ogbeide, S.; Giannese, F.; Mincarelli, L.; Macaulay, I. C. Into the Multiverse: Advances in Single-Cell Multiomic Profiling. *Trends Genet.* **2022**, *38* (8), 831–843. https://doi.org/10.1016/j.tig.2022.03.015.

(7) Aldridge, S.; Teichmann, S. A. Single Cell Transcriptomics Comes of Age. *Nat. Commun.* **2020**, *11* (1), 9–12. https://doi.org/10.1038/s41467-020-18158-5.

(8) Klein, A. M.; Mazutis, L.; Akartuna, I.; Tallapragada, N.; Veres, A.; Li, V.; Peshkin, L.; Weitz, D. A.; Kirschner, M. W. Droplet Barcoding for Single-Cell Transcriptomics Applied to Embryonic Stem Cells. *Cell* **2015**, *161* (5), 1187–1201. https://doi.org/10.1016/j.cell.2015.04.044.

(9) Ståhlberg, A.; Thomsen, C.; Ruff, D.; Åman, P. Quantitative PCR Analysis of DNA, RNAs, and Proteins in the Same Single Cell. *Clin. Chem.* **2012**, *58* (12), 1682–1691. https://doi.org/10.1373/clinchem.2012.191445.

(10) Labib, M.; Kelley, S. O. Single-Cell Analysis Targeting the Proteome. *Nat. Rev. Chem.* **2020**, *4* (3), 143–158. https://doi.org/10.1038/s41570-020-0162-7.

(11) Aebersold, R.; Agar, J. N.; Amster, I. J.; Baker, M. S.; Bertozzi, C. R.; Boja, E. S.; Costello, C. E.; Cravatt, B. F.; Fenselau, C.; Garcia, B. A.; Ge, Y.; Gunawardena, J.; Hendrickson, R. C.; Hergenrother, P. J.; Huber, C. G.; Ivanov, A. R.; Jensen, O. N.; Jewett, M. C.; Kelleher, N. L.; Kiessling, L. L.; Krogan, N. J.; Larsen, M. R.; Loo, J. A.; Ogorzalek Loo, R. R.; Lundberg, E.; Maccoss, M. J.; Mallick, P.; Mootha, V. K.; Mrksich, M.; Muir, T. W.; Patrie, S. M.; Pesavento, J. J.; Pitteri, S. J.; Rodriguez, H.; Saghatelian, A.; Sandoval, W.; Schlüter, H.; Sechi, S.; Slavoff, S. A.; Smith, L. M.; Snyder, M. P.; Thomas, P. M.; Uhlén, M.; Van Eyk, J. E.; Vidal, M.; Walt, D. R.; White, F. M.; Williams, E. R.; Wohlschlager, T.; Wysocki, V. H.; Yates, N. A.; Young, N. L.; Zhang, B. How Many Human Proteoforms Are There? *Nat. Chem. Biol.* **2018**, *14* (3), 206–214. https://doi.org/10.1038/nchembio.2576.

(12) Kamies, R.; Martinez-Jimenez, C. P. Advances of Single-Cell Genomics and Epigenomics

in Human Disease: Where Are We Now? *Mamm. Genome* **2020**, *31* (5–6), 170–180. https://doi.org/10.1007/s00335-020-09834-4.

(13) Method of the Year 2019: Single-Cell Multimodal Omics. *Nat. Methods* **2020**, *17* (1).

(14) Stoeckius, M.; Hafemeister, C.; Stephenson, W.; Houck-loomis, B.; Chattopadhyay, P. K.; Swerdlow, H.; Satija, R.; Smibert, P. Large-Scale Simultaneous Measurement of Epitopes and Transcriptomes in Single Cells. *Nat. Methods* **2017**, *14* (9), 865–868. https://doi.org/10.1038/nmeth.4380.Large-scale.

(15) Gayoso, A.; Lopez, R.; Regier, J.; Nazor, K. L.; Yosef, N.; Sciences, C.; Arbor, A.; Arbor, A.; Diego, S.; Biohub, Z.; Francisco, S. Joint Probabilistic Modeling of Single-Cell Multi-Omic Data with TotalVI. *Nat. Methods* **2021**, *18* (3), 272–282. https://doi.org/10.1038/s41592-020-01050-x.Joint.

(16) Demaree, B.; Delley, C. L.; Vasudevan, H. N.; Peretz, C. A. C.; Ruff, D.; Smith, C. C.; Abate, A. R. Joint Profiling of DNA and Proteins in Single Cells to Dissect Genotype-Phenotype Associations in Leukemia. *Nat. Commun.* **2021**, *12* (1), 1–10. https://doi.org/10.1038/s41467-021-21810-3.

(17) Li, J. J.; Bickel, P. J.; Biggin, M. D. System Wide Analyses Have Underestimated Protein Abundances and the Importance of Transcription in Mammals. *PeerJ* **2014**. https://doi.org/10.7717/peerj.270.

(18) Budnik, B.; Levy, E.; Harmange, G.; Slavov, N. SCoPE-MS: Mass Spectrometry of Single Mammalian Cells Quantifies Proteome Heterogeneity during Cell Differentiation. *Genome Biol.* **2018**, *19* (1), 1–12. https://doi.org/10.1186/s13059-018-1547-5.

(19) Hughes, A. J.; Spelke, D.; Xu, Z.; Kang, C. C.; Schaffer, D.; Herr, A. E. Single-Cell Western Blotting. *Nat. Methods* **2015**, *11* (7), 455–464. https://doi.org/10.1007/978-1-4939-2694-7_46.

(20) Vlassakis, J.; Herr, A. E. Effect of Polymer Hydration State on In-Gel Immunoassays. *Anal. Chem.* **2015**, *87* (21), 11030–11038. https://doi.org/10.1021/acs.analchem.5b03032.

(21) Shi, M.; Geng, X.; Wang, C.; Guan, Y. Quantification of Low Copy Number Proteins in Single Cells. *Anal. Chem.* **2019**, *91* (18), 11493–11496. https://doi.org/10.1021/acs.analchem.9b02989.

(22) Hendrickson, E. R.; Truby, T. M. H.; Joerger, R. D.; Majarian, W. R.; Ebersole, R. C. High Sensitivity Multianalyte Immunoassay Using Covalent DNA-Labelled Antibodies and Polymerase Chain Reaction. *Nucleic Acids Res.* **1995**, *23* (3), 522–529.

(23) Schweitzer, B.; Wiltshire, S.; Lambert, J.; O'Malley, S.; Kukanskis, K.; Zhu, Z.; Kingsmore, S. F.; Lizardi, P. M.; Ward, D. C. Immunoassays with Rolling Circle DNA Amplification: A Versatile Platform for Ultrasensitive Antigen Detection. *Proc. Natl. Acad. Sci.* **2000**, *97* (18), 10113–10119. https://doi.org/10.1073/pnas.170237197.

(24) Choi, J.; Love, K. R.; Gong, Y.; Gierahn, T. M.; Love, J. C. Immuno-Hybridization Chain Reaction for Enhancing Detection of Individual Cytokine-Secreting Human Peripheral Mononuclear Cells. *Anal. Chem.* **2011**, *83* (17), 6890–6895.

https://doi.org/10.1038/jid.2014.371.

(25) Chattopadhyay, P. K.; Winters, A. F.; Iii, W. E. L.; Laino, A. S.; Woods, D. M. High-Parameter Single-Cell Analysis. *Annu. Rev. Anal. Chem.* **2019**, *12* (2).

(26) Goltsev, Y.; Samusik, N.; Kennedy-Darling, J.; Vazquez, G.; Black, S.; Correspondence, G. P. N.; Bhate, S.; Hale, M.; Nolan, G. P. Deep Profiling of Mouse Splenic Architecture with CODEX Multiplexed Imaging In Brief A DNA Barcoding-Based Imaging Technique Uses Multiplexed Tissue Antigen Staining to Enable the Characterization of Cell Types and Dynamics in a Model of Autoimmune Diseas. *Cell* **2018**, *174* (4), 1–14. https://doi.org/10.1016/j.cell.2018.07.010.

(27) Gopal, A.; Herr, A. E. Multiplexed In-Gel Microfluidic Immunoassays: Characterizing Protein Target Loss during Reprobing of Benzophenone-Modified Hydrogels. *Sci. Rep.* **2019**, *9* (1), 1–12. https://doi.org/10.1038/s41598-019-51849-8.

(28) Gerdes, M. J.; Sevinsky, C. J.; Sood, A.; Adak, S.; Bello, M. O. Highly Multiplexed Single-Cell Analysis of Formalin- Fi Xed , Paraf Fi n-Embedded Cancer Tissue. *Proc. Natl. Acad. Sci. U. S. A.* **2013**, *110* (29), 11982–11987. https://doi.org/10.1073/pnas.1300136110/-/DCSupplemental.www.pnas.org/cgi/doi/10.1073/pnas.1300136110.

(29) Gerdes, M. J. *Patent: US007741045B2*; 2011; Vol. 2.

(30) Bordeaux, J.; Welsh, A. W.; Agarwal, S.; Killiam, E.; Baquero, M. T.; Hanna, J. A.; Anagnostou, V. K.; Rimm, D. L. Antibody Validation. *Biotechniques* **2010**, *48* (3), 197–209. https://doi.org/10.2144/000113382.

(31) Brodbelt, J. S. Deciphering Combinatorial Post-Translational Modifications by Top-down Mass Spectrometry. *Curr. Opin. Chem. Biol.* **2022**, *70*. https://doi.org/10.1016/j.cbpa.2022.102180.

(32) Kang, C.; Ward, T. M.; Bockhorn, J.; Schiffman, C.; Huang, H.; Pegram, M. D.; Herr, A. E. Electrophoretic Cytopathology Resolves ERBB2 Forms with Single-Cell Resolution. *npj Precis. Oncol.* **2018**, No. February, 1–10. https://doi.org/10.1038/s41698-018-0052-3.

(33) Tentori, A. M.; Yamauchi, K. A.; Herr, A. E.; John, L.; Dewar, L.; Distinguished, L. Detection of Isoforms Differing by a Single-Charge Unit in Individual Cells. *Angew. Chemie - Int. Ed.* **2017**, *55* (40), 12431–12435. https://doi.org/10.1002/anie.201606039.

(34) Rosàs-Canyelles, E.; Modzelewski, A. J.; Geldert, A.; He, L.; Herr, A. E. Multimodal Detection of Protein Isoforms and Nucleic Acids from Mouse Pre-Implantation Embryos. *Nat. Protoc.* **2021**, *16* (2), 1062–1088. https://doi.org/10.1038/s41596-020-00449-2.

(35) Chung, K.; Wallace, J.; Kim, S.; Kalyanasundaram, S.; Andalman, A. S.; Davidson, T. J.; Mirzabekov, J. J.; Zalocusky, K. A.; Mattis, J.; Denisin, A. K.; Pak, S.; Bernstein, H.; Ramakrishnan, C.; Grosenick, L.; Gradinaru, V.; Deisseroth, K. Structural and Molecular Interrogation of Intact Biological Systems. *Nature* **2013**, *497*, 332–339. https://doi.org/10.1038/nature12107.

(36) Chen, F.; Tillberg, P. W.; Boyden, E. S. Expansion Microscopy. *Science (80-.).* **2015**, *347*

(6221), 543–548.

(37) Wassie, A. T.; Zhao, Y.; Boyden, E. S. Expansion Microscopy: Principles and Uses in Biological Research. *Nat. Methods* **2019**, *16* (January), 33–41. https://doi.org/10.1038/s41592-018-0219-4.

(38) Xiao, P. F.; Cheng, L.; Wan, Y.; Sun, B. L.; Chen, Z. Z.; Zhang, S. Y.; Zhang, C. Z.; Zhou, G. H.; Lu, Z. H. An Improved Gel-Based DNA Microarray Method for Detecting Single Nucleotide Mismatch. *Electrophoresis* **2006**, *27* (19), 3904–3915. https://doi.org/10.1002/elps.200500918.

(39) Amsden, B. Solute Diffusion within Hydrogels. Mechanisms and Models. *Macromolecules* **1998**, *31*, 8382–8395. https://doi.org/10.1021/ma980765f.

(40) Atrazhev, A.; Manage, D. P.; Stickel, A. J.; Crabtree, H. J.; Pilarski, L. M.; Acker, J. P. In-Gel Technology for PCR Genotyping and Pathogen Detection. *Anal. Chem.* **2010**, *82* (19), 8079–8087. https://doi.org/10.1021/ac1013157.

(41) Stellwagen, N. C. Apparent Pore Size of Polyacrylamide Gels: Comparison of Gels Cast and Run in Tris-Acetate-EDTA and Tris-Borate-EDTA Buffers. *Electrophoresis* **1998**, *19* (10), 1542–1547. https://doi.org/10.1002/elps.1150191004.

(42) Tong, J.; Anderson, J. L. Partitioning and Diffusion of Proteins and Linear Polymers in Polyacrylamide Gels. *Biophys. J.* **1996**, *70* (3), 1505–1513. https://doi.org/10.1016/S0006-3495(96)79712-6.

(43) Su, A.; Smith, B. E.; Herr, A. E. In Situ Measurement of Thermodynamic Partitioning in Open Hydrogels. *Anal. Chem.* **2019**, *92* (2), 875–883. https://doi.org/10.1021/acs.analchem.9b03582.

Chapter 2: Sequential Fluorophore Quenching as a Multiplexing Strategy for In-Gel Immunoassays

2.1 Introduction

Immunoassay protein target multiplexing is becoming increasingly important to study complex biological systems, with desired multiplexing in the high 10s-100s of protein targets per tissue sample or per cell[1,2]. Multiplexing in protein assays is more limited than multiplexing in nucleic acid assays owing to the types of readouts employed in each. Common sequencing-based nucleic acid assays are capable of detecting thousands of genes or transcripts per cell[3], while protein assays often employ fluorescence-based immunoassay readouts that suffer from limited multiplexing due to spectral overlap of the fluorophores[4]. Various strategies have been developed to overcome these limitations. Some assays completely forego fluorescence readouts, opting instead to conjugate short DNA sequences to antibodies to harness the power of DNA technologies for improved multiplexing and signal amplification[1,5–7]. Mass cytometry is another method that improves immunoassay multiplexing by conjugating metal mass tags to antibodies and employing a mass spectrometry readout[8]. DNA-based readouts and mass cytometry are powerful tools, but they require specialized equipment, extensive training, and are not suitable for all assay formats. Other studies have demonstrated improved multiplexing strategies that are compatible with fluorescence-based immunoassays. Two primary strategies involve sequential rounds of immunoprobing following either (1) stripping of antibodies from their protein targets with harsh detergent buffers[9,10] or (2) quenching of the fluorophores with H_2O_2[2,11]. These multiplexing strategies allow for researchers to improve multiplexing without needing to substantially modify their well-established fluorescence-based immunoassay workflows.

Single-cell immunoblotting (scIB) is a set of single-cell protein assays developed by our group that include the single-cell western blot (scWB)[9] and single-cell isoelectric focusing (scIEF)[12]. Both assays consist of a microscale electrophoretic separation in a polyacrylamide hydrogel followed by UV photocapture of the proteins to the gel matrix via a photoactive benzophenone moiety and subsequent immunoprobing with primary antibodies followed by fluorophore-labeled secondary antibodies[9,12]. As the microarray scanner is limited to 4 fluorescence channels, multiplexing of more than 4 targets requires sequential antibody stripping and re-probing[9]. Antibody stripping steps consist of exposing the gel to a hot buffer that contains SDS and β-mercaptoethanol, resulting in denaturation and removal of the antibodies from their epitopes. While generally an effective multiplexing strategy, antibody stripping suffers from some key limitations. The primary limitation of the antibody stripping protocol is protein loss from the gel that occurs during stripping rounds, reducing the sensitivity for protein targets that are immunoprobed in later rounds[10]. Additionally, the stripping process takes hours and requires harsh chemicals. Members of our group have also noticed that antibody stripping becomes impossible for gel samples that have been stored longer than a couple days. For these reasons, scIB would benefit from a multiplexing strategy that does not rely on antibody stripping.

Fluorophore quenching is an attractive alternative to antibody stripping, as it is also compatible with fluorescence-based immunoassays and would be simple to incorporate into the scIB workflow. Gerdes et al. demonstrated a simple quenching protocol that exposed fixed tissue

samples stained with Cy3 and Cy5 labeled antibodies to a 0.5% H_2O_2 solution for 15 min to quench the fluorophores prior to subsequent re-probing steps[2,11]. They demonstrated multiplexing of up to 61 targets after 30 cycles of quenching and re-probing. Additionally, Gerdes et al. found that there was no significant epitope damage or protein loss after 100 cycles of H_2O_2 quenching, which suggests that multiplexing on the order of hundreds of targets is likely possible. H_2O_2 quenching offers additional advantages over the antibody stripping protocol, including a shorter time (15 min vs hours) and the use of milder chemicals. We hypothesize that H_2O_2 fluorophore quenching will result in less protein loss and signal degradation than antibody stripping due to the use of milder chemicals, ultimately resulting in improved scIB multiplexing. Prior to applying H_2O_2 fluorophore quenching to scIB, there is also a need to validate that the method is effective in polyacrylamide gels and to study the quenching behavior of the Alexa Fluor fluorophores commonly used in scIB[9].

Here, we study the quenching behavior of various fluorophores when exposed to H_2O_2, both in solution and in polyacrylamide gels, as a step toward applying H_2O_2 quenching as a multiplexing strategy in scIB assays. To understand the effect of H_2O_2 treatment on three Alexa Fluor (AF) dyes commonly used in scIB and determine the optimal quenching conditions, we first evaluate the effect of H_2O_2 treatment on the fluorescence in solution. Complete in-solution quenching of all the Alexa Fluor dyes led us to then evaluate the quenching of the AF dyes in two polyacrylamide gel systems, one that contained electrophoresed and photocaptured fluorophore-labeled ovalbumin, and one that employed probing for electrophoresed and photocaptured ovalbumin with fluorophore-labeled antibodies. We demonstrate significant and nearly complete in-gel quenching of AF555 and AF647 in both the gels that contained labeled ovalbumin and the immunoprobed gels. The in-gel quenching observed in this study is a promising step toward employing H_2O_2 fluorophore quenching to scIB assays for multiplexing.

2.2 Materials and Methods

Reagents

Rabbit anti-ovalbumin (ab181688), and Cy3 and Cy5 labeling kits that contained free dye were purchased from AbCAM. Alexa Fluor 555 and Alexa Fluor 647 labeling kits, Alexa Fluor 647-labeled donkey anti-rabbit (A31573), and Alexa Fluor 488-labeled ovalbumin were purchased from Thermo Fisher Scientific. Ovalbumin, bovine serum albumin (BSA, urea, sodium dodecyl sulfate, sodium deoxycholate, Triton X-100, tetramethylethylenediamine (TEMED), ammonium persulfate (APS), 3-(trimethoxylsilyl)propyl methacrylate, dichlorodimethylsilane, 30% acrylamide/bis-acrylamide solution (29:1), Dimethyl Sulfoxide (DMSO), and 30% H_2O_2 solution were purchased from Sigma-Aldrich. N-[3-[(3-Benzoylphenyl)formamido]propyl] methacrylamide (BPMAC) was custom synthesized by Pharm-Agra Laboratories. De-ionized (DI) water was prepared with Ultrapure water system from Millipore.

In-Solution Quenching Experiments

Stock solutions of each fluorophore were prepared to a concentration of 1 mg/mL in DMSO. Fluorophore solutions were then prepared to a concentration of 2 µM in quenching buffer (0.25 M $NaHCO_3$, adjusted to pH 10 with NaOH). H_2O_2 solutions were prepared in quenching buffer at concentrations of 0.2%, 1%, and 3%. The fluorophore solutions were then mixed 1:1 with the H_2O_2 solutions to yield final fluorophore concentrations of 1 µM, and H_2O_2 concentrations of 0.1%, 0.5%, and 1.5%, respectively. Next, samples were transferred to flat black 96-well plates, where each well contained a total of 100 µL. Finally, the fluorescence was measured with a Tecan Infinite M200 plate reader at the specified time points.

Protein Labeling with Fluorophores

Ovalbumin was labeled with AF555 and AF647 fluorophores via amine-reactive chemistry using commercially available microscale protein labeling kits from Invitrogen. Ovalbumin solutions were prepared at a concentration of 1 mg/mL in 1xPBS for each of the labeling reactions. Kit protocols were followed for the labeling reactions and product purification. Labeled protein concentration and degree of labeling (DOL) were calculated with Beer-Lambert Law after measuring the absorbance of each solution on a Nanodrop 2000 spectrophotometer. The average DOL of the AF555-labeled ovalbumin was 2.8, and the average DOL of the AF647-labeled ovalbumin was 0.7.

Gel Fabrication

Polyacrylamide gels were fabricated on silicon wafer substrates with 40 µm rails and 32 µm diameter microposts patterned in SU-8, as previously reported[9,13]. Gel precursor solutions containing acrylamide/bis-acrylamide stock solution (30%, 29:1) were prepared to a concentration of 8% T and 3.3% C. BPMAC was added to a concentration of 3mM, followed by degassing via sonication for 5 min. APS and TEMED were then added to the precursor to a concentration of 0.08% each before pipetting the solution between the SU-8 patterned wafer (rendered hydrophobic by treatment with dichlorodimethylsilane) and a glass microscope slide functionalized with 3-(trimethoxysilyl)propyl methacrylate. After a 15-min chemical polymerization, the slides with the attached gels were lifted from the wafers and washed in 1xPBS for at least 1 h prior to use in experiments.

Polyacrylamide Gel Electrophoresis

Ovalbumin protein solutions were prepared at a concentration of 1 µM in 1xPBS. For each half slide gel, 50 µL of protein solution was pipetted onto the surface of a glass plate, and the gel sandwiched carefully against the glass plate using tape spacers to avoid bubbles, as described in the scWB probing protocol[13]. Gels were incubated for 30 min with the protein solutions to allow for the protein to diffuse and partition into the microwells. Thermodynamic partitioning results in a higher concentration of protein in the microwells than in the surrounding gel[14]. After the incubation step, the gels were removed from the glass plate and briefly rinsed by pouring a few mL of 1xPBS over the gels at an angle. Gels were then placed in a scWB electrophoresis chamber and 12 mL of 55ºC 1xRIPA buffer poured into the corner of the chamber, as in the

scWB[13]. Gels were exposed to the RIPA buffer for 30 s to allow for protein denaturation prior to a 30 s electrophoresis step at 40 V/cm and a 45 s photocapture step with a Hamamatsu LC5 Spot Light Source.

In-Gel Quenching

After immunoprobing and imaging, the dehydrated gels were placed in a 4-well dish, and 10 mL of quenching solution was added to each well of the dish. The quenching solution consisted of 0.5% H_2O_2 in 0.25 M $NaHCO_3$, adjusted to pH 10 with NaOH. Gels were incubated in the quenching solution for 15 min on an orbital shaker. The quenching solution was then aspirated off and the gels washed in 10 mL of 1xTBST for 30 min. Gels were finally rinsed briefly 3x with DI water and dehydrated with an N_2 stream prior to re-imaging to confirm the quenching.

Immunoprobing

Immunoprobing followed the standard scWB protocol[9,13]. Each half slide gel was probed with 50 µL of antibody solution. The primary antibody (rabbit anti-ovalbumin) and secondary antibodies (AF555 and AF647-labeled donkey anti-rabbit) were diluted 1:10 in 2% BSA in 1xTBST. Gels were incubated for 2 h with the primary antibody, washed in 1xTBST, incubated for 1 h with the secondary antibodies, and washed again in 1xTBST.

Gel Imaging and Data Analysis

Imaging of the dehydrated gels was conducted using a GenePix 4300A microarray scanner equipped with 488 nm, 532 nm, 594 nm, and 635 nm lasers. AF488 gels were imaged with the 488 nm laser, AF555 gels with the 532 nm laser, and AF647 gels with the 635 nm laser. Imaging settings were chosen for high dynamic range without achieving saturation. Images were then analyzed with the scWB analysis pipeline[15] to generate ROIs from each lane of the gel, calculate intensity profiles, fit gaussian peaks to the protein bands, and extract the intensity of the gaussian peaks. An R^2 threshold of 0.7 was chosen to identify good gaussian fitted peaks. SNRs were defined as the fluorescence signal intensity at the center of the fitted gaussian peak divided by the standard deviation of a 5 pixel gutter region that served as the background. SNRs were calculated with a custom MATLAB function (Appendix A). Post-treatment gel images were transformed with the Landmark Correspondences plugin of FIJI to ensure that the same exact locations of the gel were analyzed before and after treatment.

2.3 Results and Discussion

Here, we report on three approaches to evaluate the quenching behavior of fluorophores exposed to H_2O_2. First, we assessed in-solution H_2O_2 quenching of a select set of common fluorophores. Second, we evaluated in-gel H_2O_2 quenching of three Alexa Fluor dyes with electrophoresed labeled ovalbumin. Finally, we demonstrated quenching of immunoprobed protein bands in response to H_2O_2 treatment

In-Solution Quenching Results

We first sought to understand the fluorescence quenching response of different fluorophores in solution when exposed to varied H_2O_2 concentrations and incubation times. Investigating the fluorescence response to H_2O_2 treatment in solution prior to investigating an in-gel system served three purposes: (1) to determine which fluorophores can be quenched with H_2O_2, (2) to choose fluorophore candidates for in-gel quenching experiments, and (3) to determine the minimum H_2O_2 concentration and incubation time for complete quenching. The minimal H_2O_2 concentration and incubation time was desired to reduce the chance of damage to protein epitopes. Three fluorophores that were previously evaluated in the literature were included in these experiments (FITC, Cy3, and Cy5)[2,11], along with AF488, AF555, and AF647, as they are the primary fluorophores used in scIB[9].

Based on the literature, Cy3 and Cy5 are susceptible to H_2O_2 quenching, while fluorescein is not susceptible to quenching[2,11]. A proposed mechanism for the irreversible quenching of cyanine dyes upon exposure to reactive oxygen species is oxidation and cleavage of carbon-carbon double bonds that connect the two characteristic aromatic rings[16]. Unlike cyanine dyes, the chemical structure of fluorescein consists of conjugated aromatic rings and does not contain any simple carbon-carbon double bonds, explaining the lack of quenching observed in response to H_2O_2 treatment (Fig. 2-1). Alexa Fluor dyes are often derivatives of other fluorophores that have been optimized for improved yield and/or stability, as indicated by their chemical structures. AF488 is a derivative of fluorescein (Fig. 2-1A), while AF555 and AF647 are derivatives of Cy3 and Cy5, respectively (Fig. 2-1B). We hypothesized that AF555 and AF647 would be susceptible to H_2O_2 quenching, as both are derivatives of cyanine dyes, while AF488 would not be susceptible to quenching, as it is a derivative of fluorescein.

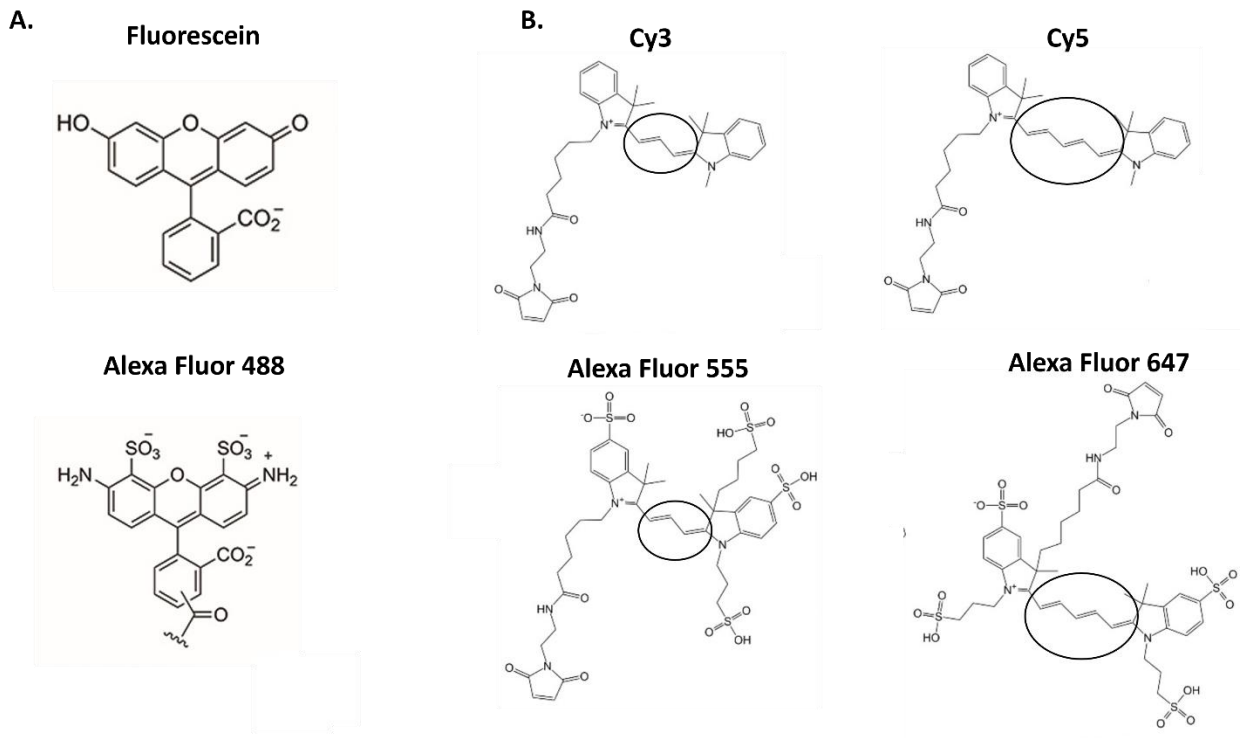

Figure 2-1: Fluorophore chemical structures indicate that Alexa Fluor dyes are similar to other commonly used fluorophores that have been previous evaluated for H_2O_2 quenching.
(A) Alexa Fluor 488 is a derivative of fluorescein[17]. (B) Alexa Fluor 555 and Alexa Fluor 647 are derivatives of Cy3 and Cy5, respectively[18]. Carbon-carbon double bonds in cyanin-based dyes circled to demonstrate the location of hypothesized cleavage upon exposure to H_2O_2.

All fluorophores evaluated exhibited a decrease in fluorescence in response to H_2O_2 treatment (Fig. 2-2). Decreasing fluorescence were observed with increasing H_2O_2 concentrations and incubation times for all fluorophores, except for FITC. The measured decrease in the fluorescence of FITC was not dependent on H_2O_2 concentration or incubation time, plateauing at a constant ~15% of the intensity of the untreated controls. The Alexa Fluor dyes, especially AF555 and AF647, exhibited the largest decrease in fluorescence in response to H_2O_2 treatment, such that the normalized fluorescence intensity reached 0 after exposure to 0.5% H_2O_2 for 15 min. Controls that consisted of samples of each of the fluorophores that did not contain H_2O_2 revealed stable fluorescence for all the Alexa Fluor dyes, and a decrease in fluorescence of 20-30% for FITC and Cy5, likely attributable to photobleaching.

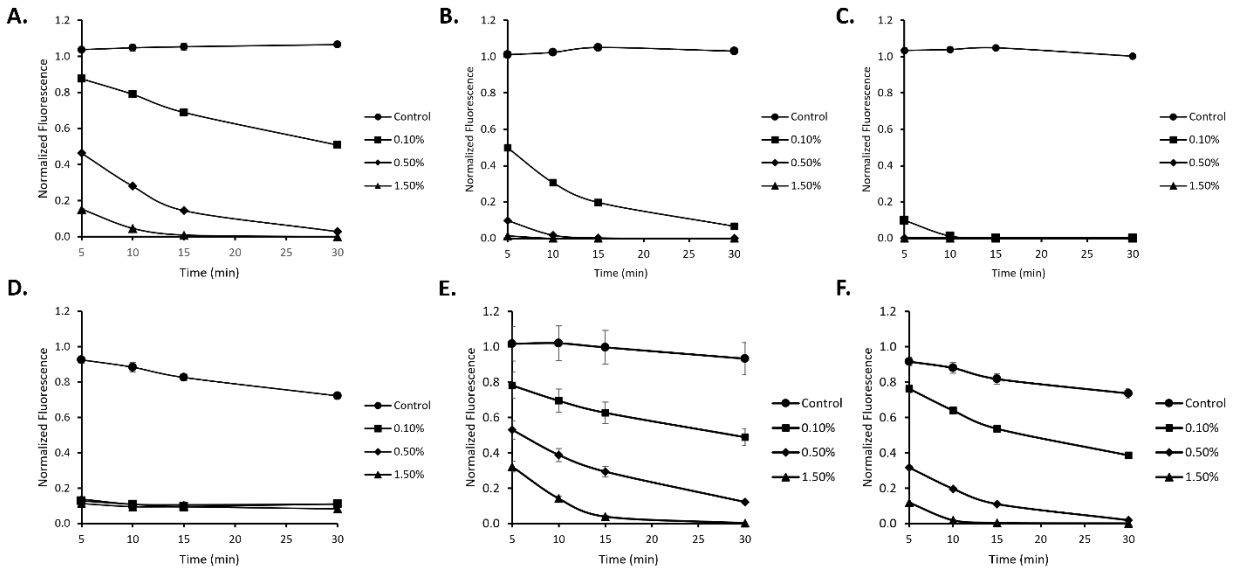

Figure 2-2: In-solution experiments reveal that H_2O_2 quenches the fluorescence of the majority of fluorophores evaluated with reduced fluorescence at higher H_2O_2 concentrations and longer incubation times. The following fluorophores at concentrations of 1 µM were exposed to varied H_2O_2 concentrations ranging from 0% (control) to 1.5%: (A) AF 488, (B) AF 555, (C) AF 647, (D) FITC, (E) Cy3, (F) Cy5. All measurements were taken in triplicate with mean values and standard deviation error bars displayed.

The results of the in-solution quenching experiments allow us to conclude that AF555 and AF647 are the fluorophores most susceptible to H_2O_2 quenching, with complete quenching achieved in 15 min with 0.5% H_2O_2. In fact, AF555 and AF647 are more sensitive to H_2O_2 treatment than Cy3 and Cy5, the fluorophores quenched in previous work for improved multiplexing. AF488 appears to also be quenchable with H_2O_2 treatment but requires a higher concentration of H_2O_2 and/or a longer incubation time than AF555 and AF647. All the Alexa Fluor dyes exhibit increased sensitivity to H_2O_2 quenching than their unmodified counterparts. In the case of AF555 and AF657, we posit that this increased sensitivity to H_2O_2 is due to chemical modifications to the cyanine dyes that result in carbon-carbon double bonds that are more susceptible to cleavage upon exposure to H_2O_2. Our in-solution quenching results for Cy3 and Cy5 after 15 min exposure to 0.5% H_2O_2 match the results in literature of 60% and 80% reductions in fluorescence, respectively[2]. Surprisingly, and in contrast to results in the literature and our hypothesis, both FITC and AF488 exhibited decreases in fluorescence in response to H_2O_2 treatment. We currently do not have an explanation for this unexpected result. It would be an interesting topic of further study.

Based on the results of this in-solution study, we decided to focus our in-gel experiments on the Alexa Fluor dyes and employ a 15 min quenching step with 0.5% H_2O_2. Ultimately, the knowledge gained from this study is beneficial for application of H_2O_2 quenching to assays that employ Alexa Fluor dyes. Additionally, these results will inform assay design with respect to the choice of H_2O_2 concentrations and incubation times needed depending on the fluorophore choice.

In-Gel Quenching with Labeled Ovalbumin

To evaluate in-gel H_2O_2 fluorophore quenching, we developed a system that employed electrophoresis of fluorophore-labeled ovalbumin (Fig. 2-3A). Briefly, ovalbumin was labeled with Alexa Flour dyes via amine-reactive chemistry, partitioned into microwells in 8% T polyacrylamide gels, exposed to 1xRIPA buffer, electrophoresed for 30 s at 40 V/cm, exposed to UV, washed, and imaged. After the first imaging step, the gels were exposed to H_2O_2 for 15 min and imaged again. Handling controls that were treated with same alkaline buffer used in the quenching step, except without the addition of H_2O_2, were included. General choices of gel format and assay conditions were chosen to closely match the scWB[9]. The H_2O_2 quenching conditions were chosen based on our in-solution quenching results and the conditions employed in the literature[2]. Since H_2O_2 is a small molecule, we anticipated that there would not be any substantial transport limitations in the gel, and that H_2O_2 would readily be able to access the fluorophores for the degradation reaction to take place. Thus, we hypothesized that complete quenching of AF555 and AF647, and partial quenching of AF488 would occur after a 15 min incubation with H_2O_2. Qualitatively, AF555 and AF647 were completely quenched after H_2O_2 treatment, as indicated by micrographs of a gel lane before and after treatment (Fig. 2-3B).

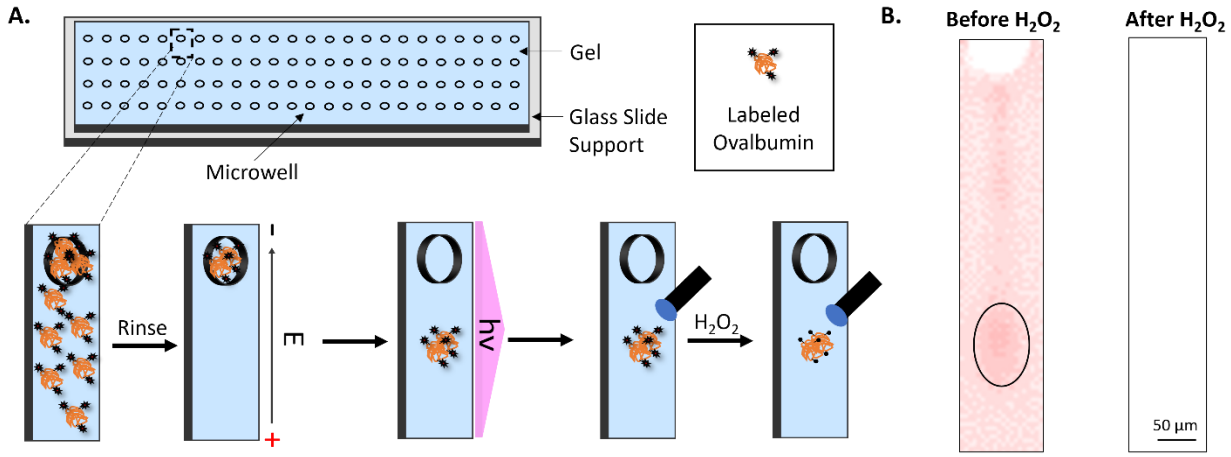

Figure 2-3: In-gel fluorophore quenching in response to H_2O_2 treatment evaluated with fluorophore-labeled ovalbumin. (A) Fluorophore-labeled ovalbumin at a concentration of 1 µM was partitioned into microwells, electrophoresed, photocaptured, and imaged prior to H_2O_2 treatment and subsequent imaging. (B) Diminished fluorescence in response to H_2O_2 treatment was observed (showing one gel lane containing AF555-ovalbumin with protein band circled).

Next, we quantitatively analyzed the immobilized ovalbumin protein peaks with the scWB MATLAB analysis pipeline[15], since the gel dimensions and assay format are comparable to the scWB. The signal-to-noise ratio (SNR) before and after treatment was chosen as the primary analysis metric because SNR>3 is commonly defined as the threshold for choosing protein peaks to analyze in the scWB[9,15]. The indices of the gel lanes were tracked in the analysis pipeline to ensure that the same subset of lanes from each gel were analyzed before and after H_2O_2 treatment. Tracking the indices was also necessary because the post-treatment lanes with SNRs<3 would normally not pass quality control and not be analyzed in the scWB pipeline.

Significant decreases in the SNRs after H_2O_2 treatment were observed for both AF555 and AF647 (Fig. 2-4). The average SNR for the AF555-labeled protein bands decreased from 7.20 ± 4.89 before H_2O_2 treatment to 2.52 ± 2.01 after H_2O_2 treatment. AF647 exhibited an even stronger response to H_2O_2 treatment with average SNRs of 5.25 ± 2.77 before treatment and 0.303 ± 0.688 after H_2O_2 treatment. There was no statistically significant difference in the SNRs before and after treatment in the AF555 and AF647 control gels, indicating that the H_2O_2 was responsible for the observed decreases. Surprisingly, there was a statistically significant increase in the SNRs for both the control and H_2O_2 treated AF488 gels.

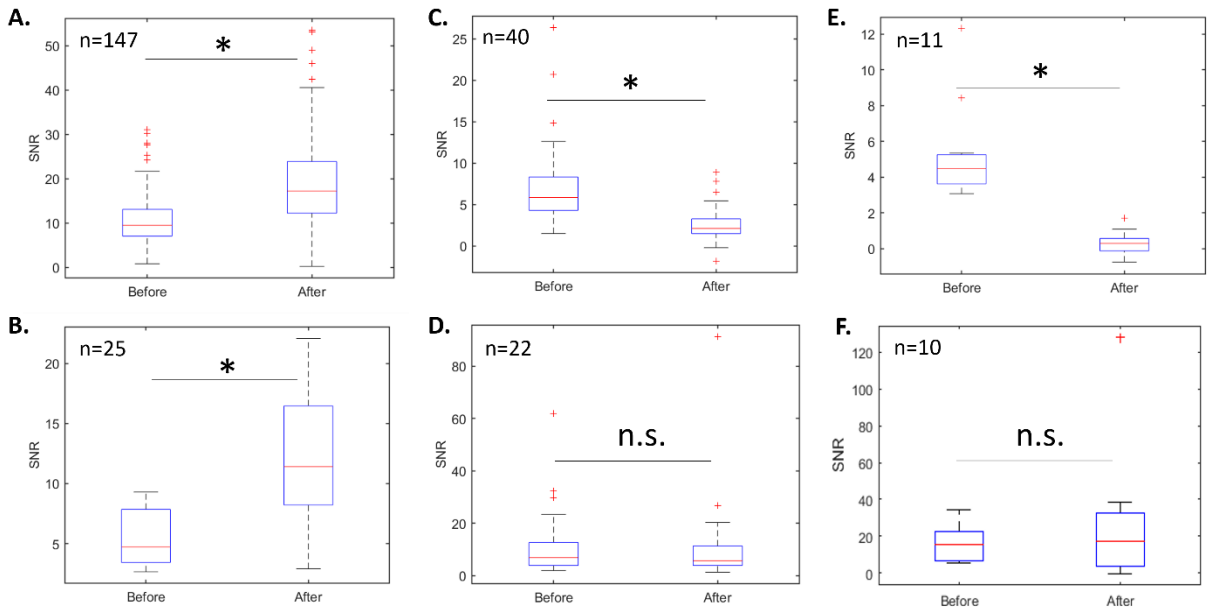

Figure 2-4: In-gel experiments with photocaptured fluorescently labeled ovalbumin reveal significant changes in the SNRs of protein peaks in gels exposed to 0.5% H_2O_2. (A) AF 488 H_2O_2 treated gel, (B) AF 488 handling control gel that was exposed alkaline buffer minus the H_2O_2, (C) AF 555 H_2O_2 treated gel, (D) AF 555 handling control gel, (E) AF 647 H_2O_2 treated gel, (F) AF 647 handling control gel. Statistical significance was determined with Mann-Whitney U-tests, where * represents $p<0.001$. Sample size on charts refers to the number of protein bands analyzed from one gel.

An average SNR value of much less than 3 in the AF647 gel indicates good quenching performance after exposure to H_2O_2, as an SNR<3 is below the cutoff for analysis in the scWB pipeline such that all lanes with SNR<3 would not be identified as a protein peak. While the average SNR of the AF555 gel is less than 3, the large error bars indicate that the SNR of many protein peaks was greater than 3 after H_2O_2. Additionally, a few of the analyzed peaks before quenching had SNRs<3 because there were so few protein peaks to analyze due to the weak fluorescence. We attribute the weak fluorescence to a low degree of labeling of the ovalbumin, and protein loss during the RIPA buffer treatment and subsequent electrophoresis steps.

Generally, the observed quenching of both AF555 and AF647 was consistent with the results of our in-solution experiments.

In-Gel Quenching of Immunoprobed Protein Bands

For application to scIB protocols, the in-gel quenching process must be compatible with immunoprobed proteins. Following the successful in-gel quenching results with fluorescently labeled ovalbumin, we evaluated H_2O_2 quenching of immunoprobed ovalbumin protein bands. The protocol for protein loading, electrophoresis, and photocapture was the same as described in the previous set of experiments, except that unlabeled ovalbumin was used in place of labeled ovalbumin. Gels were then probed with anti-ovalbumin primary antibodies followed by fluorophore-labeled secondary antibodies (Fig. 2-5A).

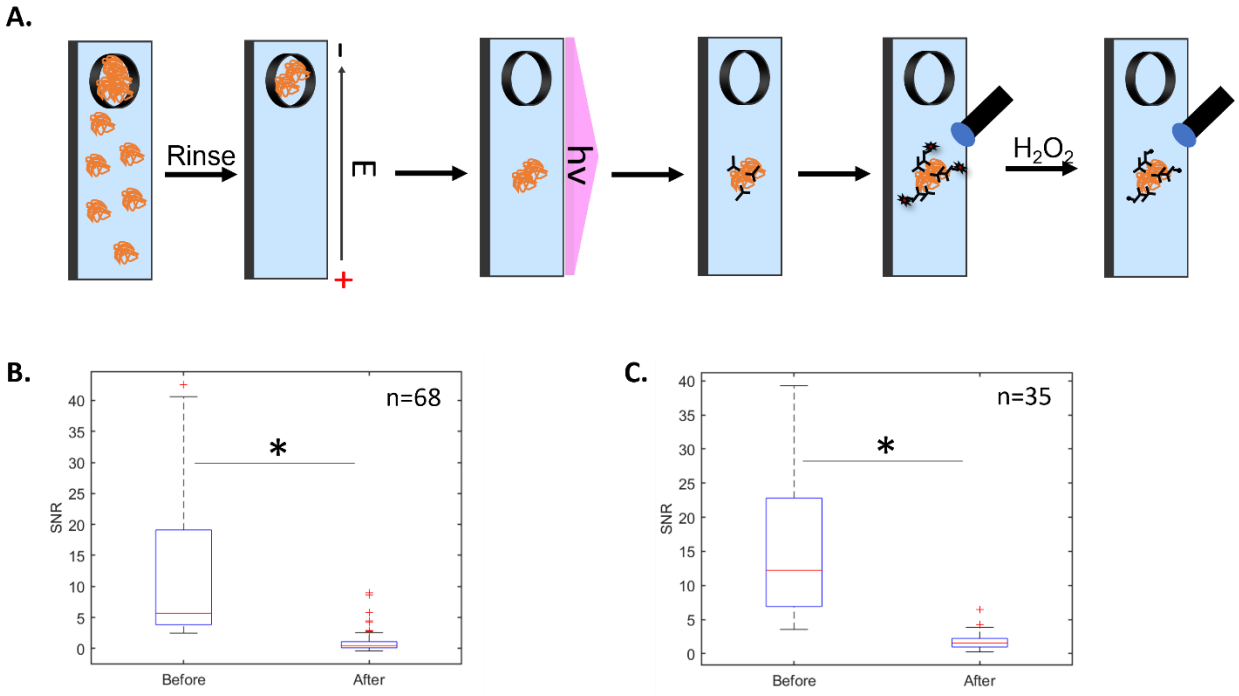

Figure 2-5: Decreases in the SNRs of immunoprobed ovalbumin protein peaks suggest complete fluorophore quenching after gels are exposed to 0.5% H_2O_2. (A) Ovalbumin was partitioned into microwells in a gel, electrophoresed, photocaptured, immunoprobed with primary antibodies and fluorescently labeled secondary antibodies, imaged, treated with H_2O_2, and subsequently imaged. (B) A gel probed with AF555-labeled antibodies exhibited SNRs<3 after H_2O_2 treatment. (C) A gel probed with AF647-labeled antibodies exhibited SNRs<3 after H_2O_2 treatment. Statistical significance was determined with Mann-Whitney U-tests, where * represents $p<0.001$. Sample size on charts refers to the number of protein bands analyzed from one gel.

Both AF555 and AF647 exhibited a strong quenching response to H_2O_2 exposure. The mean SNR of AF555 protein bands decreased from 11.9 ± 10.8 to 1.07 ± 1.81 after H_2O_2 treatment,

and the mean SNR of AF647 protein bands decreased from 15.9 ± 10.5 to 1.85 ± 1.27. These results demonstrate that the decrease in SNRs was greater in the immunoprobed system than in the system with labeled ovalbumin. A possible explanation for the greater drop in the SNRs of the immunoprobed peaks is that the fluorophores conjugated to the directly labeled ovalbumin are less accessible to H_2O_2 due to the photocapture step. Another important point to note is that the majority of lanes (63/68 for AF555 and 30/35 for AF647) had an SNR<3 after quenching, indicating nearly complete fluorophore quenching. It is possible that the few lanes with SNR>3 after H_2O_2 treatment contained noise in the protein band region that was detected and would be challenging to identify without visual inspection of each lane.

Some areas of future work include (1) evaluating quenching of more gels, as only one gel was evaluated for each condition, (2) further analysis of lanes with SNR>3 after quenching, (3) evaluating sequential quenching and re-probing of gels, (4) applying the quenching method to immunoprobed proteins from electrophoresed single cells, and (5) evaluating protein and/or epitope damage during the quenching protocol to compare to antibody stripping. The last point is especially important to determine whether quenching is advantageous over the standard antibody stripping protocol. Overall, these results suggest that H_2O_2 could be feasibly applied to scIB assays.

2.4 Conclusions

We sought to evaluate fluorophore quenching with H_2O_2 in polyacrylamide hydrogels as a strategy for improved multiplexing in scIB assays. Here, we first evaluated H_2O_2 quenching of six common fluorophores in solution to determine which fluorophores are good candidates for quenching in scIB assays and to determine optimal H_2O_2 concentrations and incubation times. The Alexa Fluor dyes evaluated were all quenched in solution after exposure to a sufficient H_2O_2 concentration for a sufficient time, which depended on the fluorophore. AF555 and AF647 were far more sensitive to H_2O_2 treatment than AF488 with complete quenching observed after a 15 min treatment with 0.5% H_2O_2. In-gel quenching of AF488, AF555, and AF647 was then studied in a system that employed electrophoresed and photocaptured fluorophore labeled ovalbumin. Statistically significant decreases in the SNRs of AF555 and AF647-labeled protein bands was observed in gels that underwent H_2O_2 treatment, while no significant difference was observed in handling control gels. Surprisingly, significant increases in the fluorescence were observed in both the AF488 treatment and handling control gels. We finally evaluated quenching of ovalbumin protein bands that were immunoprobed with antibodies labeled with AF555 and AF647. Again, statistically significant decreases in the SNRs after H_2O_2 treatment were observed with the majority of lanes exhibiting an SNR<3 after treatment, indicating complete fluorophore quenching. Taken as a whole, our initial results represent a promising first step toward H_2O_2 quenching of AF555 and AF647 as an alternative to antibody stripping for multiplexing in scIB assays.

2.5 Bibliography

(1) Goltsev, Y.; Samusik, N.; Kennedy-Darling, J.; Vazquez, G.; Black, S.; Correspondence, G. P. N.; Bhate, S.; Hale, M.; Nolan, G. P. Deep Profiling of Mouse Splenic Architecture with CODEX Multiplexed Imaging In Brief A DNA Barcoding-Based Imaging Technique Uses Multiplexed Tissue Antigen Staining to Enable the Characterization of Cell Types and Dynamics in a Model of Autoimmune Diseas. *Cell* **2018**, *174* (4), 1–14. https://doi.org/10.1016/j.cell.2018.07.010.

(2) Gerdes, M. J.; Sevinsky, C. J.; Sood, A.; Adak, S.; Bello, M. O. Highly Multiplexed Single-Cell Analysis of Formalin- Fi Xed , Paraf Fi n-Embedded Cancer Tissue. *Proc. Natl. Acad. Sci. U. S. A.* **2013**, *110* (29), 11982–11987. https://doi.org/10.1073/pnas.1300136110/-/DCSupplemental.www.pnas.org/cgi/doi/10.1073/pnas.1300136110.

(3) Gierahn, T. M.; Wadsworth, M. H.; Hughes, T. K.; Bryson, B. D.; Butler, A.; Satija, R.; Fortune, S.; Christopher Love, J.; Shalek, A. K. Seq-Well: Portable, Low-Cost Rna Sequencing of Single Cells at High Throughput. *Nat. Methods* **2017**, *14* (4). https://doi.org/10.1038/nmeth.4179.

(4) Kage, D.; Hoffmann, K.; Nifontova, G.; Krivenkov, V.; Sukhanova, A.; Nabiev, I.; Resch-Genger, U. Tempo-Spectral Multiplexing in Flow Cytometry with Lifetime Detection Using QD-Encoded Polymer Beads. *Sci. Rep.* **2020**, *10* (1), 1–11. https://doi.org/10.1038/s41598-019-56938-2.

(5) Stoeckius, M.; Hafemeister, C.; Stephenson, W.; Houck-loomis, B.; Chattopadhyay, P. K.; Swerdlow, H.; Satija, R.; Smibert, P. Large-Scale Simultaneous Measurement of Epitopes and Transcriptomes in Single Cells. *Nat. Methods* **2017**, *14* (9), 865–868. https://doi.org/10.1038/nmeth.4380.Large-scale.

(6) Peterson, V. M.; Zhang, K. X.; Kumar, N.; Wong, J.; Li, L.; Wilson, D. C.; Moore, R.; Mcclanahan, T. K.; Sadekova, S.; Klappenbach, J. A. Multiplexed Quantification of Proteins and Transcripts in Single Cells. *Nat. Biotechnol.* **2017**, *35* (10), 936–939. https://doi.org/10.1038/nbt.3973.

(7) Assarsson, E.; Lundberg, M.; Holmquist, G.; Björkesten, J.; Thorsen, S. B.; Ekman, D.; Eriksson, A.; Dickens, E. R.; Ohlsson, S.; Edfeldt, G.; Andersson, A. C.; Lindstedt, P.; Stenvang, J.; Gullberg, M.; Fredriksson, S. Homogenous 96-Plex PEA Immunoassay Exhibiting High Sensitivity, Specificity, and Excellent Scalability. *PLoS One* **2014**, *9* (4). https://doi.org/10.1371/journal.pone.0095192.

(8) Spitzer, M. H.; Nolan, G. P. Isolation of Mammalian SG Cores for RNA-Seq Analysis. *Cell* **2016**, *165* (4), 780–791. https://doi.org/10.1016/j.cell.2016.04.019.Mass.

(9) Hughes, A. J.; Spelke, D.; Xu, Z.; Kang, C. C.; Schaffer, D.; Herr, A. E. Single-Cell Western Blotting. *Nat. Methods* **2015**, *11* (7), 455–464. https://doi.org/10.1007/978-1-4939-2694-7_46.

(10) Gopal, A.; Herr, A. E. Multiplexed In-Gel Microfluidic Immunoassays: Characterizing Protein Target Loss during Reprobing of Benzophenone-Modified Hydrogels. *Sci. Rep.*

2019, *9* (1), 1–12. https://doi.org/10.1038/s41598-019-51849-8.

(11) Gerdes, M. J. *Patent: US007741045B2*; 2011; Vol. 2.

(12) Tentori, A. M.; Yamauchi, K. A.; Herr, A. E.; John, L.; Dewar, L.; Distinguished, L. Detection of Isoforms Differing by a Single-Charge Unit in Individual Cells. *Angew. Chemie - Int. Ed.* **2017**, *55* (40), 12431–12435. https://doi.org/10.1002/anie.201606039.

(13) Kang, C. C.; Yamauchi, K. A.; Vlassakis, J.; Sinkala, E.; Duncombe, T. A.; Herr, A. E. Single Cell-Resolution Western Blotting. *Nat. Protoc.* **2016**, *11* (8), 1508–1530. https://doi.org/10.1038/nprot.2016.089.

(14) Su, A.; Smith, B. E.; Herr, A. E. In Situ Measurement of Thermodynamic Partitioning in Open Hydrogels. *Anal. Chem.* **2019**, *92* (2), 875–883. https://doi.org/10.1021/acs.analchem.9b03582.

(15) Vlassakis, J.; Yamauchi, K. A.; Herr, A. E. Summit: Automated Analysis of Arrayed Single-Cell Gel Electrophoresis. *SLAS Technol.* **2021**, *26* (6), 637–649. https://doi.org/10.1177/24726303211036869.

(16) Wu, T.; Lin, T.; Zhao, J.; Hidaka, H.; Serpone, N. TiO2-Assisted Photodegradation of Dyes. 9. Photooxidation of a Squarylium Cyanine Dye in Aqueous Dispersions under Visible Light Irradiation. *Environ. Sci. Technol.* **1999**, *33* (9), 1379–1387. https://doi.org/10.1021/es980923i.

(17) Marquez, R.; Flachbartova, Z. A Bright Future for Molecular Probes. *Drug Target Rev.* **2015**, No. 3.

(18) Gebhardt, C.; Lehmann, M.; Reif, M. M.; Zacharias, M. Molecular and Spectroscopic Characterization of Green and Red Cyanine Fluorophores from the Alexa Fluor and AF Series **. *ChemPhysChem* **2021**, *22*, 1566–1583. https://doi.org/10.1002/cphc.202000935.

Chapter 3: In-gel fluorescence detection by DNA polymerase elongation

Reprinted with permission from A.C. Moss and A. E. Herr, *"In-gel fluorescence detection by DNA polymerase elongation"*, APL Bioengineering, 2020. Copyright A.C. Moss and A.E. Herr, 2020.

3.1 Introduction

The advantageous physical, chemical, and optical properties of hydrogels make the substrate material well suited for a range of bioanalyses[1–6]. Such assays often depend on fluorescence for the readout signals, and many rely on fluorescence-based DNA readouts. Fluorescence-based DNA readouts are advantageous because these readouts harness the power of DNA technologies, namely target multiplexing capability and signal amplification, while retaining spatial information and allowing for easy incorporation into existing fluorescence imaging workflows[7–10]. In-situ sequencing is an increasingly popular application of fluorescence-based DNA readouts, which provides a base-by-base readout of a DNA sequence while preserving spatial context[7,9,10].

Recent in-situ sequencing studies have either not been carried out in a hydrogel matrix, in the case of STARmap[10], or signal amplification has been carried out before embedding the tissue in the gel matrix, as is the case in BaristaSeq[9]. A complete in-gel readout will be essential for some in-gel assays, such as single-cell immunoblotting, which involves gel electrophoretic separations of biological molecules prior to target detection[4–6]. Additionally, the in-situ sequencing methods mentioned above have utilized rolling circle amplification (RCA), which involves a ligation and an amplification step prior to fluorescence readout, resulting in a long assay with many steps. A readout with fewer steps and use of one enzyme would be advantageous, resulting in a shorter assay timescale, less complexity, use of less enzymes, and less variability introduced from additional steps. An early approach to in-situ sequencing of polymerase colonies (polonies) formed after in-gel PCR involved only a single in-gel readout step based on polymerase elongation of single-stranded overhangs with labeled nucleotides but lacked signal amplification[7]. A similar readout strategy was applied by Goltsev et al. to DNA oligomers conjugated to antibodies to achieve highly multiplexed immunohistochemical staining of mouse spleen tissue slices, but this was not an in-gel assay and again did not incorporate signal amplification[8]. The potential exists for translating such a readout to in-gel nucleic acid and protein assays for ultrasensitive target detection. However, development and characterization of a completely in-gel assay readout that incorporates signal amplification will be necessary. A comparison of various in-situ sequencing methods can be found in Table 3-1.

Table 3-1: Comparison of in-situ sequencing technologies.

Technology	# enzymes employed	# of steps to readout	In-gel polymerase elongation?	Signal amplification
Polony FISSEQ[7]	1	2	Yes	No
BaristaSeq[9]	2	4	No	Yes
STARmap[10]	2	4	No	Yes

More broadly, thorough characterization of these polymerase elongation processes within hydrogels is lacking. Hydrogels introduce transport limitations, since diffusion is hindered in the porous bulk of the material[11,12]. Size exclusion-based thermodynamic partitioning, which limits the concentration of solute in the gel at equilibrium, is another factor in hydrogel-based assays[13]. Mitra et al. evaluated in situ sequencing of polymerase colonies (polonies) in a 40 μm thick, 8% total acrylamide (8% T) polyacrylamide gel and observed an incomplete reaction after incubation times of up to 6 min[7]. They concluded that the reaction was inefficient but did not characterize the process with regards to reaction kinetics or diffusive transport. Characterizing these aspects of polymerase elongation of DNA within hydrogel matrices would inform assay design.

Also important to the design of the fluorescence readout mechanism is the relationship between fluorescence signal, number of incorporated labeled nucleotides per strand, and spacing between labeled nucleotides. In investigating readout of multiple base repeats, Mitra et al. observed attenuated fluorescence signals,[7] which the authors attributed to self-quenching of the adjacent fluorophores. Relevant to mitigating signal attenuation, increased spacing between labeled nucleotides may be an option, when the sequence of interest is attached to a readout probe. Given that previous studies have scrutinized only a single labeled nucleotide incorporated per DNA strand, incorporation of multiple labeled nucleotides may also form the basis for design of signal amplification strategies[8]. Such an approach would allow for a one-step reaction for integration of signal amplification with the polymerase elongation readout[7,8]. Understanding the impact of DNA sequence design on the fluorescence signal generated by polymerase elongation with labeled nucleotides will ultimately inform assay design to maximize fluorescence signal.

Studies of hydrogel-based assays have modeled the transport of reagents into a gel and the reaction kinetics in the gel to inform assay design parameters such as reaction times and gel thicknesses[11,14–16]. One particularly useful framework is the Damköhler number (Da), which describes the ratio of the characteristic transport time to the characteristic reaction time. Damköhler analysis has provided insight into the contributions of transport and reaction kinetics to the assay timescale and concentration profiles in the gel under different conditions[11,14–16]. Specifically, modeling of the transport and reaction kinetics of in-gel polymerase elongation will provide an understanding of whether the process is limited by the transport of the polymerase into the gel or the polymerase elongation reaction of the immobilized DNA strands.

In this study, we develop design rules for polymerase elongation as a mechanism for fluorescence signal readout and amplification in hydrogel-based assays. To this end, we prepare

polyacrylamide gels with DNA immobilized in the bulk to (i) characterize the effects of the reaction kinetics and transport properties on the in-gel polymerase elongation timescale and (ii) characterize the effects of DNA sequence design on the fluorescence signal. We scrutinize two hypotheses; first, that the timescale of polymerase elongation is limited by polymerase transport and reaction kinetics, versus inherent reaction inefficiency. Second, that the fluorescence signal is modulated by both the number and spacing of incorporated labeled nucleotides per strand, which leads to a tunable approach to signal amplification.

3.2 Materials and Methods

Transport and Reaction Models

For our transport model shown in Fig. 2, the partial differential equation with respect to time and one spatial dimension was solved with the pdpe numerical solver in MATLAB. The z-directional in-gel diffusion profile and Da plots were generated in MATLAB. All values used in the model are tabulated in Table 3-2.

Table 3-2: Table of values used in polymerase transport and reaction modeling.

Symbol	Variable Name	Value
K_c	Proportionality constant for gel diffusivity	0.045 nm[11]
R_h	Hydrodynamic radius of polymerase	3.53 nm[17]
R_f	Polymer fiber radius	0.81-0.88 nm (6-10% T)[18]
ϕ	Gel polymer volume fraction	0.029-0.055 (6-10% T)[18]
k_{on}	Polymerase association rate constant	1.2×10^7 M^{-1} s^{-1} ref: 19
k_{off}	Polymerase dissociation rate constant	0.06 s^{-1} ref: 19
[E]	Polymerase concentration	0.166 µM
D_{soln}	Diffusion coefficient of polymerase in solution	6.26×10^{-11} m^2/s
µ	Viscosity of water at 21ºC (for Stokes-Einstein)	9.74×10^{-4} Pa-S[20]

T	Temperature (for Stokes-Einstein)	21ºC

For estimation of the retarded diffusion parameters, the 10 μM FWHM data were fitted to the mean square displacement diffusion model in MATLAB using the lsqcurvefit function and an effective diffusion coefficient was extracted. A 95% confidence interval for the fitted diffusion coefficient was then obtained with the nlparci function.

Diffusion coefficients from the real-time diffusion experiments were fitted to the PDE diffusion model in MATLAB. Prior to model fitting the images were processed as follows:

1. A 300 pixel ROI of pixel 500-800 of the 1392 pixels in the x-direction was selected
2. Pixels above the intensity threshold were identified, zeroed out, and eliminated
    a. The purpose was to eliminate all pixels that contained the free solution in the well and determine the y = 0 point at the well-gel interface
    b. Intensity threshold was detrmined by taking the average intensity of a row of pixels in the well with protein solution and multiplying by the estimated partition coefficient of the polymerase to estimate the fluorescence intensity at the well-gel interface
3. The intensity values of all pixels in each ROI were summed to create a 1-D vector in the y-direction of the intensity values for each time point
4. Background subtraction: for each nonzero time point, the intensity values of the corresponding summed pixels from the t = 0 image were subtracted
5. Normalization: the fluorescence intensity values of each timepoint vector were normalized to the to the max intensity value in each vector

The normalized, background subtracted fluorescence data were then fitted to the PDE model with the least squares fitting function *lsqcurvefit* in conjunction with the PDEPE solver in MATLAB to obtain a diffusion coefficient. A guess value of the diffusion coefficient for the model was selected as 3.4×10^{-7} cm^2/s based on previous model predictions for the polymerase using literature values of the hydrodynamic radius. Goodness of fit was evaluated with an R^2 - like metric that was calculated by dividing the sum of the squared residuals output of the least squares fitting functions by the sum of the total squares. MATLAB code is included in Appendix B.

Chemical Reagents

All DNA oligomers were purchased from IDT (Coralville, IA, USA), including oligomers with 5' acrydite groups for incorporation into the gel matrix (see Table 3-3 for all DNA sequences). dATP (R0141), dGTP (R0161), and dCTP (R0151) were purchased as 100 mM stock solutions from Thermo Fisher Scientific (Waltham, MA, USA). Alexa Fluor aha dUTP (A32763), AlexaFluor 488 microscale protein labeling kit (A30006), SYBR Gold nucleic acid stain (S11494), SYBR Green I nucleic acid stain (S7563), and Triton X-100 (BP-151) were also purchased from Thermo Fisher. Tetramethylethylenediamine (TEMED, T9281), ammonium persulfate (APS, A3678), 3-(trimethoxylsilyl)propyl methacrylate (440159),

dichlorodimethylsilane (440272), and 30%T/3.3%C acrylamide/bis-acrylamide (29:1) (A3574) were purchased from Sigma-Aldrich (St. Louis, MO, USA). N-[3-[(3-Benzoylphenyl)formamido]propyl] methacrylamide (BPMAC) was custom synthesized by Pharm-Agra Laboratories (Brevard, NC, USA). Deionized water (18.2 MΩ) was obtained using an Ultrapure water system from Millipore. TE and TBE buffers were prepared according to standard protocols[21].

Table 3-3: DNA sequences evaluated with the adenine bases, which serve as incorporation sites for AF 647-labeled dUTP, underlined and spacing between labeled nucleotide incorporation sites described. All oligos were synthesized by IDT.

Sequence (5'—3')	# Labeled NT Incorporation Sites	Spacing	Figures Included	Notes
acrydite—TCGCTGATACTTGAATCC	N/A	N/A	All figures	Immobilized in the gel via acrydite
CCTCTATCTCTTCGGATTCAAGTATCAGCGA	1	N/A	Fig. 3-3, Fig. 3-4, and Fig. 3-6	Strand used for all kinetics and transport-related experiments
AF 647—CCTCTATCTCTTCGGATTCAAGTATCAGCGA	1	N/A	Fig. 3-3B	Positive control strand with fluorophore
TCCCTCCCTCCCTCCCTCCCAGGATTCAAGTATCAGCGA	1	N/A	Fig. 3-7A and Fig. 3-7B	
TCCCTCCCTCCCTCCCACCCAGGATTCAAGTATCAGCGA	2	3	Fig. 3-7A, Fig. 3-7B, Fig. 3-7C, and Fig. 3-7D	
TCCCTCCCTCCCACCCACCCAGGATTCAAGTATCAGCGA	3	3	Fig. 3-7A	
TCCCTCCCACCCACCCACCCAGGATTCAAGTATCAGCGA	4	3	Fig. 3-7A	
TCCCACCCACCCACCCACCCAGGATTCAAGTATCAGCGA	5	3	Fig. 3-7F	
TCCCTCCCTCCCACCCTCCCAGGATTCAAGTATCAGCGA	2	7	Fig. 3-7B, Fig. 3-7C, and Fig. 3-	

			7D	
TCCCTCCCACCCTCCCTCCCAGGATTCAAGTATCAGCGA	2	11	Fig. 3-7B, Fig. 3-7C, and Fig. 3-7D	
TCCCACCCTCCCTCCCTCCCAGGATTCAAGTATCAGCGA	2	15	Fig. 3-7B, Fig. 3-7C, and Fig. 3-7D	
AGGGTGGGTGGGTGGATTCAAGTATCAGCGA	1	N/A	Fig. 3-7E	Incorporation site for labeled nucleotide at the end of the strand

In-Solution Polymerase Experiments

DNA oligomers with complementary regions were mixed in a 1:1 ratio from 100 µM stock solutions prepared in 1xTE buffer and concentrated NaCl solution added to reach a final concentration of 0.32 M NaCl. The mixture was then incubated for 20 min at 42ºC for hybridization to occur. Hybridized DNA was mixed with polymerase elongation solution to a final DNA concentration of 10 µM in a total volume of 20 µL and incubated for the specified times for the polymerase elongation reaction. Polymerase elongation solution consisted of 50 µM each of dATP, dGTP, dCTP, Alexa Fluor 647 aha dUTP, and 0.125 U/µL (unless otherwise specified) of Klenow (exo-) polymerase (NEB, Ipswich, MA, USA; M0212) in 10 mM Tris with 150 mM NaCl, 10 mM $MgCl_2$, and 0.1% Triton X-100. After the polymerase elongation step, 0.2 µg of each reaction was extracted, diluted to 15 µL in 1xTBE buffer, mixed 1:1 with 2x RNA loading dye (NEB; B0363S), and heated at 70ºC for 10 min to inactivate the polymerase and denature the DNA. The samples were cooled and 20 µL of sample loaded into each lane of a 15% TBE-Urea gel (Thermo Fisher Scientific). Gels were run at 200 V in 1xTBE buffer until the bromophenol blue band from the loading dye reached the bottom of the gel, ~50 min. The run was then stopped and the gels stained in 1xSYBR Gold for 30 min. Gels were imaged for SYBR Gold and Alexa Fluor 647 on an epifluorescence microscope (Olympus IX51 inverted fluorescence microscope equipped with a Photometrics CoolSNAP HQ2 CCD camera, ASI motorized stage, and a Lumen Dynamics X-Cite shuttered mercury lamp light source, controlled by MetaMorph software by Molecular Devices) with a 2x objective (PlanApo by Olympus, N.A. = 0.08) using a 100 ms exposure time. Images were inverted in FIJI (ImageJ) software and regions-of-interest (ROIs) drawn around the bands to evaluate the fluorescence intensity. Background subtraction consisted of subtracting the fluorescence intensity of an ROI the same size as the band that was placed in a blank section of the lane.

Gel Fabrication

Polyacrylamide gels were fabricated on silicon wafer substrates with 40 μm rails patterned in SU-8, as previously reported[4]. Gel precursor solutions containing acrylamide/bis-acrylamide stock solution (30%, 29:1) were prepared to a concentration of 8% T, 3.3% C. BPMAC was added to a concentration of 3 mM and DNA with a 5' acrydite group added to a concentration of 10 μM, unless otherwise specified (Fig. 3B), before degassing via sonication for 5 min. APS and TEMED were then added to the precursor to a concentration of 0.08% each before pipetting the solution between the SU-8 wafer (rendered hydrophobic by treatment with dichlorodimethylsilane) and a placing glass microscope slide functionalized with 3-(trimethoxylsilyl)propyl methacrylate on top. After a 15-minute chemical polymerization, the slides with the attached gels were lifted from the wafers and washed in 1xTBE buffer for at least 1 h.

In-Gel Polymerase Elongation Experiments

Gels were fluidically addressed in a microarray cassette (1 x 16 hybridization cassette, Arrayit, Sunnyvale, CA, USA). In order to create a single-stranded overhang for polymerase elongation, solutions of DNA with complementary regions to the DNA immobilized in the gel were prepared to a concentration of 10 μM in 0.32 M NaCl in 1xTE buffer and 100 μL pipetted into each region of the microarray cassette. The hybridization reaction was carried out at 21ºC for 2 h and followed by aspirating off the DNA solution and washing twice with 100 μL of 1xTBE buffer. Polymerase elongation solution (see composition above) was then added (60 μL per region of the microarray cassette) and the reaction run at 21ºC for the specified times. The volume of reaction solution added to each gel region was over an order of magnitude greater than the gel volume to promote constant source diffusion of the reagents into the gel. After the elongation reaction, each region was briefly washed twice with 100 μL of 1xTBE buffer before removing the gel from the cassette and washing for 30 min in a bath of wash buffer (10 mM Tris with 650 mM NaCl, 10 mM $MgCl_2$, and 0.1% Triton X-100). Gels were then rinsed in DI water and dehydrated under a N_2 stream for imaging.

Confocal Microscopy

Following established methods from a previous study, confocal images were acquired on a Carl Zeiss LSM 710 AxioObserver inverted laser scanning confocal microscope using a C-Apochromat 40×/1.1 NA water-immersion objective with correction collar[13]. The 633 nm line of a helium−neon laser was used to excite Alexa Fluor 647 and to perform reflected light confocal microscopy of the coverslip−sample interface to find the optimal correction collar setting. Fluorescence was imaged using a 488/561/633 nm dichroic filter and a pinhole set to 1.0 Airy units. Reflected light confocal images were acquired using a T80/R20 partial mirror over a 212.55 μm × 212.55 μm field of view with 0.71 μm × 0.71 μm × 0.10 μm cubic voxels. The correction collar position was chosen using our previously established method[13].

Imaging and Data Processing

Imaging of the dehydrated gels was conducted using a GenePix 4300A microarray scanner equipped with a 635-nm laser. Imaging settings of 250 PMT gain and 100% power were chosen, optimized for maximum dynamic range without achieving saturation. Images were analyzed in FIJI (ImageJ) software. ROIs of 500 x 500 pixels were drawn in the center of the gel regions created by the microarray cassette and the integrated fluorescence (AUC) evaluated. All fluorescence values were background subtracted by subtracting the AUC of a blank gel ROI of the same size.

Direct Measurement of In-Gel Protein Diffusion

The 1 mm thick gels for real-time diffusion experiments were fabricated on methacrylate-functionalized glass slides with the same composition as in all other experiments (8% T, 3.3% C, 3 mM BPMA). ssDNA and dsDNA precursors were prepared with the 5'-acrydite single-stranded DNA at a concentration of 1 µM, while the noDNA precursors did not include DNA. Following a previously developed gel fabrication protocol from our group[22], gels were fabricated on a flat glass plate with 1 mm spacers (C.B.S Scientific Gel Wrap) in place of a silicon wafer mold using 1 mL of gel precursor per 25 x 75 mm slide. Wells were formed by punching the gel with a 4 mm biopsy punch and removing the gel plugs with tweezers. The dsDNA condition consisted of single-stranded overhangs that were formed by placing gels in a bath of a strand with a complementary region plus an overhang at a concentration of 1 µM for 24 hours and washing overnight. Gels were then patted against a Kimwipe to remove excess fluid from the surface, and the Kimwipe was rolled up to dab fluid from the inside of each punched well prior to introducing the polymerase soltuion. Twelve microliters of AF 488 labeled polymerase solution at a concentration of 0.165 µM, the same concentration as in the polymerase elongation experiments, was then pipetted into each well. Thirty minute timelapse images with 5 minute image acquisition increments and an exposure time of 500 ms were acquired on an Olympus IX-51 with an Olympus PlanApo 2x objective (N.A. 0.08).

3.3 Results and Discussion

In-Gel Polymerase Elongation Model Suggests a Transport-Limited Process

Our model system consists of a polyacrylamide gel copolymerized with 5' acrydite-terminated DNA oligomers. Single-stranded overhangs are generated by hybridizing a longer strand to the immobilized DNA. Polymerase elongation solution that contains Klenow (exo-) polymerase and Alexa Fluor 647-labeled dUTP is then introduced to the top of the gel, allowing the reagents to diffuse into the gel in the z-direction and elongate the single-stranded overhangs. We assume that the process will not be limited by diffusion of the dNTPs due to their small size[23] and that depletion zones will not form due to the large excess of fluid volume above each gel region. Therefore, the two primary factors governing this process are the polymerase transport into the gel and the polymerase reaction kinetics, as illustrated in Fig. 3-1. In considering both polymerase transport into the gel matrix and polymerase reaction kinetics, we used a Damköhler number (Da) to delineate transport and reaction limited regimes for the system. The Da is the ratio of the characteristic transport time to the characteristic reaction time, such that $Da>>1$ indicates a transport limited process, while $Da<<1$ indicates a reaction limited process[14].

Previous studies have utilized Da analysis as an assay design framework to achieve maximized, uniform fluorescence signal and minimized assay time[15,16]. Da>>1 in our system represents a case where the polymerase is diffusing into the gel much slower than the immobilized DNA is elongated, while Da<<1 indicates that the polymerase is diffusing throughout the depth of the gel at a much higher rate than the elongation reaction is occurring. Understanding the regime in which the in-gel polymerase elongation process operates will inform optimization of assay design parameters, including the incubation time and gel thickness, for a complete and uniform reaction throughout the depth of the gel.

In our model, polymerase transport in the gel was represented with Fickian diffusion in one dimension (Eqn. 3-1) and a modified Stokes-Einstein diffusivity with a correction that accounts for hindered diffusion within the gel matrix (Eqn. 3-2)[11,12,17,18,20]. A characteristic transport time can then be calculated with Eqn. 3-3.

$$\frac{\partial C}{\partial t} = D_{gel}\frac{\partial^2 C}{\partial z^2} \quad \text{(Equation 3-1)}$$

$$D_{gel} = D_{soln}e^{-K_c R_h \varphi^{0.75}} \quad \text{(Equation 3-2)}$$

$$\tau_{transport} = \frac{h^2}{2D_{gel}} \quad \text{(Equation 3-3)}$$

where C is the concentration of the polymerase (M), D_{gel} is the diffusion coefficient in the gel (m^2/s), D_{soln} is the diffusion coefficient in the solution calculated with the Stokes-Einstein equation (m^2/s), K_c is a proportionality constant (m), R_h is the hydrodynamic radius of the species diffusing (m), φ is the polymer volume fraction of the gel (dimensionless), and h is the gel height (m). All values included in the models are tabulated in Table 3-2. Constant source diffusion in the z-direction was assumed with a zero-flux boundary at the gel-glass interface.

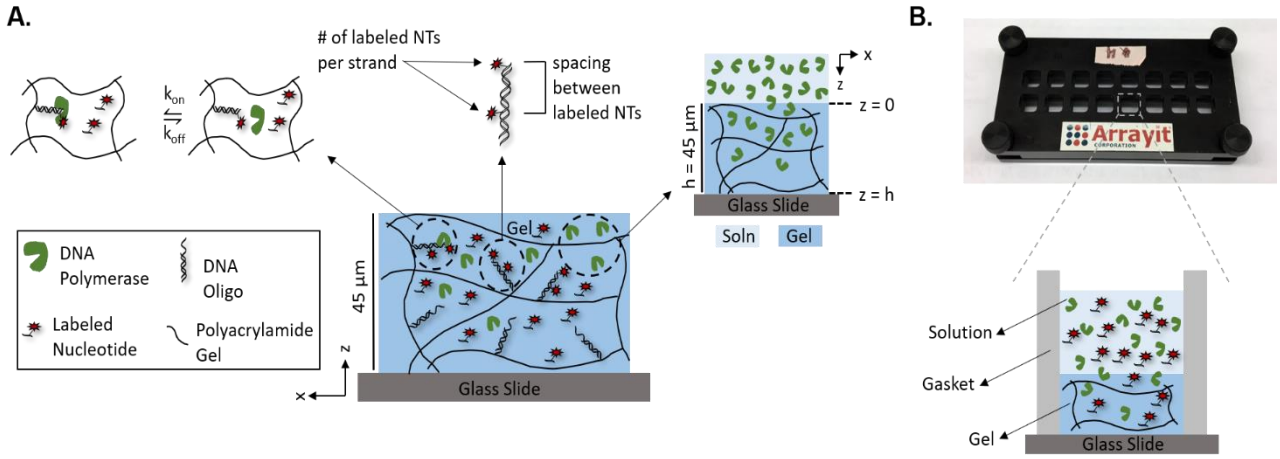

Figure 3-1: Polymerase reaction kinetics, DNA sequence design, and polymerase transport in the gel are the primary factors hypothesized to impact fluorescence signal resulting from polymerase elongation in hydrogels. (A) We hypothesize (1) that the process is transport limited, and (2) that signal amplification can be achieved by strategic DNA sequence design. The rate limiting step of the polymerase elongation reaction (schematic on the left) is the detachment of the polymerase from an elongated strand of DNA, which gives a characteristic time of 1.0 s.

The characteristic transport time for the polymerase (R_h = 3.5 nm) through a 45 µm thick gel (schematic on the right) is 74 s, assuming a modified Stokes-Einstein diffusion coefficient that takes into account hindered diffusion in the gel pores, suggesting a transport limited process. DNA sequence designs that increase the number of labeled nucleotides incorporated per strand and the spacing between labeled nucleotides (schematic in center) are hypothesized to increase the fluorescence signal. (B) The device consists of a gel bonded to a glass slide and mounted in a microarray cassette. Gel regions are separated by a gasket. Reagent solutions are applied to the top of each gel region and diffuse into the gel.

We also constructed a model (Eqn. 3-4) for the polymerase reaction kinetics based on the literature[19], which suggests that the rate-limiting step for Klenow (exo-) polymerase is the detachment of the polymerase from the elongated DNA strand (Fig. 3-1). A resulting characteristic reaction time based on this model can then be calculated with Eqn. 3-5. For the calculation of characteristic reaction time, the in-gel enzyme concentration was estimated based on the Ogston model of size-exclusion based thermodynamic partitioning, which yielded a partition coefficient of 0.46 for Klenow (exo-) polymerase in an 8% T gel[13].

$$DE \underset{k_{off}}{\overset{k_{on}}{\rightleftharpoons}} D + E \quad \text{(Equation 3-4)}$$

$$\tau_{rxn} = \frac{1}{k_{off} + K[E]k_{on}} \quad \text{(Equation 3-5)}$$

where D is the concentration of elongated DNA strand immobilized in the gel (M), E is the concentration of the polymerase enzyme (M), K is the partition coefficient (dimensionless), k_{on} ($M^{-1}s^{-1}$) is the kinetic rate constant of binding, and k_{off} (s^{-1}) is the kinetic rate constant of dissociation of the polymerase from the elongated strand.

These models predict a characteristic transport time of 74 s and a characteristic reaction time of 1.0 s in our system, which consists of a 3.5 nm (68 kDa) Klenow (exo-) polymerase diffusing through a 45 µm thick 8% T gel. The resulting value of Da is ~70, which indicates that the system is transport limited. For comparison, the resulting value of Da for the dNTPs is ~3, which suggests a transport timescale on the same order of magnitude as the reaction timescale. The Da regime estimate suggests polymerase transport is the limiting factor. Given the expected transport limited regime of this system, we estimated that diffusion of the polymerase throughout the depth of the gel (in the z-direction) occurs within 5 min (Fig. 3-2A). More broadly speaking, Da analysis indicates that the process is largely transport limited even in solution, indicating that the process is transport limited across different gel densities with Da scaling with the square of the gel thickness (Fig. 3-2B).

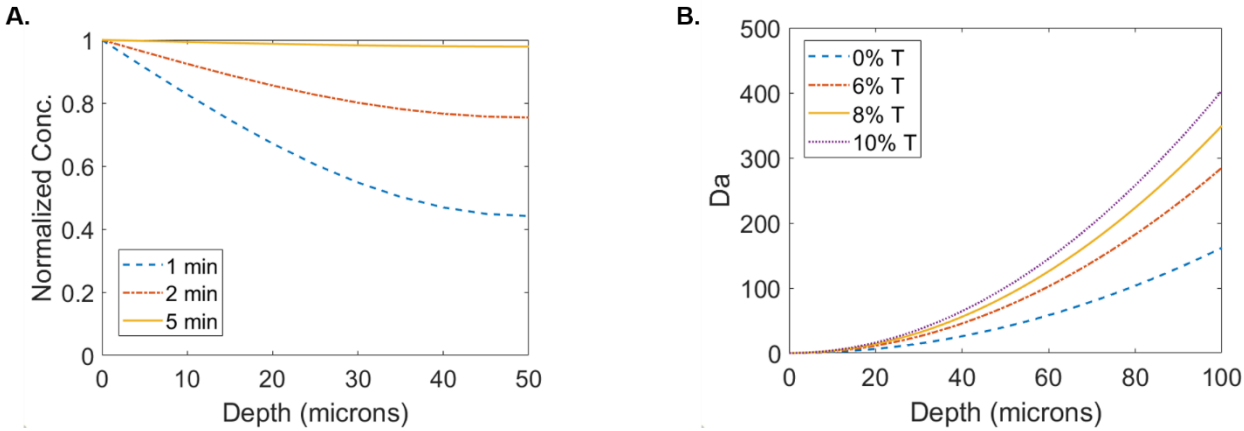

Figure 3-2: Models of in-gel polymerase diffusion and reaction indicate that the process is transport limited across conditions. (A) Transient 1D model of constant source diffusion of Klenow (exo-) DNA polymerase indicates that a uniform concentration profile in the z-direction is reached after about 5 min, (B) The diffusion and polymerase elongation reaction models predict Da>1 across a wide range of gel thicknesses and all gel densities, including free solution (0% T), which suggests that the process is transport limited across the vast majority of conditions.

In-gel Polymerase Elongation Kinetics are Slower than Predicted by Reaction and Transport Limitations

Next, we measured the timescale of in-gel polymerase elongation. First, we sought to evaluate the background signal attributable to retention of fluorescently labeled nucleotides within the gel during the polymerase elongation process. As retention of fluorescent probes is a direct contributor to in-gel assay background and noise, it is important to understand how much additional background in the gel arises due to the introduction of fluorescently labeled nucleotides[13,14]. Fluorescence signal was evaluated by exposing regions of gel that contained immobilized DNA to a polymerase elongation solution that contained Klenow (exo-) polymerase and dNTPs (including AF 647-labeled dUTP substituted for dTTP). Background signal arising from retention of labeled nucleotides was estimated using negative controls that contained the labeled nucleotides but omitted either the polymerase or the immobilized DNA. The negative controls exhibited fluorescence signal that was three orders of magnitude lower than the full reaction condition, indicating minimal background from retained fluorescently labeled nucleotides (Fig. 3-3A). Strong fluorescence signal and minimal background suggest that polymerase elongation with fluorescently labeled nucleotides is an effective strategy for DNA readout in polyacrylamide gels.

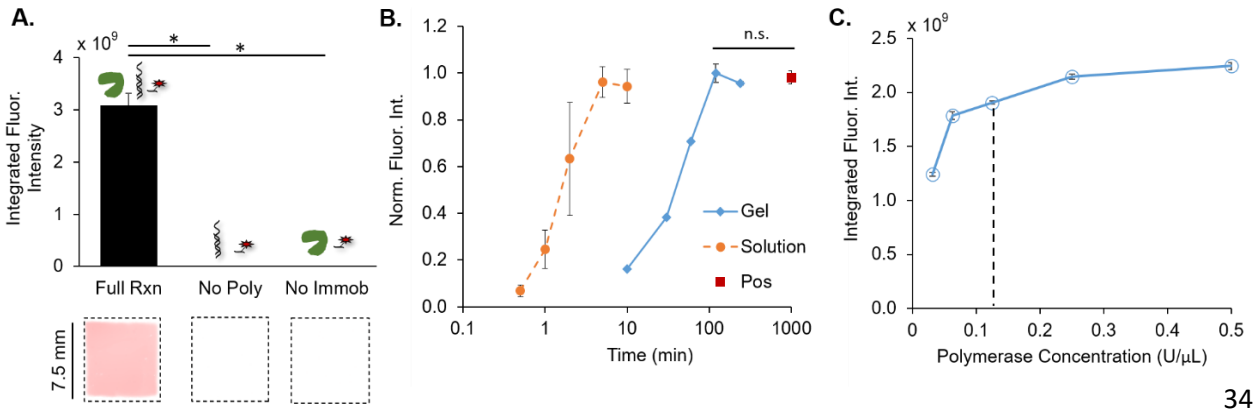

Figure 3-3: In-gel polymerase elongation generates strong signal with minimal background and reaches completion after a 2 h incubation at room temperature. (A) Integrated fluorescence intensity and corresponding micrographs from the complete in-gel reaction demonstrate strong fluorescence signal, while minimal fluorescence was observed in the negative controls that omitted polymerase (No Poly) or immobilized DNA (No Immob) (n=5), (B) normalized integrated fluorescence intensity of gels exposed to polymerase elongation solution demonstrates complete elongation after 2 h, as indicated by a positive control of a hybridized labeled complementary strand (Pos), while completion is achieved in ≤5 min in solution (n=3, normalization to max intensity of each condition), (C) in-gel experiments with an increased concentration of polymerase above the 0.125 U/μL used in most experiments (indicated by the dotted line) resulted in minimal increase in fluorescence for a 30 minute incubation (n=3). Statistical significance was determined by pairwise Mann-Whitney U-tests, * $p<0.05$, standard deviation error bars shown.

Second, we evaluated how the kinetics of the in-gel polymerase elongation process differs from in-solution kinetics. A previous study evaluated polymerase reaction kinetics on a surface with immobilized DNA, another assay format that employs immobilized DNA, and found that the polymerase reaction kinetics were comparable to in solution[24]. Additionally, the literature suggests that hydrogels are advantageous environments for reactions—as compared to on surfaces—due to a larger number of possible accessible molecular orientations[25,26]. Therefore, we predict that the in-gel polymerase reaction kinetics will occur at the same rate as in solution. The hypothesis of comparable in-gel reaction kinetics is supported by in-gel PCR studies that employed standard PCR protocols without any need for increasing the times of the elongation steps[27,28]. However, as compared to this study, the previous in-gel PCR studies saw all reagents diffused into the gel (rather than immobilized), higher temperatures employed, and use of different polymerases. In the most direct comparison to our study, where immobilized DNA was isothermally elongated with fluorescently labeled nucleotides in a 40 μm thick 8% T gel, Mitra et al. found that the reaction was not complete within the expected time scale of <6 min[7]. They attributed the incomplete reaction to inefficient incorporation of the nucleotides but did not run the reaction to completion. Our transport model indicates that the time necessary for diffusion of the polymerase into the gel is on the same order of magnitude as even the longest reaction times employed by Mitra et al. Thus, we hypothesize that the reaction was not run to completion due to the transport limitations in the gel. As the polymerase is often at a low concentration in PCR and thus the rate-limiting species, increasing the polymerase concentration has been shown to result in a linear increase in the fluorescence for a given time point[29]. Therefore, modulating the polymerase concentration will allow us to evaluate whether reaction limitations are dominant in the system.

While polymerase elongation in solution reached completion after 5 min, the fluorescence signal of the in-gel reaction increased for room-temperature incubation times up to 2 h, at which point the fluorescence plateaued (Fig. 3-3B). No statistically significant differences (Mann-Whitney U-tests, $p>>0.05$) in the normalized fluorescence intensity were observed between the 2 h timepoint (1.0 ± 0.03 relative fluorescence units (RFU)), the 4 h timepoint (0.96 ± 0.03 RFU), and the positive control (0.98 ± 0.03 RFU), in which a fluorescently labeled complementary strand was hybridized to the immobilized DNA in the gel. Comparable signal between the

fluorescence plateau values and the positive control indicate that all of the immobilized DNA in the gel is elongated by the polymerase after long incubation times. The observed discrepancy between in-gel and in-solution kinetics could be attributed to either reaction limitations or transport limitations resulting from diffusion of the polymerase. To evaluate whether reaction limitations are dominant, we varied the concentration of the polymerase, the rate-limiting species. Increasing the concentration of the polymerase from 0.125 U/μL to 0.5 U/μL resulted in an 18% increase in the fluorescence signal after a 30-min incubation at room temperature (Fig. 3-3C). The resultant 18% increase in fluorescence from quadrupling the polymerase concentration is minimal compared to the expected linear relationship between polymerase concentration and reaction progress based on the literature[29]. Taken together, the results presented here indicate that the reaction is efficient, as all immobilized DNA in the gel is elongated upon reaction completion, and that the discrepancy between the in-gel and in-solution kinetics is likely not due to reaction limitations. Therefore, we posit that transport limitations are responsible for the discrepancy between the in-gel and in-solution kinetics of the polymerase elongation process.

Confocal Microscopy Reveals a Nonuniform Fluorescence Profile Throughout the Depth of the Gel

To investigate the hypothesis of transport limitations contributing to the slow in-gel polymerase elongation process, we sought to measure the post-reaction fluorescence profiles throughout the depth of the gels. A high Da indicates that diffusion is occurring slower than the reaction can take place, which results in a nonuniform profile throughout a gel[16]. Based on Da analysis of our system and the result of minimal signal increase from increasing the polymerase concentration, we hypothesize that we will observe increased fluorescence penetration into the gel with increased incubation time. Confocal microscopy with reflection images of the glass coverslip and glass slide to delineate the gel bounds allowed us to observe how deep the fluorescence penetrated into the gel at different time points (Fig. 3-4A). Fluorescence that reaches from the glass coverslip on top of the gel to the glass slide on the bottom was observed in the 4 h time point**,** while fluorescence was observed through less than a quarter of the gel in the 10 min time point. While there was a substantial difference in the fluorescence penetration, the maximum fluorescence intensity in the brightest portions of the gel is similar in both the 10 min and 4 h time points at 2.51 ± 0.16 and $2.54 \pm 0.06 \times 10^4$ arbitrary fluorescence units (AFU), respectively ($n = 3$). This result is consistent with transport limitations rather than reaction limitations. In the case of a reaction limited system with a low value of Da, we would have expected to see an increase in the maximum fluorescence intensity rather than the fluorescence penetration, since diffusion of the polymerase would be occurring at a much faster rate than the reaction. While the theoretical analysis indicated a transport limited process, the extent of this limitation turned out to be much greater than predicted. Our diffusion model predicted that the polymerase would diffuse through the thickness of the gel within 5 min, which is much less than the 2-4 hours necessary for complete fluorescence penetration. This discrepancy suggests additional contributing factors, such as retarded diffusion. Retarded diffusion is a phenomenon that has been observed when DNA oligomers are hybridized to single-stranded DNA immobilized in a gel and occurs as a result of interactions between the DNA strands that hinders the diffusion through the thickness of the gel[30]. The amount of retardation is proportional to the concentration of immobilized DNA in the gel and the affinity between the interacting species, and the resulting

rate of diffusion can be orders of magnitude slower than simple diffusion[30]. While retarded diffusion of enzymes in this manner has not been previously described, polymerase binding of a DNA template occurs with similar high affinity to that of DNA hybridization[19]. Thus, it is possible that an analogous mechanism of retarded diffusion of the polymerase is resulting in the slow in-gel elongation kinetics that we have observed.

To further evaluate our hypothesis of retarded diffusion, in-gel polymerase elongation was evaluated with different concentrations of immobilized DNA, as the characteristic diffusion time in retarded diffusion is proportional to the concentration of immobilized DNA. Polyacrylamide gels with 1 µM and 5 µM immobilized DNA were evaluated, in addition to the gels with 10 µM immobilized DNA that were evaluated in all other experiments. We hypothesized that the time for complete fluorescence penetration throughout the depth of the gel would be dependent on the concentration of immobilized DNA in the gel. Fluorescence intensity profiles in the z-direction were again measured by confocal microscopy with the length in the z-direction that exhibited >50% of the max fluorescence intensity (FWHM) designated as a quantitative metric for the depth of fluorescence penetration in the gel. The results suggest that complete polymerase elongation throughout the depth of the gel, indicated by a plateau FWHM value of ~65-70 µm, was achieved in under 30 min for 1 µM immobilized DNA, 1 h for 5 µM immobilized DNA, and under 4 h for 10 µM immobilized DNA (Fig. 3-4B). Plateau times were determined by a Kruskal-Wallis test, which resulted in $p>0.05$ when the 30 min, 1 h, and 2 h time points were grouped together for the 1 µM condition, and when the 1 h, 2 h, and 4 h time points were grouped together for the 5 µM condition. These reaction completion times suggest that the time for completion of in-gel polymerase elongation is proportional to the concentration of immobilized DNA, which is consistent with our hypothesis of retarded diffusion. Further support for the retarded diffusion hypothesis was obtained by fitting a 1D diffusion model based on mean square displacement (Eqn. 3-6) to the FWHM data from the 10 µM immobilized DNA condition. There is a literature precedent for this type of fitting strategy, where the position of the diffusion front was represented by the distance corresponding to half the maximum signal and fitted to a mean square displacement model[31]. Only the 10 µM data were fitted due to the lack of data points for a complete curve in the other conditions. The model was a good fit ($R^2 = 0.948$), with a fitted effective diffusion coefficient of 0.172±0.06 µm/s (Fig. 3-4C, 95% C.I.). When compared to the predicted in-gel diffusion coefficient for simple diffusion, the fitted effective diffusion coefficient was 80-fold smaller. In retarded diffusion, the effective diffusion coefficient can be related to the simple diffusion coefficient by the retardation coefficient K (Eqn. 3-7), where K is the product of the association constant of the interacting species (equivalent to k_{on}/k_{off}) and m, the concentration of immobilized DNA (Eqn. 3-8)[30].

$$z = \sqrt{2D_{eff}t} \quad \text{(Equation 3-6)}$$

$$D_{eff} = \frac{D_{gel}}{K} \quad \text{(Equation 3-7)}$$

$$K = \frac{k_{on}}{k_{off}} m \quad \text{(Equation 3-8)}$$

Based on the retarded diffusion equations and the model fit, the retardation coefficient for our system is K = 80. Estimation of K based on the association constant from literature[19] yields a value of K = 2000, which is higher than our estimated value. This discrepancy could be

explained by the difference between DNA hybridization, which the retarded diffusion model is based on, and polymerase elongation. Polymerase elongation is a more complex process that involves association, extension of the DNA strand, and dissociation. Therefore, it is likely that modifications to the retarded diffusion model are necessary and a topic for future investigation. Overall, the dependence of the fluorescence penetration depth on the DNA concentration and the good fit to a diffusion model support a retarded diffusion-type mechanism.

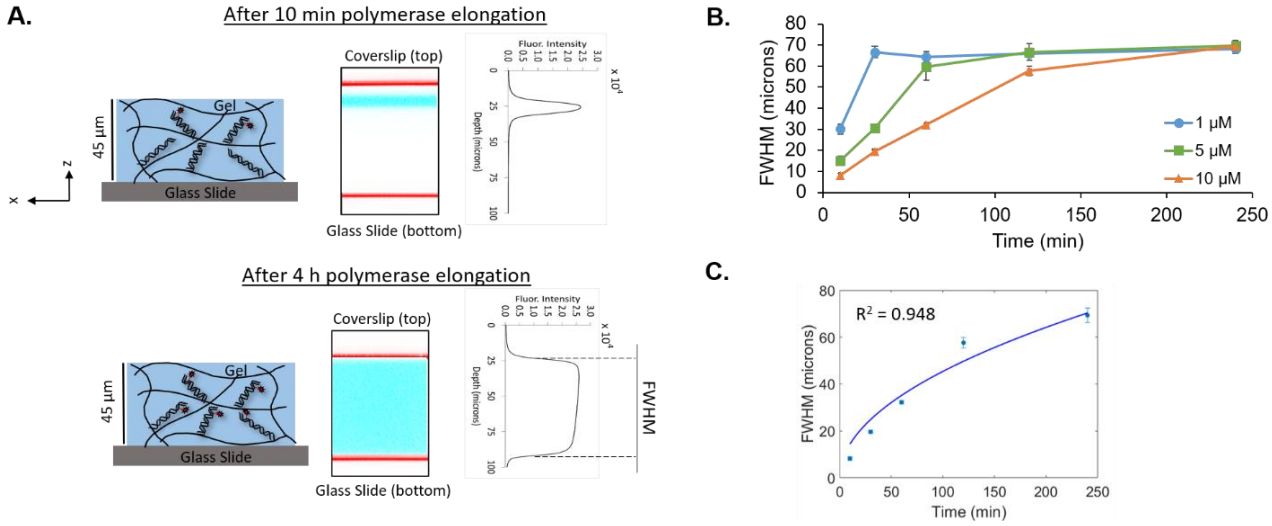

Figure 3-4: Confocal analysis suggests that the in-gel polymerase elongation process is transport limited and supports retarded diffusion. (A) Fluorescence micrographs demonstrate increased fluorescence penetration after a 4 h incubation with the polymerase elongation solution (polymerase + labeled dUTP, washed before imaging) than after a 10 minute incubation, with similar maximum fluorescence intensity values in the brightest portions of the gel (red = glass, blue = gel fluorescence, white space between coverslip and gel at 10 min due to a fluid layer). (B) Line plots of the full width at half maximum (FWHM) fluorescence within the gels for various concentrations of immobilized DNA indicates that the time for complete fluorescence penetration throughout the gel is proportional to the concentration of immobilized DNA (n=3, standard deviation error bars). (C) A good fit (R^2 = 0.948) was obtained when the FWHM data for the 10 µM immobilized DNA condition were fitted to a mean square displacement (MSD) function, yielding an effective diffusion coefficient of 0.172±0.06 µm/s (95% C.I.).

While our study specifically focused on thin, dense gels with immobilized DNA concentrations of ≥1 µM, these findings likely apply to many other hydrogel-based systems, such as gel cleared tissue. Gel-cleared tissue studies employ gels that are less dense than the gels used in our study but are often 1-2 orders of magnitude thicker[1]. Additionally, specific intracellularly expressed proteins are often immobilized in hydrogels at concentrations on the order of 0.1-1.0 µM[4], the upper end of which, after binding with DNA-labeled antibodies, would be close to what was investigated in our study. Since our Damköhler analysis indicates that even less dense gels are highly transport limited (Fig. 3-2), the slow transport phenomenon described here could be observed in a 1-mm thick 4% T gel with 0.5 µM of a specific protein, a realistic scenario for gel-cleared tissue. The broader implication is that an understanding of slow transport through thick

matrices containing immobilized species will inform assay design parameters including concentrations, timescales, and methods of introducing reagents. Our findings suggest that an understanding of the local in-gel concentrations of an immobilized species could be important, as variable local concentration in a gel has the potential to introduce spatial non-uniformity, particularly in the z-direction. Therefore, running the reaction to completion will be essential to ensure spatial uniformity. As the slow transport of the polymerase results in a slow, cumbersome assay, in-gel polymerase elongation could benefit from the development of strategies that reduce the assay time. While employing smaller engineered polymerases would ameliorate the slow transport to some extent, such an approach would be fundamentally limited because retarded diffusion has a larger dependance on the affinity-based interactions than on the hydrodynamic radius of the enzyme. Alternative approaches, such as the method implemented by Mitra et al. where the polymerase was incorporated in a denser gel precursor that was poured on top of the primary gel and polymerized before adding other reaction components[7], hold promise. Building on the results presented in our study has the potential to further advance strategies that improve transport in hydrogel matrices. These results also suggest that slower than expected transport may occur in other hydrogel systems that involve reactions and/or affinity-based interactions. In conclusion, further study will be necessary to understand these transport phenomena in hydrogels and develop assay design rules for applications that rely on thick gels, dense gels, and gels with high concentrations of immobilized DNA.

Direct Measurements of Protein Diffusion Coefficients in Polyacrylamide Gels

One of the limitations of our previous measurements is that the distribution of the polymerase elongation reaction products was measured as a proxy for the polymerase diffusion, rather than direct polymerase diffusion measurements. Here, we sought to develop an experimental setup to measure real-time diffusion of DNA polymerase in polyacrylamide gels with the ultimate goal of measuring retarded diffusion phenomena. Our system employed 1 mm thick polyacrylamide gels (8% T) with 4 mm diameter wells that were filled with AF488-labeled Klenow exo- polymerase, and the diffusion was monitored by timelapse epifluorescence imaging (Fig. 3-5). Diffusion of the labeled polymerase from the microwell into the surrounding gel was clearly visible by imaging (Fig. 3-5C).

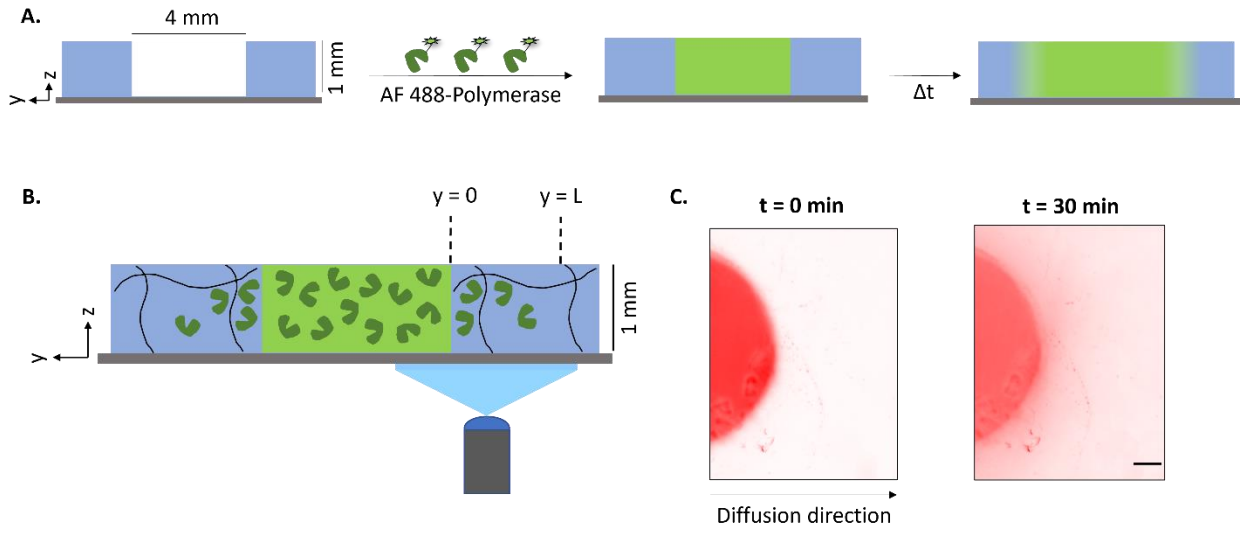

Figure 3-5: Diffusion of AF488-labeled Klenow exo- polymerase in polyacrylamide gels was measured via timelapse imaging. (A) Experimental workflow involves filling 4 mm punched wells in 1 mm thick with AF488-labeled polymerase and observing the diffusion into the gel. (B) Diffusion was measured from the gel-microwell interface (length y = 0) to edge of the imaging field of view (length y = L) for fitting to a diffusion model. (C) Images taken at t = 0 and t = 30 min illustrate the diffusion out of the microwell into the surrounding gel. Scale bar is 500 µm.

The diffusion data were then fitted via least squares fitting to a 1-D unsteady-state partial differential equation (PDE) diffusion model (Eqn 3-8) with the following initial condition and boundary conditions (Eqns 3-9, 3-10, and 3-11).

$$\frac{\partial C}{\partial t} = D\frac{\partial^2 C}{\partial y^2}$$ (Equation 3-8)

I.C.: $C = 0$ @ $t = 0$ (Equation 3-9)

B.C. 1: $C = C_0$ @ $y = 0$ (Equation 3-10)

B.C. 2: $\frac{\partial C}{\partial t} = 0$ @ $y = L$ (Equation 3-11)

where C is concentration, C_0 is the initial concentration, t is time, and D is the diffusion coefficient (cm^2/s). The second boundary condition is assuming semi-infinite diffusion. The same governing equation and boundary conditions have been applied to similar systems in the literature[32,33]. Normalized fluorescence values were assumed to be proportional to the concentration. Other assumptions include constant-source diffusion, 1-D diffusion in the radial direction, which can be approximated as rectangular 1-D diffusion in the center of the well, and the y = 0 point (gel interface) defined as the point that exhibited a fluorescence value equal to the product of the estimated partition coefficient and the in-well fluorescence.

Preliminary results suggest that the data fit the diffusion model well (Fig. 3-6A). Fits for multiple replicates of each condition resulted in an R^2 metric of 0.89-0.96. The measured diffusion

coefficients were in the range of $5x10^{-7}$-$1x10^{-6}$ cm^2/s, which is up to one order of magnitude higher than our estimated diffusion coefficient for Klenow exo- polymerase. Overall, the fit appears to be better in the region closer to the well than in the region farther from the well.

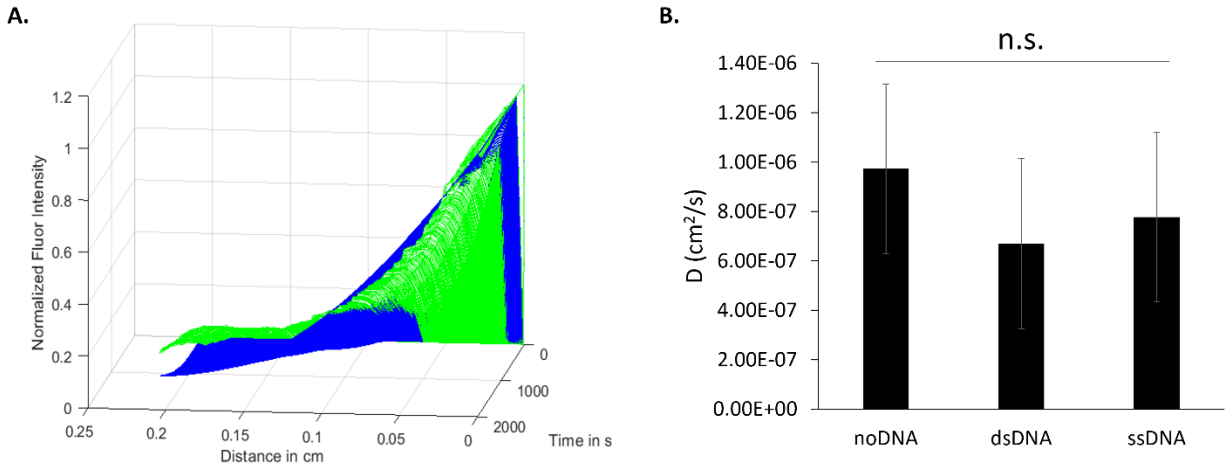

Figure 3-6: Fitting of the diffusion data yields diffusion coefficients for AF488-labeled Klenow exo- polymerase. (A) The diffusion model fits the data well, as illustrated by the surface plot (blue = fitted model, green = experimental data) and the R^2 value of 0.93. (B) There was no significant difference in the fitted polymerase diffusion coefficients between gels that did not contain immobilized DNA (noDNA), gels that contained single-stranded immobilized DNA (ssDNA), and gels that contained double stranded DNA with a single-stranded overhang (dsDNA). Mean with standard deviation error bars are reported and all data were collected in triplicate. Statistical significance was evaluated with a Kruskal-Wallace Test ($p>0.05$).

There is a precedent for measured diffusion coefficients that are substantially higher than predicted by standard models. In-gel diffusion coefficients measured by Lewus and Carta[32] were orders of magnitude higher than predicted. Their hypothesis, which is supported by the literature, is that interactions between the protein and the charged gel matrix result in faster diffusion. While our gels are not charged, they contain the hydrophobic molecule BPMA, which has been shown to result in hydrophobic interactions between proteins and the gel matrix[13]. Our working hypothesis is that interactions between the protein and the BPMA result in faster diffusion. As we are primarily interested in the relative difference in the diffusion of the polymerase in the presence and absence of DNA, the ratio of the diffusion coefficients under different conditions is more important than the absolute value. For this reason, we decided to go ahead with retarded diffusion experiments and report the ratio of the diffusion coefficients.

To test our hypothesis that retarded diffusion of the polymerase is governed by interactions between the polymerase and the single-stranded DNA overhangs, we evaluated three experimental conditions: no immobilized DNA, immobilized single-stranded DNA, and immobilized double-stranded DNA with single-stranded overhangs capable of being polymerase elongated. The polymerase elongation solution contained the AF 488 labeled polymerase and all four dNTPs, including AF 647-dUTP, to be able to measure the fluorescently labeled reaction products after running the experiments. The result of our preliminary experiment was no significant difference between the three conditions (Fig. 3-6B).

Upon further investigation, no reaction products were observed around the wells when imaging in the AF 647 channel after an overnight wash. This result suggests that the polymerase may have not been interacting normally with the immobilized DNA in the gel. We posit that either reduced polymerase activity due to overlabeling or incomplete hybridization of the second strand that forms the single-stranded overhang is responsible for the lack of fluorescently labeled reaction products in the gel. A similar result of no difference in the measured diffusion coefficients between the experimental conditions was observed in a previous experiment. In that case, we confirmed in our standard 45 μm thick gel system that the polymerase was overlabeled such that all its activity was lost. The batch of labeled polymerase used in the above experiment had a degree of labeling (DOL) of 4.22, compared to 6.64 in the previous batch, and it exhibited ~50% of the activity of unlabeled polymerase in our standard system. To test our hypothesis of incomplete hybridization of the second strand, gels were stained with SYBR Green I nucleic acid stain, which preferentially stains double-stranded DNA. Strong fluorescence was observed near the edge of the well, while the fluorescence was weak in the rest of the gel. The result was the same in both the ssDNA and dsDNA gels. No visible difference between the ssDNA and dsDNA gels was a surprising result that warrants further investigation. Improper or incomplete hybridization is likely a contributing factor to the lack of observed retarded diffusion. Longer hybridization times or polymerizing the double-stranded DNA into the gel are possible solutions to the issue.

There is a general need to improve the robustness and reproducibility of this experimental setup. We observed a great deal of variability in the extracted diffusion coefficients among each of the three replicates for each of the experimental conditions, as demonstrated by the large error bars (Fig. 3-6B). There was also a discrepancy in the measured diffusion coefficients between the experimental runs from different days. Additionally, the R^2 values in the later sets of experiments were ~0.75, compared to ~0.9 in the earlier sets of experiments. Our working hypothesis is that residual free dye was not completely removed from the labeled polymerase during the purification step and contributes to the variability between the measurements from different experiments, as earlier experiments used the inactive batch of labeled polymerase with the higher DOL. This hypothesis is supported by our observation that the background in the region of the image farthest away from the well was higher than in gels that were exposed to the lower DOL batch of labeled polymerase at all nonzero timepoints. Additionally, the fit was poor in the regions farthest from the well with experimental data normalized fluorescence values higher than the fitted model values. Residual free dye from the protein labeling reaction that was not removed by the purification process is a likely explanation for the high background and poor fit in the regions farther from the well since free dye diffuses faster than the labeled protein. Further experiments to study the effects of residual free dye and improve the purification of the labeled polymerase are warranted.

As a whole, our preliminary results for measuring diffusion of labeled polymerase in real-time are promising. With further modifications and improvements, such a system has the potential to measure retarded diffusion.

Increased Number of and Spacing between Labeled Nucleotides Results in Increased Fluorescence Signal

The second goal of this work was to evaluate various DNA sequence designs that incorporate multiple labeled nucleotides to determine the effect on the fluorescence signal, as one labeled nucleotide incorporated per strand has been the focus of previous studies. Ultimately, we sought to develop design rules for signal amplification via in-gel polymerase elongation and improve the reading out of repeat bases. Two key sequence design parameters were evaluated: the number of labeled nucleotides incorporated per strand and the spacing of unlabeled nucleotides between each labeled nucleotide. To our knowledge, no other studies have evaluated the effect of varying a specified number of labeled nucleotides incorporated into a DNA strand via polymerase elongation in a hydrogel matrix. A previous in-solution study evaluated chemically labeled DNA strands and found that for strands of a similar length, up to five Cy3 labels per strand resulted in increased fluorescence[34]. Additionally, previous in-solution studies have successfully incorporated multiple labeled nucleotides per strand via polymerase elongation, but did not thoroughly characterize the fluorescence increase that results from a specified increase in the number of labeled nucleotides incorporated[35,36]. As the in-gel molecular accessibility of DNA is thought to be comparable to in solution[25,26], we hypothesized that the relationship between the in-gel fluorescence increase and number of incorporated labeled nucleotides would be similar to in-solution studies. Other key sequence design factors that we will be evaluating include the spacing between labeled nucleotides and distance of labeled nucleotide incorporation sites from the end of the DNA strand. When fluorophores are <10 nm apart, self-quenching can occur due to homo-FRET[37,38]. Additionally, formation of truncation products during polymerase elongation with labeled nucleotides has been observed when the labeled nucleotide is incorporated close to the end of the strand[35,36]. Thus, we hypothesized that increasing the spacing between labeled nucleotides while be cognizant of the distance from the end of the strand will result in increased fluorescence signal.

We first evaluated DNA sequence designs (Table 3-3) that could incorporate multiple labeled nucleotides with a spacing of three unlabeled nucleotides between each labeled nucleotide.

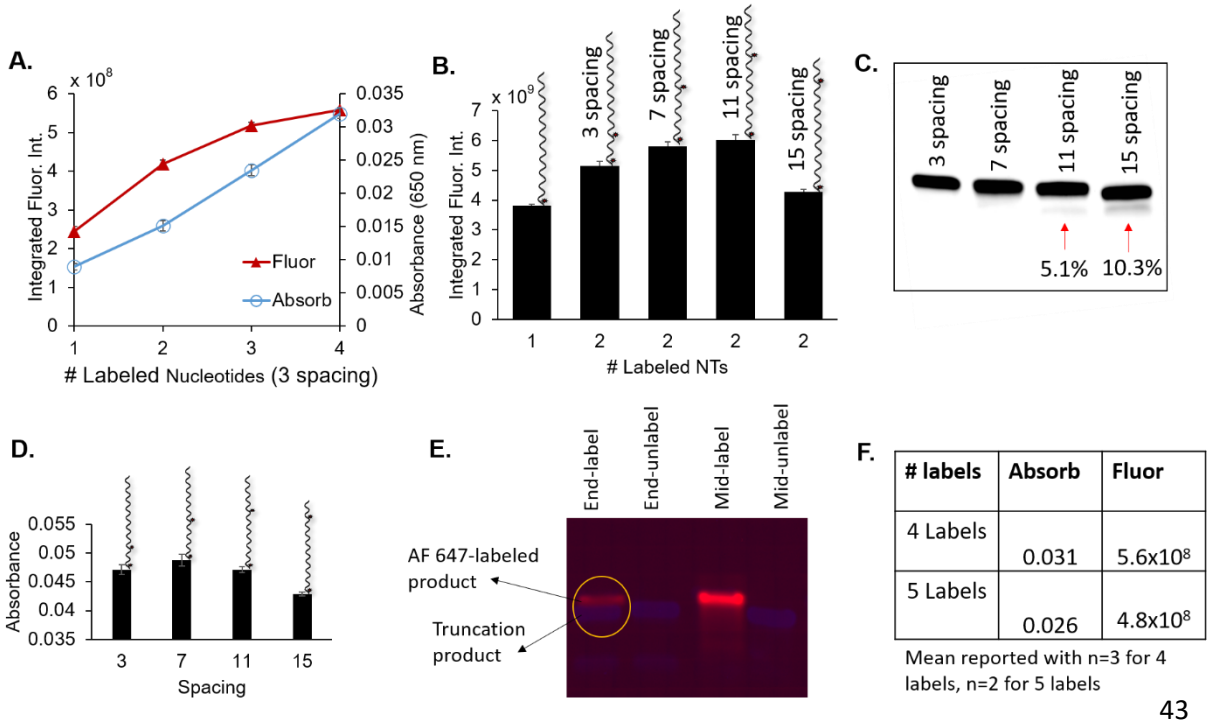

# labels	Absorb	Fluor
4 Labels	0.031	5.6×10^8
5 Labels	0.026	4.8×10^8

Mean reported with n=3 for 4 labels, n=2 for 5 labels

Figure 3-7: Fluorescence signal can be increased through incorporation of multiple labeled nucleotides and increased spacing between labeled nucleotides. (A) in-gel fluorescence intensity increases at a decreasing rate as multiple labeled nucleotides are incorporated, while absorbance increases at 650 nm indicate complete incorporation of the labeled nucleotides, (B) DNA sequences with increased spacing between labeled nucleotides (representative schematic above each bar on plot) result in increased in-gel fluorescence (sp indicates spacing), (C) sequences with varied spacing between labeled nucleotide incorporations were polymerase elongated in solution and run on a 15% TBE-Urea gel, revealing lower molecular weight bands (circled) below the primary band for the sequences with 11 and 15 spacing that comprise 5.1% and 10.3% of the total signal, respectively. This indicates the formation of truncation products that contain only one labeled nucleotide, (D) The absorbance after polymerase elongation in gel decreases for spacings greater than 7, which is indicative of polymerase truncation, (E) Polymerase truncation is observed when the labeled nucleotide is incorporated at the end of a strand, as indicated by the two circled bands on the 15% TBE-urea gel (red is AF 647 from labeled nucleotides, blue is SYBR gold stain, label = AF 647-dUTP, unlabel = dUTP), (F) a decrease in fluorescence and absorbance was observed when increasing the number of labeled nucleotides from 4 to 5 with 3 spacing between. n=3 replicates with standard deviation error bars unless otherwise specified.

Sequences that allowed for the incorporation of multiple labeled nucleotides resulted in increased fluorescence for up to 4 incorporated labeled nucleotides (Fig. 3-7A). However, the increase tapered off for increasing numbers of labeled nucleotides such that a 2.3-fold signal increase was observed in a strand that incorporated four labeled nucleotides when compared to a strand that incorporated one labeled nucleotide. We did not observe this tapering off in the absorbance reading for each additional incorporated labeled nucleotide, indicating that the polymerase was incorporating the predicted number of labeled nucleotides into each sequence (Fig. 3-7A). Interestingly, the fluorescence and absorbance decreased 15% and 18%, respectively, when the number of incorporated labeled nucleotides increased from 4 to 5 (Fig. 3-7F). The decreases in fluorescence and absorbance are hypothesized to be due to incomplete incorporation of the labeled nucleotides that results from premature dissociation of the polymerase, resulting in truncation products. In agreement with other studies[34–36], we have observed in solution that DNA sequences in which the labeled nucleotides are incorporated at the end of the strand result in truncation products (Fig. 3-7E). Additionally, our results closely match a previous study, in which increases in the fluorescence signal were observed for up to 5 labeled nucleotides per strand[34]. The tapering off of fluorescence signal is likely a result of self-quenching, since the spacing of 3 nucleotides between each labeled nucleotide corresponds to ~1 nm (assuming 0.34 nm/nucleotide)[39].

To test our hypothesis of self-quenching, we investigated the effect of increased spacing between labeled nucleotides on the gel fluorescence. Increased spacing was hypothesized to mitigate self-quenching and result in increased fluorescence. When the spacing between two labeled nucleotide incorporation sites was increased from 3-7 unlabeled nucleotides, a 13% increase in fluorescence signal was observed, and when increased from 3-11 unlabeled nucleotides, a 17% increase was observed (Fig. 3-7B). When the spacing was increased from 11-15, a decrease in fluorescence was observed. A reaction in solution followed by separation on a 15% TBE-urea

gel revealed a truncation product for the 11 and 15 spacing sequences that was especially prevalent with the 15 spacing sequence, constituting 10% of the signal in that lane of the gel (Fig. 3-7C). The truncation hypothesis was corroborated by absorbance readings of the gels that, when compared to the 7 spacing case, revealed a 12% decrease in the absorbance for 15 spacing and a 3.4% decrease for 11 spacing (Fig. 3-7D). We hypothesize that the formation of a truncation product is due to the second labeled nucleotide being incorporated closer to the end of the strand in the 11 and 15 spacing cases (Table 3-3). While increased spacing resulted in increased fluorescence signal, even the signal corresponding to the 11 nucleotide spacing was still far from double that of one incorporated labeled nucleotide. Additionally, the fluorescence increase from 7-11 spacing was minimal at 3.8%, indicating diminishing returns for longer spacers. Diminishing returns in additional fluorescence for longer spacers is consistent with the theory on self-quenching because homo-FRET decreases exponentially with increasing distance between fluorophores[37]. Considering that DNA strand length increases 0.34 nm per additional base and homo-FRET occurs when fluorophores are less than 10 nm apart, we hypothesize that a strand length of up to ~30 bases may be necessary to completely eliminate self-quenching[37,39]. Overall, our results support the hypothesis that self-quenching due to homo-FRET results in reduced fluorescence when multiple labeled nucleotides are incorporated.

More broadly, our results suggest that signal amplification via incorporation of multiple labeled nucleotides is possible with further sequence optimization followed by experimental validation. As incorporation of multiple labeled nucleotides with short spacers results in a limited increase in fluorescence, mitigating the diminishing signal increases with each incorporated labeled nucleotide will be essential for achieving signal amplification and/or accurate quantification of repeat bases. Achieving our optimum observed spacing of 11 nucleotides on a strand that could incorporate 5 labeled nucleotides would require a strand length of approximately 70 bases. We predict that such a sequence would result in over 3-fold signal amplification. In the case of DNA-based antibody readouts, longer strands could be a limiting factor, since 80 base long DNA strands have been shown to substantially reduce antibody binding when compared to 30 base long strands[40]. Further evaluation of the tradeoff between antibody binding kinetics and strand length will be necessary when developing readouts for antibody-based systems. Overall, the advantages of signal amplification incorporated into an in-situ sequencing readout would be an improved assay timescale and fewer steps that introduce error or variability. However, it is possible that the maximum amount of signal amplification could be limited by self-quenching and/or truncation during elongation. Therefore, further investigation of this strategy as a strategy for signal amplification is warranted.

3.4 Conclusions

In this study, we found that a polymerase elongation reaction in a polyacrylamide hydrogel is efficient when run to completion but reaches completion 1-2 orders of magnitude slower than predicted based on simple reaction or transport limitations. The minimal effect on reaction completion observed when quadrupling the concentration of the rate-limiting species, the polymerase, and an uneven fluorescence profile throughout the depth of the gel support our hypothesis that the process is transport limited. Additionally, the observed proportionality between the immobilized DNA concentration and the time for complete reaction throughout the

gel support the hypothesis of retarded diffusion of the polymerase due to interactions between the polymerase and the immobilized DNA. The broader implication for assay design is that consideration of the increased time for complete transport to ensure a complete, spatially uniform reaction throughout the gel is essential. Our work provides a jumping off point for the study of these phenomena toward the goal of more informed hydrogel-based assay design.

In this study, we also evaluated DNA sequence designs for the incorporation of multiple labeled nucleotides per strand via polymerase elongation. Our findings indicate that incorporating multiple labeled nucleotides per strand results in an increase in fluorescence. However, the increase tapers off with additional labeled nucleotides if the labeled nucleotides are spaced close together, such that only a 2.3-fold increase in fluorescence was observed when increasing the number of incorporated labeled nucleotides from 1 to 4. Increasing the spacing between labeled nucleotides from 3 unlabeled nucleotides to 11 labeled nucleotides increased the fluorescence signal by 18%, supporting our hypothesis of self-quenching. However, a crucial caveat that we discovered is that the final incorporated labeled nucleotide must not be too close to the end of the DNA strand, otherwise a truncation product will form due to the inability of the polymerase to completely incorporate the nucleotide. The broader implication of this work is that careful DNA sequence design that increases the spacing between incorporated labeled nucleotides has the potential to improve the reading out of repeat bases and introduce signal amplification into these readouts.

3.5 Bibliography

(1) Chung, K.; Wallace, J.; Kim, S.; Kalyanasundaram, S.; Andalman, A. S.; Davidson, T. J.; Mirzabekov, J. J.; Zalocusky, K. A.; Mattis, J.; Denisin, A. K.; Pak, S.; Bernstein, H.; Ramakrishnan, C.; Grosenick, L.; Gradinaru, V.; Deisseroth, K. Structural and Molecular Interrogation of Intact Biological Systems. *Nature* **2013**, *497*, 332–339. https://doi.org/10.1038/nature12107.

(2) Chen, F.; Tillberg, P. W.; Boyden, E. S. Expansion Microscopy. *Science (80-.).* **2015**, *347* (6221), 543–548.

(3) Wassie, A. T.; Zhao, Y.; Boyden, E. S. Expansion Microscopy: Principles and Uses in Biological Research. *Nat. Methods* **2019**, *16* (January), 33–41. https://doi.org/10.1038/s41592-018-0219-4.

(4) Hughes, A. J.; Spelke, D.; Xu, Z.; Kang, C. C.; Schaffer, D.; Herr, A. E. Single-Cell Western Blotting. *Nat. Methods* **2015**, *11* (7), 455–464. https://doi.org/10.1007/978-1-4939-2694-7_46.

(5) Tentori, A. M.; Yamauchi, K. A.; Herr, A. E.; John, L.; Dewar, L.; Distinguished, L. Detection of Isoforms Differing by a Single-Charge Unit in Individual Cells. *Angew. Chemie - Int. Ed.* **2017**, *55* (40), 12431–12435. https://doi.org/10.1002/anie.201606039.

(6) Kang, C.; Ward, T. M.; Bockhorn, J.; Schiffman, C.; Huang, H.; Pegram, M. D.; Herr, A. E. Electrophoretic Cytopathology Resolves ERBB2 Forms with Single-Cell Resolution. *npj Precis. Oncol.* **2018**, No. February, 1–10. https://doi.org/10.1038/s41698-018-0052-3.

(7) Mitra, R. D.; Shendure, J.; Olejnik, J.; Krzymanska-Olejnik, E.; Church, G. M. Fluorescent in Situ Sequencing on Polymerase Colonies. *Anal. Biochem.* **2003**, *320* (1), 55–65. https://doi.org/10.1016/S0003-2697(03)00291-4.

(8) Goltsev, Y.; Samusik, N.; Kennedy-Darling, J.; Vazquez, G.; Black, S.; Correspondence, G. P. N.; Bhate, S.; Hale, M.; Nolan, G. P. Deep Profiling of Mouse Splenic Architecture with CODEX Multiplexed Imaging In Brief A DNA Barcoding-Based Imaging Technique Uses Multiplexed Tissue Antigen Staining to Enable the Characterization of Cell Types and Dynamics in a Model of Autoimmune Diseas. *Cell* **2018**, *174* (4), 1–14. https://doi.org/10.1016/j.cell.2018.07.010.

(9) Chen, X.; Sun, Y.; Church, G. M.; Lee, J. H.; Zador, A. M. Efficient in Situ Barcode Sequencing Using Padlock Probe-Based BaristaSeq. *Nucleic Acids Res.* **2018**, *46* (4), 1–10. https://doi.org/10.1093/nar/gkx1206.

(10) Wang, X.; Allen, W. E.; Wright, M. A.; Sylwestrak, E. L.; Samusik, N.; Vesuna, S.; Evans, K.; Liu, C.; Ramakrishnan, C.; Liu, J.; Nolan, G. P.; Bava, F.; Deisseroth, K. Three-Dimensional Intact-Tissue Sequencing of Single-Cell Transcriptional States. **2018**, *5691*. https://doi.org/10.1126/science.aat5691.

(11) Hughes, A. J.; Lin, R. K. C.; Peehl, D. M.; Herr, A. E. Microfluidic Integration for Automated Targeted Proteomic Assays. *Proc. Natl. Acad. Sci.* **2012**, *109* (16), 5972–5977. https://doi.org/10.1073/pnas.1108617109.

(12) Amsden, B. Solute Diffusion within Hydrogels. Mechanisms and Models. *Macromolecules* **1998**, *31*, 8382–8395. https://doi.org/10.1021/ma980765f.

(13) Su, A.; Smith, B. E.; Herr, A. E. In Situ Measurement of Thermodynamic Partitioning in Open Hydrogels. *Anal. Chem.* **2019**, *92* (2), 875–883. https://doi.org/10.1021/acs.analchem.9b03582.

(14) Vlassakis, J.; Herr, A. E. Effect of Polymer Hydration State on In-Gel Immunoassays. *Anal. Chem.* **2015**, *87* (21), 11030–11038. https://doi.org/10.1021/acs.analchem.5b03032.

(15) Pregibon, D. C.; Doyle, P. S. Optimization of Encoded Hydrogel Particles for Nucleic Acid Quantification. *Anal. Chem.* **2009**, *81* (12), 4873–4881. https://doi.org/10.1021/ac9005292.

(16) Tentori, A. M.; Nagarajan, M. B.; Kim, J. J.; Zhang, W. C.; Slack, F. J.; Doyle, P. S. Quantitative and Multiplex MicroRNA Assays from Unprocessed Cells in Isolated Nanoliter Well Arrays. *Lab Chip* **2018**, *18* (16), 2410–2424. https://doi.org/10.1039/c8lc00498f.

(17) Joubert, A. M.; Byrd, A. S.; LiCata, V. J. Global Conformations, Hydrodynamics, and X-Ray Scattering Properties of Taq and Escherichia Coli DNA Polymerases in Solution. *J. Biol. Chem.* **2003**, *278* (28), 25341–25347. https://doi.org/10.1074/jbc.M302118200.

(18) Williams, J. C.; Mark, L. A.; Eichholtz, S. Partition and Permeation of Dextran in Polyacrylamide Gel. *Biophys. J.* **1998**, *75* (1), 493–502. https://doi.org/10.1016/S0006-3495(98)77538-1.

(19) Kuchta, R. D.; Mizrahi, V.; Benkovic, P. A.; Johnson, K. A.; Benkovic, S. J. Kinetic Mechanism of DNA Polymerase I (Klenow). *Biochemistry* **1987**, *26* (25), 8410–8417. https://doi.org/10.1021/bi00399a057.

(20) Likhachev, E. R. Dependence of Diffusion on Temperature and Pressure. *Tech. Phys.* **2007**, *48* (4), 127–149. https://doi.org/10.1007/978-3-540-71488-0_8.

(21) *Cold Spring Harbor Protocols*; Sever, R., Ed.; Cold Spring Harbor Laboratory Press, 2020.

(22) Grist, S. M.; Mourdoukoutas, A. P.; Herr, A. E. 3D Projection Electrophoresis for Single-Cell Immunoblotting. *Nat. Commun.* **2020**, *11*, 1–17. https://doi.org/10.1038/s41467-020-19738-1.

(23) Ma, S.; Loufakis, D. N.; Cao, Z.; Chang, Y.; Achenie, L. E. K.; Lu, C. Diffusion-Based Microfluidic PCR for "One-Pot" Analysis of Cells. *Lab Chip* **2014**, *14* (16), 2905–2909. https://doi.org/10.1039/c4lc00498a.

(24) Niikura, K.; Matsuno, H.; Okahata, Y. Direct Monitoring of DNA Polymerase Reactions on a Quartz-Crystal Microbalance. *J. Am. Chem. Soc.* **1998**, *7863* (98), 8537–8538. https://doi.org/10.1021/ja980967r.

(25) Fotin, A. V; Drobyshev, A. L.; Proudnikov, D. Y.; Perov, A. N.; Mirzabekov, A. D. Parallel Thermodynamic Analysis of Duplexes on Oligodeoxyribonucleotide Microchips.

Nucleic Acids Res. **1998**, *26* (6), 1515–1521.

(26) Halperin, A.; Buhot, A.; Zhulina, E. B. On the Hybridization Isotherms of DNA Microarrays : The Langmuir Model and Its Extensions On the Hybridization Isotherms of DNA Microarrays : *J. Phys. Condens. Matter* **2006**, *18*, S463-490. https://doi.org/10.1088/0953-8984/18/18/S01.

(27) Chetverina, H. V.; Samatov, T. R.; Ugarov, V. I.; Chetverin, A. B. Molecular Colony Diagnostics: Detection and Quantitation of Viral Nucleic Acids by in-Gel PCR. *Biotechniques* **2002**, *33* (1), 150–156.

(28) Atrazhev, A.; Manage, D. P.; Stickel, A. J.; Crabtree, H. J.; Pilarski, L. M.; Acker, J. P. In-Gel Technology for PCR Genotyping and Pathogen Detection. *Anal. Chem.* **2010**, *82* (19), 8079–8087. https://doi.org/10.1021/ac1013157.

(29) Montgomery, J. L.; Wittwer, C. T. Influence of PCR Reagents on DNA Polymerase Extension Rates Measured on Real-Time PCR Instruments. *Clin. Chem.* **2014**, *60* (2), 334–340. https://doi.org/10.1373/clinchem.2013.212829.

(30) Livshits, M. A.; Mirzabekov, A. D. Theoretical Analysis of the Kinetics of DNA Hybridization with Gel- Immobilized Oligonucleotides. *Biophys. J.* **1996**, *71* (5), 2795–2801. https://doi.org/10.1016/S0006-3495(96)79473-0.

(31) Kimmich, R.; Klemm, A.; Weber, M.; Seymour, J. D. Flow, Diffusion, Dispersion, and Thermal Convection in Percolation Clusters: NMR Experiments and Numerical FEM/FVM Simulations. *Mater. Res. Soc. Symp. Proc.* **2001**, *651*.

(32) Lewus, R. K.; Carta, G. Protein Diffusion in Charged Polyacrylamide GelsVisualization and Analysis. *J. Chromatogr. A* **1999**, *865* (1–2), 155–168. https://doi.org/10.1016/S0021-9673(99)00862-6.

(33) Tong, J.; Anderson, J. L. Partitioning and Diffusion of Proteins and Linear Polymers in Polyacrylamide Gels. *Biophys. J.* **1996**, *70* (3), 1505–1513. https://doi.org/10.1016/S0006-3495(96)79712-6.

(34) Randolph, J. B.; Waggoner, A. S. Stability, Specificity and Fluorescence Brightness of Multiply-Labeled Fluorescent DNA Probes. *Nucleic Acids Res.* **1997**, *25* (14), 2923–2929. https://doi.org/10.1093/nar/25.14.2923.

(35) Tasara, T.; Angerer, B.; Damond, M.; Winter, H.; Dörhöfer, S.; Hübscher, U.; Amacker, M. Incorporation of Reporter Molecule-Labeled Nucleotides by DNA Polymerases. II. High-Density Labeling of Natural DNA. *Nucleic Acids Res.* **2003**, *31* (10), 2636–2646. https://doi.org/10.1093/nar/gkg371.

(36) Giller, G.; Tasara, T.; Angerer, B.; Mühlegger, K.; Amacker, M.; Winter, H. Incorporation of Reporter Molecule-Labeled Nucleotides by DNA Polymerases. I. Chemical Synthesis of Various Reporter Group-Labeled 2′-Deoxyribonucleoside-5′-Triphosphates. *Nucleic Acids Res.* **2003**, *31* (10), 2630–2635. https://doi.org/10.1093/nar/gkg370.

(37) Shrestha, D.; Jenei, A.; Nagy, P.; Vereb, G.; Szöllősi, J. *Understanding FRET as a Research Tool for Cellular Studies*; 2015; Vol. 16. https://doi.org/10.3390/ijms16046718.

(38) Luchowski, R.; Matveeva, E. G.; Gryczynski, I.; Terpetschnig, E. A.; Patsenker, L.; Laczko, G.; Borejdo, J.; Gryczynski, Z. Single Molecule Studies of Multiple-Fluorophore Labeled Antibodies. Effect of Homo-FRET on the Number of Photons Available Before Photobleaching. *Curr Pharm Biotechnol* **2008**, *9* (5), 411–420.

(39) Levitt, M. How Many Base-Pairs per Turn Does DNA Have in Solution and in Chromatin? Some Theoretical Calculations. *Proc. Natl. Acad. Sci. U. S. A.* **1978**, *75* (2), 640–644. https://doi.org/10.1073/pnas.75.2.640.

(40) Sundah, N. R.; Ho, N. R. Y.; Lim, G. S.; Natalia, A.; Ding, X.; Liu, Y.; Seet, J. E.; Chan, C. W.; Loh, T. P.; Shao, H. Barcoded DNA Nanostructures for the Multiplexed Profiling of Subcellular Protein Distribution. *Nat. Biomed. Eng.* **2019**, *3* (9), 684–694. https://doi.org/10.1038/s41551-019-0417-0.

Chapter 4: In-Gel Hybridization Chain Reaction Characterization and Optimization for Nucleic Acid Signal Amplification

4.1 Introduction

Hydrogels exhibit advantageous physical, chemical, and optical properties for a wide range of bioanalyses[1–6]. However, many reactions and processes have not been thoroughly characterized within a hydrogel matrix. One such example is hybridization chain reaction (HCR), an isothermal and enzyme-free signal amplification strategy in which combination of an initiator strand of DNA with a pair of metastable DNA hairpins results in the formation of a long nicked double helix of DNA and subsequent signal amplification of multiple orders of magnitude[7,8]. In-gel HCR has been previously demonstrated for sensitive analyte detection in tissue clearing and expansion microscopy applications[9,10]. However, key assay design parameters, such as the reaction kinetics, effects of varying gel density, linear concentration dependent response, and effects of buffer composition have not been thoroughly studied.

Hydrogel-based systems exhibit some unique properties when compared to solution-based or surface-based systems. First, hydrogels introduce transport limitations, since diffusion is hindered in the porous bulk of the material[11,12]. Size exclusion-based thermodynamic partitioning, which limits the concentration of solute in the gel at equilibrium, is another factor in hydrogel-based assays[13]. Therefore, the assay timescale is not governed solely by the reaction kinetics, since the conditions within a hydrogel are not the same as in solution. One particularly useful framework for comparing the transport and reaction timescales is the Damköhler number (Da). Damköhler analysis can provide insight into the contributions of transport and reaction kinetics to the assay timescale and concentration profiles in the gel under different conditions[11,14–16]. Da is the ratio of the characteristic transport time to the characteristic reaction time, such that $Da \gg 1$ indicates a transport limited process, while $Da \ll 1$ indicates a reaction limited process[14]. For predictions of characteristic transport time in gel, diffusion can be modeled by Fickian diffusion in one dimension employing a modified Stokes-Einstein equation with a correction that accounts for hindered diffusion within the gel matrix [11,12,17–19]. Meanwhile, DNA hybridization can be modeled by pseudo first-order reaction kinetics when one strand is in excess[20], something that will be further discussed later. The understanding gained from such an analysis will ultimately inform optimization of assay design parameters, such as the incubation times and reagent concentrations.

Specific factors that have the potential to influence the assay performance are 1) the gel density, 2) the concentration dependent response, and 3) the effects of the buffer composition. Polyacrylamide gel density is typically reported in terms of the percentage of total acrylamide (%T) and percentage of bis-acrylamide crosslinker (%C), such that higher %T and %C gels are higher density and have smaller pore sizes[21]. In-gel HCR has currently only been employed in low density gels (~4% T, 1% C)[9,10]. Many other gel-based assays, such as single-cell immunoblotting, employ denser hydrogels (6-15% T)[4,5]. There is a possibility that denser gels could inhibit HCR due to the smaller pore sizes causing steric hindrance as the concatemers form

or providing unfavorable diffusion and/or partitioning characteristics. Therefore, it is essential to understand the effects of gel density on HCR for informed assay design. Evaluation of the linear concentration dependent response is also important for development of a quantitative or semi-quantitative in-gel assay[4]. Buffer composition is yet another factor than can influence the maximum fluorescence signal and the reaction kinetics. DNA hybridization reactions, including HCR, have long employed molecular crowding agents, such as dextran sulfate, to increase the rate of reaction and the amount of signal[9,22–24]. Molecular crowding agents act by restricting the DNA to the free solution space not occupied by the molecular crowding agent, which reduces the entropy and increases the free energy, resulting in an increase in the effective concentration[22,23]. Inclusion of dextran sulfate in the reaction buffer has the potential to increase both the fluorescence signal and reaction kinetics in denser polyacrylamide gels, and thus warrants evaluation.

In this study, we develop assay design rules for HCR assays in dense polyacrylamide hydrogels. To this end, we prepare polyacrylamide gels with DNA immobilized in the bulk to characterize the degree of signal amplification resulting from HCR, the reaction kinetics, the linearity of the concentration-dependent response, and effects of the buffer composition on the signal. We find that HCR results in robust signal amplification that is consistent across different gel densities and follows pseudo first-order DNA hybridization kinetics. Furthermore, we find that a buffer that contains dextran sulfate results in double the signal, and that the degree of reaction completion is essential for the linear concentration dependent response. These results indicate broad applicability of in-gel HCR as a signal amplification strategy in dense polyacrylamide gels.

4.2 Materials and Methods

Reagents

All DNA oligomers were purchased from IDT (Coralville, IA, USA), including oligomers with 5’ acrydite groups for incorporation into the gel. Tetramethylethylenediamine (TEMED, T9281), ammonium persulfate (APS, A3678), 3-(trimethoxylsilyl)propyl methacrylate (440159), dichlorodimethylsilane (440272), 30%T/3.3%C acrylamide/bis-acrylamide (29:1) (A3574), dextran sulfate (D8787), sodium chloride S9888), and sodium citrate dihydrate (W302600) were purchased from Sigma-Aldrich (St. Louis, MO, USA). 1.5 M Tris-HCl, pH 8.8, was purchased from Teknova (T1588). Tris base (3715-A) was purchased from Santa Cruz Biotechnology. 0.5 M EDTA, pH 8.0 (15575-038) was purchased from Gibco. N-[3-[(3-Benzoylphenyl)formamido]propyl] methacrylamide (BPMAC) was custom synthesized by Pharm-Agra Laboratories (Brevard, NC, USA). Deionized water (18.2 MΩ) was obtained using an Ultrapure water system from Millipore. TE, TBE, and SSC buffers were prepared according to standard protocols[25].

Gel Fabrication

Polyacrylamide gels were fabricated on silicon wafer substrates with 45 μm rails patterned in SU-8, as previously reported[4]. Gel precursor solutions containing acrylamide/bis-acrylamide stock solution (30%, 29:1) were prepared to concentrations of 6-10% T, 3.3% C. BPMAC was added to a concentration of 3 mM and the DNA initiator strand for HCR with a 5’ acrydite group added to a concentration of 100 nM, unless otherwise specified, before degassing via sonication

for 5 min. APS and TEMED were then added to the precursor to a concentration of 0.08% each before pipetting the solution between the SU-8 wafer (rendered hydrophobic by treatment with dichlorodimethylsilane) and a placing glass microscope slide functionalized with 3-(trimethoxylsilyl)propyl methacrylate on top. After a 15-minute chemical polymerization, the slides with the attached gels were lifted from the wafers and washed in 1xTBE buffer for at least 1 h.

In-Gel HCR Experiments

Gels were fluidically addressed in a microarray cassette (1 x 16 hybridization cassette, Arrayit, Sunnyvale, CA, USA). HCR was carried out at 21ºC for 10 min-24 h and followed by aspirating off the DNA solution and washing twice with 100 µL of 1xTBE buffer. HCR hairpin mixture at a concentration of 500 nM of each hairpin in 1xTE buffer with 0.32 M NaCl was then added (60 µL per region of the microarray cassette) and the reaction run at 21ºC for the specified times. The volume of reaction solution added to each gel region was over an order of magnitude greater than the gel volume to promote constant source diffusion of the reagents into the gel. After the reaction, each region was briefly washed twice with 100 µL of 1xTBE buffer before removing the gel from the cassette and washing for 30 min in a bath of 1xTBE. Gels were then rinsed in DI water and dehydrated under a N2 stream for imaging.

Imaging and Data Processing

Imaging of the dehydrated gels was conducted using a GenePix 4300A microarray scanner equipped with a 635-nm laser. Imaging settings of 400 PMT gain and 80% power were chosen (300 gain and 80% power for Fig. 4-3C), optimized for maximum dynamic range without achieving saturation. Images were analyzed in FIJI (ImageJ) software. ROIs of 500 x 500 pixels were drawn in the center of the gel regions created by the microarray cassette, and the mean fluorescence intensity and integrated fluorescence were evaluated. Plots were generated in Excel and MATLAB.

Fitting of HCR Data to Kinetics Model

In-gel HCR data were fitted to Eqn. 4-2 using the lsqcurvefit function in MATLAB. Values for K and k_2 were then extracted from the model fit. R^2 was calculated from the ratio of the residuals (resnorm from lsqcurvefit) to the total sum of squares, which consisted of subtracting the data mean from each individual data point, squaring, and taking the sum. MATLAB code is included in Appendix C.

4.3 Results and Discussion

In-Gel HCR Results in Three Orders of Magnitude of Signal Amplification

We first sought to evaluate how much signal amplification HCR provides over hybridization of a labeled complementary strand in an 8% T gel, as HCR provides signal amplification over standard FISH assays that hybridize individual labeled complementary strands[8]. Since the benefits of signal amplification can be counteracted by high background, and retention of fluorescent probes is a direct contributor to in-gel assay background and noise, it is also

important to understand how much background is attributable to non-specific retention of HCR hairpins[13,14]. The model system employed in our study consisted of a polyacrylamide gel copolymerized with a 5' acrydite-terminated version of the HCR initiator DNA oligomer employed by Dirks et al[7] (Fig. 4-1A). The HCR hairpins or complementary strand were introduced to the top of the gel, allowing the reagents to diffuse into the gel in the z-direction. For the first set of experiments, initiator strand was included in the gel at a concentration of 100 nM, and each hairpin was at a concentration of 500 nM. Fluorescence signal and background were evaluated by exposing regions of gel to either the HCR hairpins or the labeled complementary strand and comparing to a negative control that consisted of a gel that omitted the immobilized initiator strand. We hypothesized that signal amplification of 2-3 orders of magnitude would be possible based on previous in-gel HCR studies, despite the denser gels, since the pore size is not orders of magnitude smaller[9,10,26]. We also hypothesized that minimal background would arise from retention of the HCR hairpins since small hydrophilic molecules do not get trapped in the gel as much as larger and hydrophobic molecules[13]. After a 2 h incubation, HCR resulted in a three order of magnitude increase in signal over hybridization of a labeled complementary strand (Fig. 4-1B). Additionally, signal in the negative control, which consisted of gel regions without immobilized initiator that were exposed to the HCR hairpins, was three orders of magnitude lower than in the experimental condition. Hybridization of the labeled complementary strand resulted in such weak signal that it is not visible to the naked eye in the 'Comp' false color micrograph shown in Fig. 4-1B. The implication is that HCR is a promising signal amplification strategy in dense polyacrylamide hydrogels due to the high degree of signal amplification and minimal background due to retained probes.

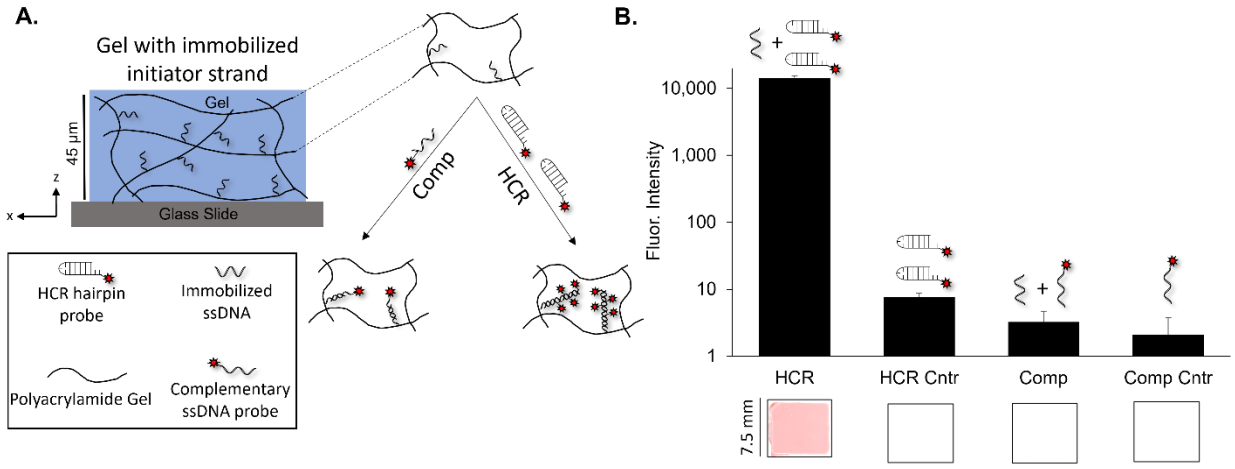

Figure 4-1: HCR results in three orders of magnitude of signal amplification in 8% T polyacrylamide gels. (A) HCR was evaluated in 45 µm thick 8% T polyacrylamide hydrogels by immobilizing an initiator strand and introducing either HCR hairpins or a labeled complementary strand as a control, (B) HCR results in strong signal with minimal background, affording three orders of magnitude of signal amplification over hybridization of a labeled complementary strand or negative controls that omitted the immobilized DNA (mean of $n \geq 3$ gel regions with standard deviation error bars, sample false color micrographs shown below plot).

In-Gel HCR Reaches Completion in 24 h Across Gel Densities

Second, we investigated the timescale for in-gel HCR completion and how it varies across different gel densities, two essential parameters for assay design. We hypothesized that the time for reaction completion would be substantially slower in gel than on a surface due to transport limitations. Previous HCR studies on surfaces have employed incubation times of 10 min-2 h[27–30]. However, the porous structure of the hydrogel matrix introduces transport limitations. Assuming that the HCR hairpins behave as 24 nt dsDNA fragments, employing diffusion coefficient data for 20 nt dsDNA fragments from Stellwagen et al.[31], and assuming 1D constant source diffusion, we obtain a predicted characteristic transport time in the gel of ~19 s for a simple diffusion case. However, a phenomenon termed retarded diffusion that is attributed to interactions between the immobilized and diffusing strands during hybridization has been shown to result in diffusion that is orders of magnitude slower than predicted by simple diffusion models[32]. The predicted characteristic reaction time based on 24 bases per strand participating in hybridization and a NaCl concentration of 0.32 M is 3.5×10^{-5} s[20]. The resultant Damköhler number for even a simple diffusion case is 5×10^{5}, which indicates that in-gel HCR is highly transport limited. Due to the high Damköhler number, we predict that the time for completion in gel could be orders of magnitude slower than in solution. Another key factor for assay design is the dependence of the reaction kinetics and final fluorescence signal on the gel density. Ideally, there would be minimal dependence such that the fluorescence signal and reaction time would not need to be adjusted depending on the gel density. Since formation of long HCR concatemers has the potential to block the gel pores, we hypothesized that denser gels would exhibit lower plateau fluorescence values. The predicted pore size of a 6% T, 3% C gel is 98 nm, while the predicted pore size of a 10% T, 3% C gel is 75 nm[21]. By comparison, the pore size of a 4% T, 1% C gel that is similar to what was used in previous cleared tissue experiments has a predicted pores size of 170 nm. If the process were limited by the gel pore size, we would expect to see a 25% difference in the fluorescence signal upon reaction completion in the 10% T gel compared to the 6% T gel.

Our results demonstrate that fluorescence signal continued to increase up to the 24 h timepoint, appearing to reach a plateau in all three of the gel densities evaluated (Fig. 4-2A and B). The final signal after 24 h appears to be within error and thus comparable across gel densities. The above results suggest that in-gel HCR is slower than in solution or on a surface by an order of magnitude or more[27–29]. Since the Damköhler number is high, transport limitations likely explain the discrepancy between in-gel and other assays. Interestingly, despite the 15% and 25% smaller pore sizes of the 8% and 10% T gels, compared to the 6% T gel, we observed a minimal difference in the endpoint fluorescence signal. While data from only one gel are reported for both the 6% T and 10% T conditions, we are confident that the results are representative because the intra-gel variability is comparable to the inter-gel variability observed across three 8% T gels. The three order of magnitude signal increase resulting from HCR over hybridization of a labeled complementary strand would suggest that there are 1000s more fluorophores incorporated, which would correspond to a number of DNA bases on the order of 10^{5}, as each hairpin is 48 nt. Light scattering experiments with DNA fragments of various sizes found that a 2,000 bp DNA strand, much smaller than the hypothetical length of the HCR concatemers, has a radius of gyration of ~100 nm[33]. Since a molecule with a 100 nm radius of gyration in solution would be large enough to block a pore, another mechanism is likely. It is possible that the DNA strands interact with the gel backbone such that they are roughly parallel to the backbone. Eventually, as enough DNA

accumulates, the pores would be slowly constricted. This constriction could, in turn, result in a decrease in the partition coefficient of the hairpins, resulting in the hairpins eventually being largely size excluded. The broader implication for assay design is that reaction times of 24 h or longer are necessary to ensure that the reaction reaches completion in a 45 µm thick gel. Additionally, consistent signal across different gel densities indicates that HCR is applicable to different gel systems without needing to correct for gel density.

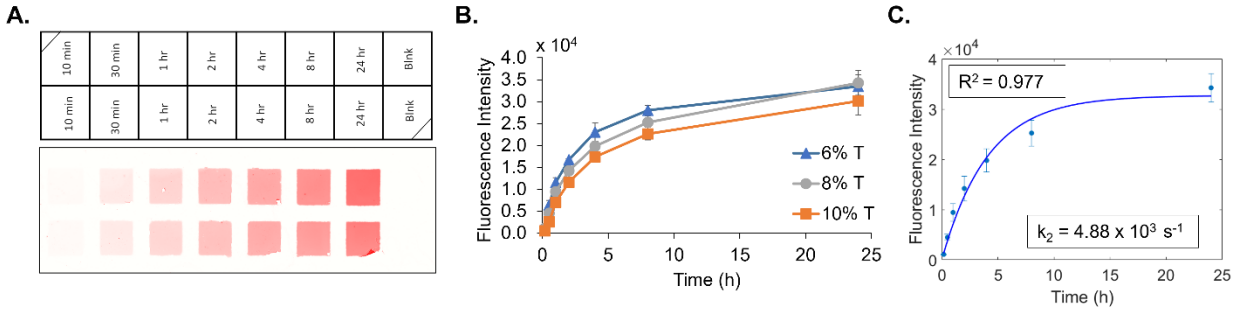

Figure 4-2: HCR in gel follows pseudo first-order DNA hybridization kinetics with a consistent time for reaction completion across gel densities. (A) gel micrograph demonstrates an increase in fluorescence intensity with time in an 8% T gel with an immobilized initiator concentration of 100 nM, (B) reaction completion occurs within 10s of hours with consistent final signal across gel densities, as indicated by signal plateaus at ~24 h, (C) a pseudo first-order model of DNA hybridization fits HCR data very well, allowing for the extraction of kinetic constants (8% T depicted but comparable fit across gel densities). Plots represent n ≥ 2 gel regions from n≥1 gel(s) with standard deviation error bars.

In-Gel HCR Follows Pseudo First-Order DNA Hybridization Kinetics

Further extending upon the measurement of the in-gel reaction timescale, we sought to fit a reaction kinetics model to the data. DNA hybridization has been shown to follow pseudo first-order kinetics when one strand is in excess[20]. The fraction of single stranded DNA is represented by the following equation:

$$f_{ss} = e^{-k_2 C_0 t} \qquad \text{(Equation 4-1)}$$

where k_2 is the kinetic constant, C_0 is molar nucleotide residue concentration, and t is the time. We hypothesized that HCR would follow pseudo first-order DNA hybridization kinetics, since HCR is inherently a DNA hybridization process. Data were fitted to the following equation, which represents the rate of formation of dsDNA as the reaction progresses:

$$\text{fluorescence} = K[1-e^{-k_2 C_0 t}] \quad \text{(Equation 4-2)}$$

where K is a proportionality constant. When the 8%T data are fitted to the pseudo first-order reaction kinetic model via least squares fitting, a very good fit is obtained with an R^2 value of 0.977 and a kinetic rate constant of 4.88 x 10^4 s^{-1} (Fig. 4-2C). Good fits are obtained across different gel densities, such that the kinetic constants were obtained for the 6% T, 8% T, and 10% T gels (Table 4-1). While the kinetic rate constant of the 8% T gel is only 13% higher than the rate constant of the 10% T gel, the rate constant of the 6% T gel is 1.7-fold higher than the

10% T gel. The good model fits observed suggest that in-gel HCR follows pseudo first-order DNA hybridization kinetics for all gel densities evaluated. Experimental kinetic rate constants are lower than predicted by theory for HCR hybridization in solution but are still within an order of magnitude of the theoretically predicted value of 2.8×10^4 s^{-1}. The slower in-gel reaction kinetics and the dependence of the reaction kinetics on the gel density are likely explained by diffusion and/or partitioning since these factors have not been specifically decoupled when fitting the models to the gel fluorescence. However, the general trend suggests that the in-gel HCR data can be fit with a pseudo first order DNA hybridization kinetics model.

Table 4-1: HCR in gel fits a DNA hybridization kinetics model with kinetics constants that decrease with increasing gel density.

Gel Density	**k_2 (s^{-1})**
6%	7.33×10^3
8%	4.88×10^3
10%	4.32×10^3

Linear Concentration Dependent Response Observed as Reaction Proceeds to Completion
Another essential aspect of a quantitative in-gel fluorescence assay is a linear concentration dependent response[4]. While in-gel HCR generates strong signal after a much shorter time than the 24 h necessary for reaction completion, differences in reaction rates could result in a nonlinear concentration dependent response for an incomplete reaction. Therefore, it is important to understand whether in-gel HCR exhibits a linear concentration dependent response and whether this response is dependent on the degree of reaction completion. When three DNA initiator concentrations ranging from 50-200 nM were evaluated, the fluorescence signal did not follow a strong linear trend for short incubation times (Fig. 4-3A). However, the response was linear for longer incubation times, as indicated by the increase in the R^2 values associated with longer incubation times (Fig. 4-3A). The results thus indicate that in-gel HCR exhibits a linear concentration dependent response, but only as the reaction proceeds toward completion. This result of increasing linearity with time is consistent with the steep initial increase in fluorescence that occurs (Fig. 4-2), which results in a larger initial difference in signal between the different concentrations. Ultimately, our results indicate that it will be important to run the reaction to completion when signal quantification is desired.

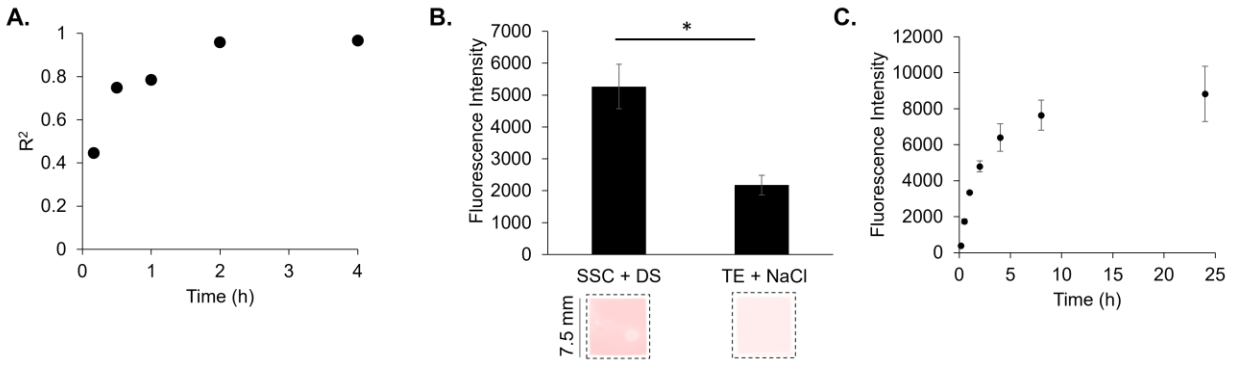

Figure 4-3: Assay time and buffer composition are key factors for HCR assay design in gel. (A) linearity of the signal-concentration dependence increases as the reaction proceeds toward

completion as indicated by an increase in the correlation coefficient (R^2) with time for three concentrations ranging from 50 nM-200 nM, (B) the use of a high salt sodium saline citrate buffer (SSC) with the molecular crowding agent dextran sulfate (DS) results in over a 2-fold increase in fluorescence signal over TE buffer with 0.32 M NaCl for a 2 h incubation time (n = 5 with standard deviation error bars), (C) Signal plateau is reached after ~24 h in buffer with DS, comparable to buffer w/o DS (n = 2 with standard deviation error bars). Statistical significance, *p<0.05, was determined by a Mann-Whitney U-test.

Changes in Buffer Composition Result in Doubling of Signal

Finally, we sought to evaluate the effects of including the molecular crowding agent dextran sulfate in the HCR buffers on the fluorescence signal and reaction kinetics. A previous microarray hybridization study found that inclusion of 10% dextran sulfate resulted in an ~3-fold increase in signal[22]. We sought to specifically evaluate the effect of 10% dextran sulfate on the degree of signal amplification and the time for reaction completion for in-gel HCR. Since our system is transport limited, we hypothesized that the time for reaction completion would not be different, but that the max signal would be higher. The resultant signal after a 2 h incubation with 10% dextran sulfate in 5xSSC buffer was twice the signal achieved when using the 0.32 M NaCl in 1xTE buffer, which was employed in all our other experiments (Fig. 4-3B). However, the overall reaction kinetics curve and time necessary for reaction completion still appear to be ~24 h despite the inclusion of dextran sulfate (Fig. 4-3C). The two-fold increase in signal for the in-gel HCR system agrees well with the microarray literature[22]. However, our system is different due to the gel pores, which size exclude the large dextran sulfate molecules. The molecular weight of the dextran sulfate is 500 kDa, which has a corresponding hydrodynamic radius of 15.9 nm, and an estimated partition coefficient in an 8% T gel of 10^{-7}, indicating near complete exclusion[34]. A resultant working hypothesis is that the size excluded dextran sulfate results in increased partitioning of the DNA hairpins into the gel, which overcomes the effect of the shrinking pores as the reaction proceeds to completion. The second result of no change in the assay timescale is consistent with the transport limited nature of the process. Overall, use of HCR buffers that contain 10% dextran sulfate is a promising strategy to maximize the fluorescence signal but does not reduce the time necessary for reaction completion.

Reproducibility Challenges

The 6% T and 10% T data shown in Fig. 4-2 and Table 4-1 come from n = 2 gel regions from one gel. Due to limited building access during the COVID-19 pandemic and work on other projects, work on this project was halted for ~1 year. When we began to run experiments again to obtain more replicates, we observed drastically different results. The plateau fluorescence intensity values at the longest time points were in the same range as previously in the 6% T gels, but the fluorescence intensity values corresponding to the shorter incubation times were much lower (Fig. 4-4). In the 10% T gels, the both the final fluorescence at 24 h and at the earlier timepoints was much lower in the later experiments (Fig. 4-4).

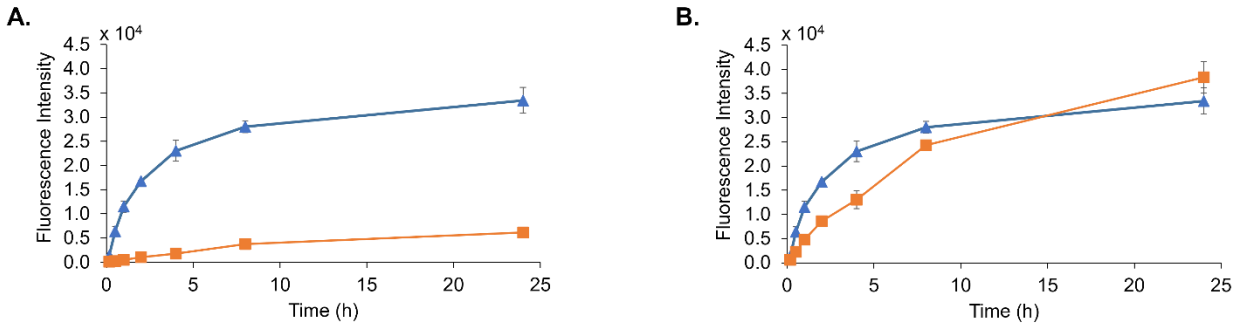

Figure 4-4: A marked difference in the fluorescence response to HCR incubation time was observed between experimental replicates in (A) 10% T gels, and (B) 6% T gels. Blue with triangular markers represents the older data set, while orange with square markers represents the newer data set. The mean of n = 2 gel regions on the same gel with standard deviation error bars is reported for each condition.

To test our hypothesis that variability resulting from different batches of HCR reagents was causing the drastically different results, we applied HCR hairpin solution to blank gel regions on one of the gels from the previous year and to a fresh gel. In the old gel, we observed results that were comparable to the previous results, while the new gel exhibited the reduced fluorescence. This led us to conclude that the issue is related to the gels rather than the HCR hairpin solution. Another hypothesis for the divergent results was that dichlorodimethylsilane residue from the silicon wafer mold was coating the gel surface, hindering the penetration of the HCR hairpins into the gel. This hypothesis came about as we observed that the surface of the new gels appeared more hydrophobic than the surface of the older gels. Such a difference in surface hydrophobicity could arise from differences in the amount of excess silane residue on the silicon wafer mold. To test the silane residue hypothesis, the silicon wafer mold was treated with NaOH to remove excess silane residue prior to gel fabrication. While the surface of the resultant gel appeared less hydrophobic, there was no substantial difference in the fluorescence after a 1 h incubation with HCR hairpin solution. This result led us to conclude that gel surface hydrophobicity is likely not the cause of the divergent results.

The data in Fig. 4-4 was obtained without inclusion of DS in the HCR hairpin solution. Surprisingly, when DS was included in the hairpin solution, the results matched the previous DS data. We do not have an explanation for why the more recent DS data matched the previous data, while the non-DS data did not. The DS result does suggest that the older data likely represents the correct trends of fluorescence increase over time for gels exposed to the HCR hairpins. However, future work is needed to troubleshoot the causes of the variability. We posit that the differences between the data sets likely involve the gels. Overall, our results from this study represent a start to detailed characterization of in-gel HCR assays.

4.4 Conclusions

In conclusion, we demonstrate that in-gel HCR reaches completion after 24 hours, follows pseudo first-order DNA hybridization kinetics, and results in three orders of magnitude of signal amplification that is consistent across different gel densities. Furthermore, we found that the linearity of the concentration dependent response depends on the degree of completion of the reaction and that employing a reaction buffer that contains the molecular crowding agent dextran sulfate results in double the fluorescence signal but does not affect the time for reaction completion. These results can be used to inform in-gel assay design with regard to the reaction times and buffer compositions for maximum signal and accurate analyte quantification. Improved in-gel HCR assays will ultimately allow for sensitive and accurate quantification of low-abundance biomolecules, which will advance biological inquiry.

4.5 Bibliography

(1) Chung, K.; Wallace, J.; Kim, S.; Kalyanasundaram, S.; Andalman, A. S.; Davidson, T. J.; Mirzabekov, J. J.; Zalocusky, K. A.; Mattis, J.; Denisin, A. K.; Pak, S.; Bernstein, H.; Ramakrishnan, C.; Grosenick, L.; Gradinaru, V.; Deisseroth, K. Structural and Molecular Interrogation of Intact Biological Systems. *Nature* **2013**, *497*, 332–339. https://doi.org/10.1038/nature12107.

(2) Chen, F.; Tillberg, P. W.; Boyden, E. S. Expansion Microscopy. *Science (80-.).* **2015**, *347* (6221), 543–548.

(3) Wassie, A. T.; Zhao, Y.; Boyden, E. S. Expansion Microscopy: Principles and Uses in Biological Research. *Nat. Methods* **2019**, *16* (January), 33–41. https://doi.org/10.1038/s41592-018-0219-4.

(4) Hughes, A. J.; Spelke, D.; Xu, Z.; Kang, C. C.; Schaffer, D.; Herr, A. E. Single-Cell Western Blotting. *Nat. Methods* **2015**, *11* (7), 455–464. https://doi.org/10.1007/978-1-4939-2694-7_46.

(5) Tentori, A. M.; Yamauchi, K. A.; Herr, A. E.; John, L.; Dewar, L.; Distinguished, L. Detection of Isoforms Differing by a Single-Charge Unit in Individual Cells. *Angew. Chemie - Int. Ed.* **2017**, *55* (40), 12431–12435. https://doi.org/10.1002/anie.201606039.

(6) Kang, C.; Ward, T. M.; Bockhorn, J.; Schiffman, C.; Huang, H.; Pegram, M. D.; Herr, A. E. Electrophoretic Cytopathology Resolves ERBB2 Forms with Single-Cell Resolution. *npj Precis. Oncol.* **2018**, No. February, 1–10. https://doi.org/10.1038/s41698-018-0052-3.

(7) Dirks, R. M.; Pierce, N. A. Triggered Amplification by Hybridization Chain Reaction. *Proc. Natl. Acad. Sci.* **2004**, *101* (43), 15275–15278. https://doi.org/10.1073/pnas.0407024101.

(8) Bi, S.; Yue, S.; Zhang, S. Hybridization Chain Reaction: A Versatile Molecular Tool for Biosensing, Bioimaging, and Biomedicine. *Chem. Soc. Rev.* **2017**, *46* (14), 4281–4298. https://doi.org/10.1039/C7CS00055C.

(9) Shah, S.; Lubeck, E.; Schwarzkopf, M.; He, T.-F.; Greenbaum, A.; Sohn, C. H.; Lignell, A.; Choi, H. M. T.; Gradinaru, V.; Pierce, N. A.; Cai, L. Single-Molecule RNA Detection at Depth by Hybridization Chain Reaction and Tissue Hydrogel Embedding and Clearing. *Development* **2016**, *143* (15), 2862–2867. https://doi.org/10.1242/dev.138560.

(10) Lin, R.; Feng, Q.; Li, P.; Zhou, P.; Wang, R.; Liu, Z.; Wang, Z.; Qi, X.; Tang, N.; Shao, F.; Luo, M. A Hybridization-Chain-Reaction-Based Method for Amplifying Immunosignals. *Nat. Methods* **2018**, *15* (4), 275–278. https://doi.org/10.1038/nmeth.4611.

(11) Hughes, A. J.; Lin, R. K. C.; Peehl, D. M.; Herr, A. E. Microfluidic Integration for Automated Targeted Proteomic Assays. *Proc. Natl. Acad. Sci.* **2012**, *109* (16), 5972–5977. https://doi.org/10.1073/pnas.1108617109.

(12) Amsden, B. Solute Diffusion within Hydrogels. Mechanisms and Models. *Macromolecules* **1998**, *31*, 8382–8395. https://doi.org/10.1021/ma980765f.

(13) Su, A.; Smith, B. E.; Herr, A. E. In Situ Measurement of Thermodynamic Partitioning in Open Hydrogels. *Anal. Chem.* **2019**, *92* (2), 875–883. https://doi.org/10.1021/acs.analchem.9b03582.

(14) Vlassakis, J.; Herr, A. E. Effect of Polymer Hydration State on In-Gel Immunoassays. *Anal. Chem.* **2015**, *87* (21), 11030–11038. https://doi.org/10.1021/acs.analchem.5b03032.

(15) Pregibon, D. C.; Doyle, P. S. Optimization of Encoded Hydrogel Particles for Nucleic Acid Quantification. *Anal. Chem.* **2009**, *81* (12), 4873–4881. https://doi.org/10.1021/ac9005292.

(16) Tentori, A. M.; Nagarajan, M. B.; Kim, J. J.; Zhang, W. C.; Slack, F. J.; Doyle, P. S. Quantitative and Multiplex MicroRNA Assays from Unprocessed Cells in Isolated Nanoliter Well Arrays. *Lab Chip* **2018**, *18* (16), 2410–2424. https://doi.org/10.1039/c8lc00498f.

(17) Joubert, A. M.; Byrd, A. S.; LiCata, V. J. Global Conformations, Hydrodynamics, and X-Ray Scattering Properties of Taq and Escherichia Coli DNA Polymerases in Solution. *J. Biol. Chem.* **2003**, *278* (28), 25341–25347. https://doi.org/10.1074/jbc.M302118200.

(18) Williams, J. C.; Mark, L. A.; Eichholtz, S. Partition and Permeation of Dextran in Polyacrylamide Gel. *Biophys. J.* **1998**, *75* (1), 493–502. https://doi.org/10.1016/S0006-3495(98)77538-1.

(19) Likhachev, E. R. Dependence of Diffusion on Temperature and Pressure. *Tech. Phys.* **2007**, *48* (4), 127–149. https://doi.org/10.1007/978-3-540-71488-0_8.

(20) Wetmur, J. G. DNA Probes : Applications of the Principles of Nucleic Acid Hybridization DNA Probes : Applications of the Principles of Nucleic Acid Hybridization. *Crit. Rev. Biochem. Mol. Biol.* **1991**. https://doi.org/10.3109/10409239109114069.

(21) Stellwagen, N. C. Apparent Pore Size of Polyacrylamide Gels: Comparison of Gels Cast and Run in Tris-Acetate-EDTA and Tris-Borate-EDTA Buffers. *Electrophoresis* **1998**, *19* (10), 1542–1547. https://doi.org/10.1002/elps.1150191004.

(22) Ku, W. C.; Lau, W. K.; Tseng, Y. T.; Tzeng, C. M.; Chiu, S. K. Dextran Sulfate Provides a Quantitative and Quick Microarray Hybridization Reaction. *Biochem. Biophys. Res. Commun.* **2004**, *315* (1), 30–37. https://doi.org/10.1016/j.bbrc.2004.01.013.

(23) Kuznetsova, I. M.; Turoverov, K. K.; Uversky, V. N. *What Macromolecular Crowding Can Do to a Protein*; 2014; Vol. 15. https://doi.org/10.3390/ijms151223090.

(24) Wetmur, J. G. Acceleration of DNA Renaturation Rates. *Biopolymers* **1975**, *14* (12), 2517–2524. https://doi.org/10.1002/bip.1975.360141208.

Chapter 5: Characterization of Immuno-Hybridization Chain Reaction for In-Gel Protein Signal Amplification

5.1 Introduction

Fluorescence immunoassays suffer from poor lower limits of detection (LLOD) due to the lack of signal amplification in most methods[1] and limitations in target multiplexing due to spectral overlap of fluorophores[2]. DNA-antibody conjugates are increasingly being employed in immunoassays to harness the power of DNA technologies for signal amplification and multiplexing. Improved LLOD and multiplexing capabilities have been achieved in many assays that use DNA-antibody conjugates[1,3–6]. One specific class of immunoassays that would benefit immensely from LLOD improvements is single-cell immunoblotting, a set of in-gel immunoassays that combine single-cell electrophoretic separations with an immunoassay stage for highly specific protein detection[7–9]. The LLOD of the single-cell western blot (scWB) is currently estimated to be ~170,000 protein copies per cell[7,10], which is close to the median protein copy number in a mammalian cell[11]. Therefore, only ~50% of proteins in a mammalian cell are expressed at a sufficient level to be detected by the scWB. Based on the distribution of protein expression in a mammalian cell[11], we estimate that a 5-fold improvement in the LLOD of the scWB would result in access to >80% of mammalian proteome, while a 20-fold improvement in the LLOD would result in access to >99% of the mammalian proteome. These dramatic improvements to the LLOD have the potential to open the door to new areas of biological inquiry, since many low-abundance proteins, such as Caspase-3, play crucial roles in cellular processes[12].

Immuno-hybridization chain reaction (HCR) is an immunoassay signal amplification strategy that involves conjugating HCR initiator sequences to antibodies, immunoprobing with the antibody conjugates, and subsequently introducing fluorescently labeled HCR hairpins for signal amplification and detection[1,6,13,14]. Multiple studies have demonstrated a 2-3 order of magnitude increase in signal from immuno-HCR compared to direct labeled antibodies both on surfaces[1] and in gel-embedded cleared tissue[6,13]. HCR is a highly advantageous signal amplification strategy because it is isothermal, enzyme-free, simple, and involves few steps for strong signal amplification, when compared to other assays, such as rolling circle amplification (RCA)[1,15,16]. Additionally, the HCR hairpin probes are small such that they will easily partition and diffuse into a hydrogel, unlike the large concatemers characteristic of immunoSABER[17]. The numerous advantages of immuno-HCR over other signal amplification strategies make it a promising signal amplification strategy to improve the LLOD of single-cell immunoblotting.

While immuno-HCR has been applied to low density polyacrylamide gels in gel-embedded cleared tissue, it has not been applied to dense (>4% T) polyacrylamide hydrogels to the best of our knowledge. There is a need to specifically evaluate and characterize the performance of immuno-HCR in dense polyacrylamide gels, as the effects of thermodynamic partitioning and hindered diffusion are more pronounced in denser hydrogels[18,19]. Additionally, there have not been thorough characterizations of how DNA conjugation affects antibody binding and

thermodynamic partitioning behavior, despite knowledge that DNA conjugation reduces the binding affinity[20,21], and increases the molecular size, which will impact thermodynamic partitioning in hydrogels. Here, we seek to (1) characterize the impact of DNA conjugation on antibody binding affinity and thermodynamic partitioning, and (2) evaluate the performance of immuno-HCR against standard immunoprobing with fluorophore-labeled antibodies both in gel and in a well plate assay.

5.2 Materials and Methods

Reagents

All DNA oligomers were purchased from IDT (Coralville, IA, USA), including the DNA initiator with a 5' acrydite group for incorporation into the gel matrix, and the HCR hairpins with 5' Alexa Fluor (AF) 647 modifications. Mouse anti-ovalbumin (ab17293) was purchased from AbCAM. TurboGFP (FP552) was purchased from Axxora. Rabbit anti-turboGFP (PA5-22688), AF647-labled donkey anti-mouse (A31571), Alexa Fluor 647-labeled donkey anti-rabbit (A31573), DBCO-PEG5-NHS (NC0973990), and NHS-biotin (20217) were purchased from Thermo Fisher Scientific (Waltham, MA). Ovalbumin (A5503), bovine serum albumin (BSA, A9418), tetramethylethylenediamine (TEMED, T9281), ammonium persulfate (APS, A3678), 3-(trimethoxylsilyl)propyl methacrylate (440159), dichlorodimethylsilane (440272), dimethyl sulfoxide (DMSO), 30%T/3.3%C acrylamide/bis-acrylamide (29:1) (A3574), dextran sulfate (D8787), and SYPRO Ruby Protein Gel Stain (S4942) were purchased from Sigma-Aldrich (St. Louis, MO, USA). N-[3-[(3-Benzoylphenyl)formamido]propyl] methacrylamide (BPMAC) was custom synthesized by Pharm-Agra Laboratories (Brevard, NC, USA). Deionized water (18.2 MΩ) was obtained using an Ultrapure water system from Millipore. Buffers were prepared according to standard protocols[22].

Preparation of DNA-Antibody Conjugates

DNA-antibody conjugates were prepared by amine-reactive copper-free click chemistry similarly to previously published protocols[23]. DBCO-PEG5-NHS stock solution was prepared at a concentration of 8 mg/mL in DMSO. A buffer exchange step was performed on antibodies that came stored in buffer that contained sodium azide and/or tris by washing 3x in 10 kDa molecular weight cutoff (MWCO) filters (EMD Millipore, UFC501024) and eluting in a final volume of 50 µL of 1xPBS. DBCO crosslinker was then added to the antibody solution at 20 mol equivalents/mol of antibody, and additional buffer added for a final reaction volume of 200 µL for 100 µg of antibody. The antibody-crosslinker linking reaction proceeded for 2 h at room temperature followed by washing 3x in a 10 kDa MWCO filter and eluting in 1xPBS. Five mol equivalents of azide-terminated HCR initiator, prepared as a 500 µM stock solution in 1xTE buffer, was then added to the activated antibodies. The azide-DBCO reaction proceeded overnight at room temperature followed by storage of the conjugates at 4°C.

Non-Reducing SDS-PAGE

DNA-antibody conjugates were characterized by non-reducing SDS-PAGE analysis. Large pore size (6% T tris glycine) slab gels (Thermo Fisher Scientific, XP00065BOX) were used. Samples were prepared by diluting with 1xPBS to the desired concentration and mixing with 4x non-reducing laemmli buffer to a final 1x concentration of 62.5 mM Tris-HCl pH 6.8, 2.5% SDS, 0.002% bromophenol blue, and 10% glycerol. Prior to electrophoresis, samples were heated to 95°C for 5 min, followed by cooling to room temperature. Each sample was run on the gel in triplicate with 500 ng of sample per lane. Spectra Broad Range Protein Ladder (Thermo Fisher Scientific, PI26634) was run alongside the samples to confirm the size of the antibodies and the DNA-antibody conjugates. Electrophoresis was run at 120 V for 90 min. After electrophoresis, gels were fixed and stained according to the SYPRO Ruby quick stain protocol. Imaging was performed on a Bio Rad ChemiDoc XRS+, where the antibodies were imaged with the SYPRO Ruby auto exposure setting, the ladder imaged colorimetrically, and the channels merged in ImageJ.

Optical Biolayer Interferometry (BLI) Measurements

TurboGFP was biotinylated in house with NHS-biotin by adding 20 molar equivalents of 10 mM NHS-biotin in DMSO to a solution of 1 mg/mL turboGFP in 1xPBS. The biotinylation reaction was allowed to proceed for 30 min at room temperature and followed by 4 washes with 10 mM Tris HCl in a 10 kDa MWCO filter. For BLI experiments, biotinylated turboGFP was diluted to a concentration of 20 nM in BLI buffer #1 (1xPBS + 0.05% Tween20 + 0.2% BSA), and anti-turboGFP was diluted serially from 6.25-150 nM in BLI buffer #2 (same as #1 except with 10 µM biotin included). ForteBio streptavidin-coated BLI tips were hydrated in BLI buffer for at least 10 min prior to each experiment. BLI experiments were run on an Octet RED384 instrument (ForteBio). The antigen loading step was 2 min, followed by a 1 min wash, 15 min association, and 15 min dissociation. Data analysis, including a global fit to a bivalent analyte model, was carried out in the Octet Data Analysis Software.

Partition Coefficient Measurements

HCR initiator was conjugated to AF647-labeled donkey anti-mouse for partition coefficient measurements. Partition coefficient measurements were taken in 6% T polyacrylamide gels fabricated on chambered coverslips, following previously established methods[18]. Unconjugated and DNA-conjugated antibodies were diluted to concentrations of 0.1 µM in 1xPBS and incubated with the gels for >1 h to reach equilibrium. Confocal imaging took place on a Carl Zeiss LSM 710 AxioObserver inverted laser scanning confocal microscope using a C-Apochromat 40×/1.1 NA water-immersion objective with correction collar, following the AC-LSCM method[18]. Analysis consisted of employing the previously developed analysis pipeline[18] with a minor modification of leaving out the median filter step due to weak fluorescence from the low concentration of labeled antibody used in this experiment.

Immuno-HCR Well Plate Assay

Ovalbumin solution was prepared in 1xPBS at a concentration of 1 µg/mL and serially diluted for experiments with lower concentrations. Antibody solutions were prepared in 2% BSA in 1xTBST at a concentration of 10 µg/mL for the primary antibody (mouse anti-ovalbumin) and 20 µg/mL for the secondary antibody (AF647-labeled donkey anti-mouse). HCR hairpin solution was prepared at a concentration of 50 nM of each hairpin in HCR reaction buffer (5xSSC + 10% dextran sulfate). To each well of a Nunc maxisorp 96-well plate (Thermo Fisher Scientific, 437111), 100 µL of ovalbumin solution was added and the plate incubated for 2 h at room temperature. Each well was washed 2x with 1xTBST and then blocked with 2% BSA in 1xTBST buffer overnight at 4°C. Primary antibodies were incubated for 2 h at room temperature, while secondary antibodies and the HCR reaction were incubated for 1 h at room temperature. Each of the antibody and HCR incubations used 50 µL of solution per well. Wells were washed twice with 1xTBST between the primary and secondary probe incubations, and three times after secondary antibody incubation or HCR reaction.

Gel Fabrication

Polyacrylamide gels were fabricated on silicon wafer substrates with 40 µm rails patterned in SU-8, as previously reported[7,24]. Gel precursor solutions containing acrylamide/bis-acrylamide stock solution (30%, 29:1) were prepared to a concentration of 8% T and 3.3% C. BPMAC was added to a concentration of 3mM, followed by degassing via sonication for 5 min. APS and TEMED were then added to the precursor to a concentration of 0.08% each before pipetting the solution between the SU-8 wafer (rendered hydrophobic by treatment with dichlorodimethylsilane) and a glass microscope slide functionalized with 3 (trimethoxysilyl)propyl methacrylate. After a 15-min chemical polymerization, the slides with the attached gels were lifted from the wafers and washed in 1xPBS for at least 1 h prior to use in experiments.

In-Gel HCR

TurboGFP was photopatterned as 100 µm diameter spots in the gels following a previously established photopatterning protocol[25]. Briefly, turboGFP was diluted to a concentration of 100 nM in 1xPBS and 60 µL of protein solution pipetted onto each half slide gel. The gel with the protein solution was sandwiched against a coverslip and incubated for 10 min. A photomask was then placed under the coverslip, the sandwich transferred to a UV light source and exposed for 300 s at ~20 mW/cm^2. After UV exposure, the sandwiches were placed in 1xTBST buffer and the coverslips gently removed prior to a 1 h wash in 1xTBST, changing out the buffer halfway through. Gels were briefly rinsed in DI water and dehydrated and imaged for endogenous turboGFP fluorescence. Gels were then immunoprobed following standard single-cell western blot immunoprobing protocols[7] with a 2 h primary antibody probing time, and either a 1 h secondary antibody probing time or a 2 h HCR reaction time. DNA-conjugated polyclonal rabbit anti-turboGFP (primary) and AF647-labeled donkey anti-rabbit (secondary) antibodies were diluted to a concentration of 50 µg/mL in 1xTBST + 2% BSA. HCR hairpin solution was prepared at a concentration of 500 nM per hairpin in HCR buffer, as described above in the well plate assay.

Gel Imaging and Data Analysis

Imaging of the dehydrated gels was conducted using a GenePix 4300A microarray scanner equipped with 488 nm, 532 nm, 594 nm, and 635 nm lasers. TurboGFP endogenous fluorescence was measured in the 488 nm channel prior to immunoprobing, while AF647 fluorescence was measured in the 635 nm channel. Imaging settings chosen for high dynamic range without achieving saturation. Images were then analyzed with a modified version of the scWB analysis pipeline adapted to analyzing protein spots[25] to generate ROIs from each lane of the gel, calculate intensity profiles, fit gaussian peaks to the protein bands, and extract the intensity of the gaussian peaks. An R^2 threshold of 0.7 was chosen to identify good gaussian fitted peaks. SNRs were defined as the fluorescence signal intensity at the center of the fitted gaussian peak divided by the standard deviation of a 5 pixel gutter region that served as the background. The same fit bounds and indices from the endogenous turboGFP fluorescence analysis were applied to the immunoprobed images to obtain the AUC ratios of immunoprobed to endogenous fluorescence.

5.3 Results and Discussion

Preparation and Characterization of DNA-Antibody Conjugates

We first prepared DNA-antibody conjugates of anti-ovalbumin with the published HCR initiator sequence from Dirks and Pierce[15]. The design requirements of our assay include (1) a small linker that will minimize detrimental effects to antibody binding affinity and partitioning, (2) a simple conjugation procedure, and (3) ideally no need for complicated purification procedures. We chose copper-free click chemistry for its simplicity, robustness, strong covalent bond with a short linker, and because it has been used in many other similar studies[21,23,26,27]. Copper-free click chemistry uses a NHS-PEG5-DBCO crosslinker that has an NHS ester on one end for amine-reactive chemistry with the antibodies and a cyclooctyne ring on the other end for copper-free click chemistry with azide-labeled DNA oligonucleotides[23]. The reaction is outlined in Fig. 5-1A in a schematic, where a monoclonal mouse anti-ovalbumin was initially chosen as a model system. Briefly, the antibody is reacted with an excess of the NHS-PEG_5-DBCO crosslinker for 2 h at room temperature, followed by washing in a molecular weight cutoff filter (MWCO) to remove excess crosslinker, addition of an excess of azide-labeled HCR initiator, and overnight incubation at room temperature. The reaction products were then characterized with non-reducing SDS-PAGE and the gels stained with SYPRO Ruby protein stain (Fig. 5-1B). The unconjugated anti-ovalbumin antibody (150 kDa) migrated as expected against the protein ladder. DNA-antibody conjugates migrated slower than the unconjugated antibody, consistent with their larger molecular weights, and presented multiple bands that represent different degrees of labeling (DOLs).

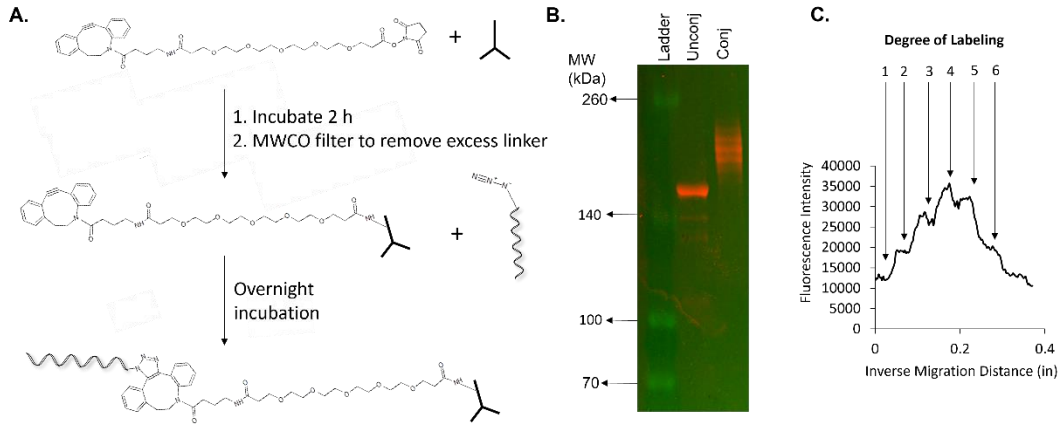

Figure 5-1: DNA-antibody conjugates with HCR initiator sequences were prepared via copper-free click chemistry and characterized by non-reducing SDS-PAGE. (A) Reaction scheme illustrates reaction of amine groups with the NHS ester of DBCO-PEG$_5$-NHS crosslinker followed by reaction of the cyclooctyne group with an azide-labeled DNA oligonucleotide. (B) Non-reducing SDS-PAGE analysis of the DNA-antibody conjugates (Conj) reveals slower migration of the conjugates and multiple bands that represent different degrees of labeling when compared to the unconjugated antibody (Unconj). (C) An intensity profile trace of the conjugate SDS-PAGE lane reveals multiple peaks representing different degrees of labeling from 1-6 DNA molecules per antibody. Note: molecular sizes not drawn to scale in schematic.

Achieving an optimal DOL is a crucial consideration when designing an immunoassay with DNA-antibody conjugates. A sufficiently high DOL for strong signal is necessary, but too high of a DOL can negatively impact antibody binding and/or partitioning. The advantage of a high DOL is that more DNA oligomers per antibody results in more initiation sites for HCR. However, too many molecules of DNA per antibody has been shown to result in interference with the antigen binding region of the antibody[21]. Over-labeling is especially a concern with non-specific amine-reactive chemistry, where DNA oligomers can bind to any region, including the antigen binding region. Other studies have found that 2-3 DNA oligos per antibody is optimal for signal with higher DOLs having a strong negative impact on antibody binding[20,21,23], so a DOL of 2-3 was our target. We selected 20 mol equivalents of crosslinker and 5 mol equivalents of azide-labeled DNA to start, since 20 equivalents of NHS-crosslinking reagent is a standard ratio for NHS reagents[28]. The reason for the lower molar ratio of the azide-labeled DNA is the higher efficiency of the click reaction[23].

Our conjugation protocol resulted in a range of 1-6 DNA oligomers per anti-ovalbumin antibody, as indicated by the peaks in the intensity profile trace of an SDS-PAGE lane (Fig. 5-1C).Based on the width of the peaks, we estimate that the average DOL is ~3.5 DNA oligomers per anti-ovalbumin, which is slightly higher than ideal but still within the optimal range of 2-5 observed by Sundah et al[20]. Therefore, we decided to move forward with this conjugation protocol for further DNA-antibody conjugate characterization and immuno-HCR experiments. In addition to conjugating the anti-ovalbumin antibody, we also conjugated AF647-labeled donkey anti-mouse for partitioning experiments and a polyclonal anti-turboGFP antibody. The average DOL of

AF647-labeled donkey anti-mouse comparable to anti-ovalbumin, but average DOL of anti-turboGFP was surprisingly drastically lower at ~1 DNA oligomer per antibody. While outside of the ideal range, a DOL of 1 is still considered acceptable for assay performance[20,21]. We do not currently have a firm hypothesis of why the DOL was so drastically different between the anti-turboGFP and the other antibodies. We observed the difference in multiple batches of both anti-ovalbumin and anti-turboGFP. Further investigation into the variability in DOL is an important aspect of future work. The primary conclusion is that we achieved conjugation of the HCR initiator DNA oligomer to our antibody probes with acceptable DOLs for our subsequent experiments.

Characterization of the Binding Affinity of DNA-Antibody Conjugates

Antibody binding kinetics govern immunoassay performance since the dissociation constant can be directly related to the amount of antigen-antibody complex formed at equilibrium and to the ratio of the kinetic rate constants (Eqn. 5-1)[29].

$$K_D = \frac{[Ab][Ag]}{[Ab\text{-}Ag]} = \frac{k_{off}}{k_{on}} \quad \text{(Equation 5-1)}$$

where K_D is the dissociation constant (M), [Ag] is the concentration of free antibody probe (M), [Ag] is the concentration of unbound antigen (M), [Ab-Ag] is the concentration of antigen-antibody complex, k_{off} is the dissociation rate constant (s^{-1}), and k_{on} is the association rate constant ($M^{-1}\ s^{-1}$).

Non-specific conjugation, especially with high degrees of labeling, is known to result in decreased antibody binding affinity[20,21]. Decreased binding affinity results in a lower concentration of antibody-antigen complex at equilibrium (Eqn. 5-1), which negatively impacts assay performance. There is a need to quantitatively characterize how antibody binding kinetics is impacted by DNA conjugation, since previous work has been largely qualitative or focused on the performance of a specific assay[20,21]. Optical biolayer interferometry (BLI) is a robust and simple technique to measure antibody binding kinetics[30]. BLI measures the interference pattern that occurs at the end of a glass tip when white light is passed between a layer with bound material and a reference layer. The change in the interference pattern as material binds to the sensor is then correlated to the thickness of the bound layer in nm, which serves as the readout. A BLI experiment involves four stages: (1) loading of biotinylated antigen onto the streptavidin pre-coated tips, (2) washing excess unbound antigen, (3) antibody binding in antibody solution to measure the kinetic association constant, (4) antibody dissociation in buffer to measure the kinetic dissociation constant. Antibody concentrations are titrated to bracket the anticipated K_D, where each sensor is dipped into a different concentration. Antibody binding affinity is then quantified in the instrument software by fitting the binding curves to a bivalent ligand binding model. BLI has been used before to measure the binding affinity of DNA-conjugated antibodies but no rigorous quantitative analysis was made[20]. Here, we seek to make quantitative measurements of the difference in antibody binding affinity between antibodies conjugated with the HCR-initiator sequence and unconjugated antibodies.

Initial BLI experiments with the anti-ovalbumin antibody indicated that it is a low affinity binder with a K_D of >300 nM. Measuring the affinity of such a low affinity binder would require

impractically high concentrations of antibody to obtain accurate measurements. For this reason, we opted for an antigen/antibody pair of turbo-GFP and a polyclonal rabbit anti-turboGFP antibody, which exhibited K_D values that were two orders of magnitude lower. When we varied the concentration of anti-turboGFP from 6.25-150 nM, we observed a concentration-dependent response to the amount of bound antibody, and less binding of the DNA-antibody conjugates compared to the unconjugated antibodies (Fig. 5-2A).

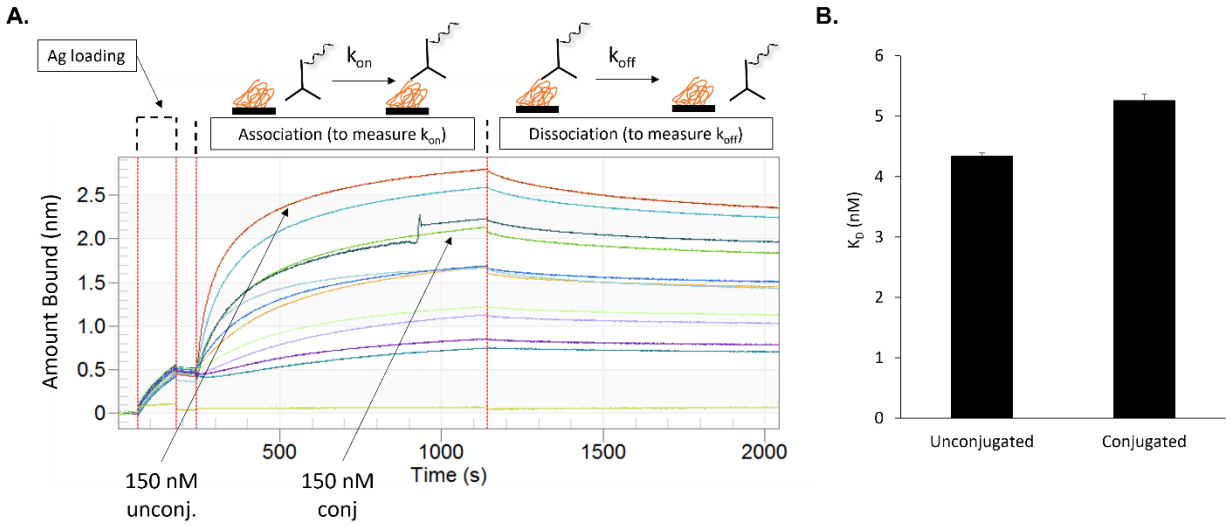

Figure 5-2: Optical biolayer interferometry measurement reveals reduced binding of DNA-antibody conjugates compared to unconjugated antibodies. (A) Each trace represents the binding of a different concentration of either unconjugated or DNA-conjugated anti-turboGFP. The traces for 150 nM unconjugated antibody and 150 nM DNA-conjugated antibody are indicated with arrows. (B) DNA conjugation results in a 17% increase in the dissociation constant values extracted from the fitted BLI data. Each condition consists of one replicate at each concentration with error bars representing deviation of the experimental data from the model fit.

The data were then fitted with a bivalent ligand model. Global fitting of a bivalent ligand model revealed fitted K_D values of ~5 nM, which indicate high-affinity binding for both the conjugates and the unconjugated antibodies (Fig. 5-2B). The DNA-conjugated antibodies exhibited a 17% higher K_D value compared to the unconjugated antibodies. The higher K_D value is indicative of weaker binding of the DNA-antibody conjugates and/or interference from the DNA labels. Despite the slight decrease in the binding affinity, the binding performance of the conjugates is strong, which suggests that assay performance will not be severely encumbered. One caveat to our results is that the quantitative K_D values may not be especially accurate. While the R^2 values of the model fits were high (>0.98), we observed that the curve shape of the model fits did not match the curve shape of the experimental data well (Fig. 5-3). There are many factors that can influence the shape of the curves and the subsequent quality of the fit in BLI, including the concentration of antigen used during antigen loading, and the buffer composition. Further

optimization would likely be necessary for improved fits and improved confidence in the quantitative values. Additionally, since each run consisted of only one replicate corresponding to each concentration, additional experimental runs are necessary to establish reproducibility and statistical significance. Despite the potential issues with the model fit and limited number of replicates, we are confident that our binding affinity measurements are in the correct order of magnitude and that the trend in the difference between conjugated and unconjugated antibodies holds. The overall trend is supported by a ~15% decrease in the amount bound of conjugated antibody bound in the 150 nM concentration, which closely matches the 17% difference obtained from the fitted values.

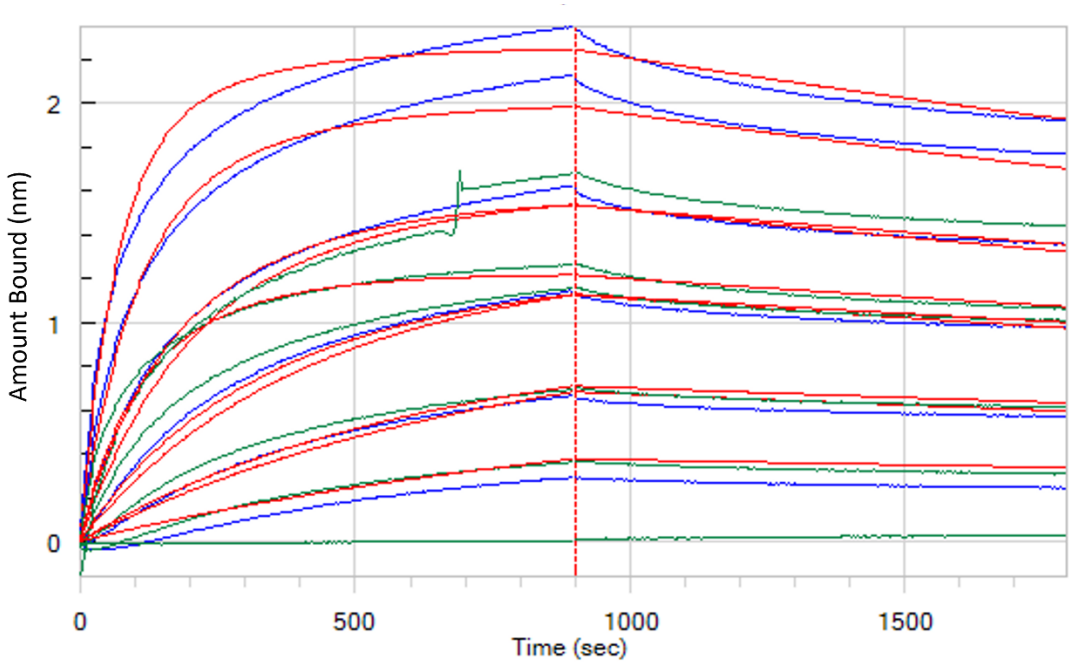

Figure 5-3: Curve shapes of bivalent analyte fits do not closely match the curve shapes of the BLI data. Red lines represent the model fits, while the blue and green curves represent the data.

Something else to note is that our results indicate less of an effect of DNA conjugation on antibody binding affinity than the results of a previous study[20]. The difference between our results and the previous results are not surprising because we conjugated a shorter DNA strand (18 nucleotides vs 30 nucleotides), and the turboGFP antibodies had a lower DOL (~1 vs 2.5) than the antibodies in the previous study. Sundah et al. found that 80 nucleotide DNA strands resulted in a substantial drop in antibody binding compared to 30 nucleotide DNA strands, which further supports this theory. An interesting area of future work would be to evaluate the effect of different degrees of labeling and DNA strand lengths on the antibody binding affinity. Additionally, the change in binding affinity upon conjugation should ideally be measured for more antigen-antibody pairs due to variability between different antibody-antigen pairs.

However, taken as a whole, our results provide a jumping off point for quantitative measurements of DNA-antibody binding affinity.

Evaluation of the Partitioning Behavior of DNA-Antibody Conjugates

Thermodynamic partitioning is a crucial property that governs in-gel assay performance[18,31]. The partition coefficient is defined as the ratio of the solute concentration in the gel to the solute concentration in the surrounding solution that is in equilibrium with the gel (Eqn. 5-2). Due to unfavorable thermodynamic interactions between solute molecules that are confined within hydrogel matrices, the solute concentration in the gel is lower than in the surrounding solution in the absence of attractive interactions between the solute and the gel matrix. Uncharged polyacrylamide gels follow the Ogston model of size-exclusion partitioning (Eqn. 5-3), which is dependent on the hydrodynamic radius of the molecule[18]. Therefore, larger molecules exhibit smaller partition coefficients in polyacrylamide hydrogels.

$$K = \frac{[\text{solute}]_{\text{gel}}}{[\text{solute}]_{\text{solution}}} \qquad \text{(Equation 5-2)}$$

$$K = \exp\left[-\phi\left(1 + \frac{R_h}{a_f}\right)^2\right] \qquad \text{(Equation 5-3)}$$

where [solute]gel is the concentration of the solute in the gel phase (M), $[\text{solute}]_{\text{solution}}$ is the concentration of the solute in the solution phase that is in equilibrium with the gel (M), Φ is the polymer volume fraction, R_h is the solute hydrodynamic radius (Å), and a_f is the polymer chain radius (Å).

An understanding of the partitioning behavior of large probes is essential for assay design, as larger probes require higher concentrations to counteract partitioning and achieve sufficiently high in-gel concentrations for complex formation. Additionally, when the partition coefficient is too small, molecules can be size excluded from the gel. The effect of DNA conjugation on antibody hydrodynamic radii, and the respective diffusion and partitioning properties, has not been thoroughly investigated before. Prior to developing in-gel assays with DNA-antibody conjugates, it is essential to understand how DNA conjugation affects the partitioning properties. Here, we test our hypothesis that conjugation of DNA oligomers to antibodies increases the hydrodynamic radius enough to result in a significant decrease in the partition coefficient

We measured the partition coefficients of DNA-conjugated Alexa Fluor (AF)647-labeled antibodies and unconjugated AF647-labeled antibodies with aberration-compensated laser scanning confocal microscopy (AC-LSCM), a technique developed by our group to make precise partition coefficient measurements in hydrogels[18] (Fig. 5-3A). Partition coefficients were measured in 6% T polyacrylamide gels that contained BPMAC and were exposed to UV prior to introduction of the antibody solution. We found that the partition coefficients of DNA-conjugated were significantly lower than the partition coefficients of the unconjugated antibodies (Fig. 5-3B). The average partition coefficient of the unconjugated antibodies was 0.0946 ± 0.0038, while the average partition coefficient of the DNA-conjugated antibodies was 63.4% lower at 0.0346 ± 0.0038.

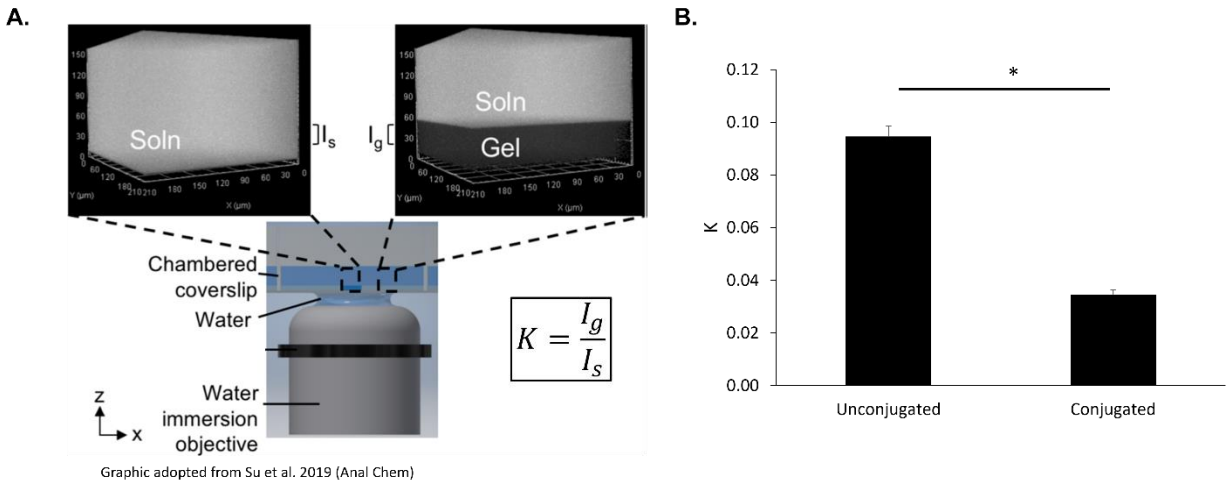

Figure 5-4: Partition coefficient measurements reveal reduced in-gel partitioning of DNA-antibody conjugates compared to unconjugated antibodies. (A) Aberration-compensated laser scanning confocal microscopy (AC-LSCM) enables precise quantification of partition coefficients by measuring the fluorescence of the gel and the solution at equilibrium while correcting for optical aberrations, (B) DNA conjugation of Alexa Fluor 647-labeled donkey anti-mouse results in a significant decrease of 63% in the partition coefficient. n = 4 gels per condition. Statistical significance was determined with a Mann-Whitney U-Test, where * = $p<0.05$.

While the partition coefficient of DNA-antibody conjugates is significantly lower than of unconjugated antibodies, a theoretical DNA signal amplification of 2-3 orders of magnitude would be sufficient to counteract the effects of reduced partitioning. However, if necessary, doubling or tripling the antibody concentration is feasible and would be sufficient to counteract the negative effect of DNA conjugation on partitioning. It is also important to note that the conjugates evaluated in this partitioning study had a high DOL of ~4 DNA oligomers per antibody. We hypothesize that there will be a lesser effect on the partitioning with a lower DOL of ~2 DNA oligomers per antibody. Studying the effect of the DOL on the partitioning behavior is an important area of future study. Overall, the results of our novel partitioning study of DNA-antibody conjugates suggest that differences in partitioning will not be large enough to counteract the benefits of signal amplification.

Characterization of Immuno-HCR in a Well Plate Assay

Prior to evaluating immuno-HCR in a polyacrylamide hydrogel system, we sought to validate immuno-HCR with our reagents and methods in a well plate fluorescence assay. The assay consisted of adsorbing ovalbumin to the well surface of 96-well plates, followed by BSA blocking, primary antibody probing (either unconjugated or DNA conjugated), and finally either HCR or probing with fluorophore-labeled secondary antibodies.

Immuno-HCR resulted in strong, detectable signal, yet standard probing with labeled secondary antibodies performed better and with less variability from run-to-run (Fig. 5-5A). We initially evaluated an antigen concentration of 1 µg/mL and thought that we may have been operating at a concentration above the linear dynamic range for immuno-HCR based on the results in Choi et al[1]. Thus, we hypothesized that immuno-HCR would perform better than standard probing with labeled secondary antibodies at lower antigen concentrations. However, standard probing with labeled secondary antibodies outperformed immuno-HCR at all concentrations evaluated (Fig. 5-5B).

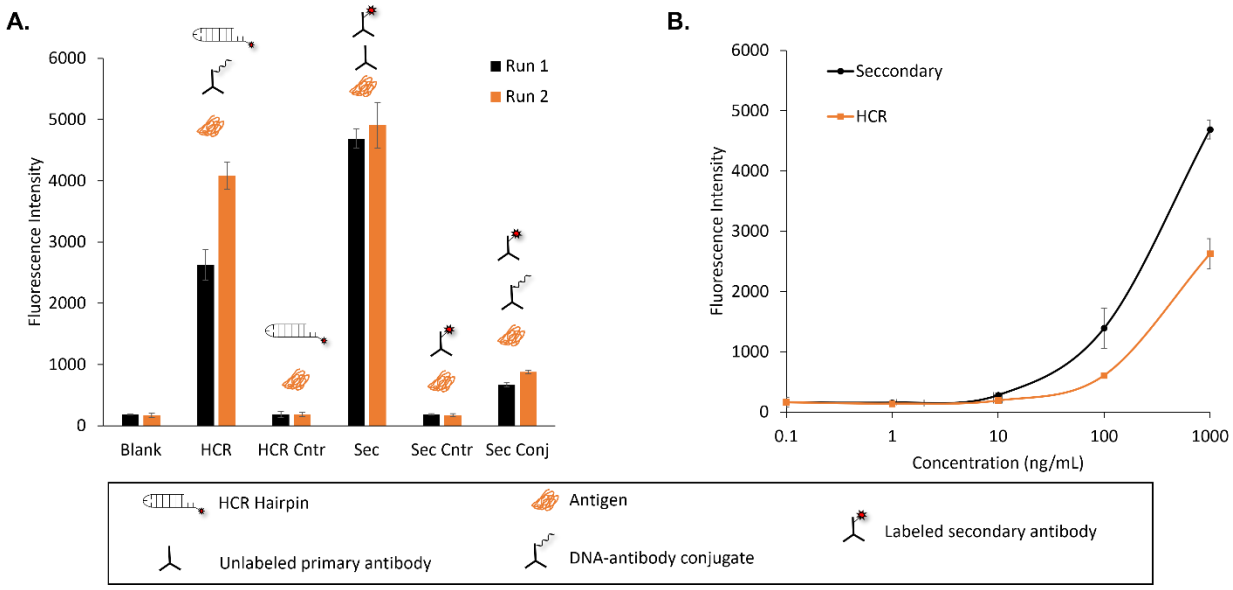

Figure 5-5: Detection of ovalbumin in well plate fluorescence immunoassays reveals that immuno-HCR results in strong signal albeit weaker signal than detection with fluorophore-labeled secondary antibodies. (A) Both immuno-HCR (HCR) and probing with unconjugated primary antibodies followed by a labeled secondary antibody (Sec) resulted in strong signal, while the controls (HCR Cntr and Sec Cntr), exhibited comparable signal to blank wells. Probing with DNA-antibody conjugates followed by labeled secondary antibodies (Sec Conj) resulted in far weaker signal than probing with unconjugated primary antibodies. (B) Varying the concentration of ovalbumin reveals a concentration-dependent fluorescence response with a lower limit of detection of 10-100 ng/mL for both the immuno-HCR and labeled secondary assays. All measurements were taken in triplicate with mean and standard deviation error bars reported.

Something of note is the generally poor performance of the well plate assay. We estimate that the LLOD is in the order of 10-100 ng/mL, which is much lower than anticipated based on the literature[1]. Lower antigen concentrations were not distinguishable from the controls, which consisted of blank wells and wells that were exposed to the fluorescently labeled probes in the absence of the antigen. In an attempt to improve the LLOD of the well plate assay, we evaluated different adsorption and blocking conditions, different concentrations of antibodies, different concentrations of HCR probes, different types of well plates designed for maximal adsorption, and multiple antigen-antibody pairs (ovalbumin and tGFP), all with similar results. Here, we are

only showing ovalbumin data since most optimized version of the assay was run with ovalbumin. Since we were not sure whether the poor performance of immuno-HCR in comparison to probing with labeled secondary antibodies was due to poor performance specific to the well plate assay, we decided to move to in-gel system to evaluate immuno-HCR.

Demonstration of In-Gel Immuno-HCR

Next, we sought to directly evaluate the performance of immuno-HCR in dense (8% T) polyacrylamide gels and compare to standard immunoprobing with fluorophore-labeled secondary antibodies. Our system to study in-gel immuno-HCR involved photopatterning proteins in polyacrylamide gels via benzophenone-chemistry with a previously established protocol[25] prior to immunoprobing. Gels were then immunoprobed with DNA-conjugated antibodies, followed by either probing with fluorophore-labeled secondary antibodies or HCR. We initially chose ovalbumin as our protein target and patterned AF555-labeled ovalbumin to be able to normalize the immunoprobed fluorescence to the fluorescence of the patterned protein spots. While the AF555-labeled ovalbumin spots were clearly detectable, the immunoprobed signal with AF647 was so weak that it was barely interpretable in all conditions. We hypothesize that the weak signal could be a result of the poor affinity of the anti-ovalbumin antibody or due to the use of labeled ovalbumin. For these reasons, we focused on the turboGFP system for in-gel experiments.

TurboGFP was photopatterned in 8% T polyacrylamide gels and subjected to either immunoprobing or immuno-HCR. Signal-to-noise ratios (SNRs) far greater than 3 were observed with both standard immunoprobing and immuno-HCR (Fig. 5-6A), suggesting good assay performance. The average SNR of a protein spot on the immuno-HCR gel was 9.06 ± 3.04, compared to 13.7 ± 8.82 on the gel that underwent standard immunoprobing. We also computed the ratios of the immunoprobed integrated fluorescence (AUC) to the endogenous turboGFP AUCs. Again, the AUC ratios of the spots on the immuno-HCR gel were significantly lower than on the standard immunoprobed gel at 0.476 ± 0.164, compared to 0.747 ± 0.581 (Fig. 5-6B). Another notable observation is that there were far more extreme high outliers on the standard immunoprobed gel than on the immuno-HCR gel.

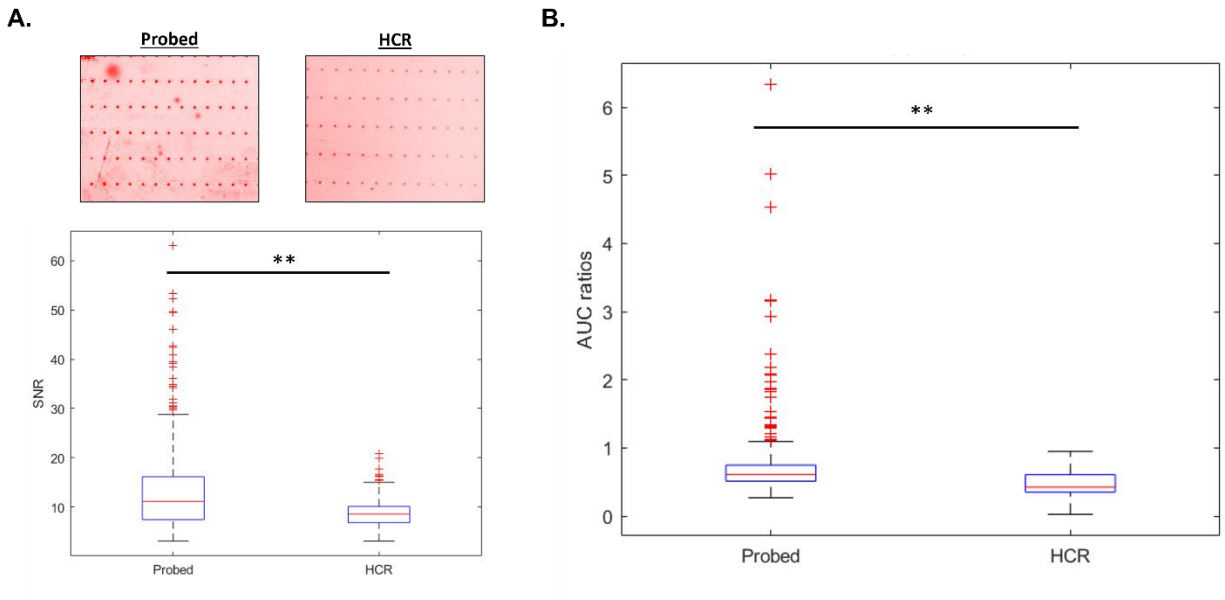

Figure 5-6: In-gel immuno-HCR of photopatterned turboGFP spots results in detectable yet weaker signal than standard immunoprobing with labeled secondary antibodies. (A) SNRs of immuno-HCR probed spots were significantly lower than SNRs of spots probed with labeled secondary antibodies, as shown quantitatively in the plot and qualitatively in the micrographs above. (B) Area under the curve fluorescence (AUC) ratios of the probed bands to the endogenous turboGFP fluorescence reveal significantly lower values for immuno-HCR than for probing with labeled secondary antibodies. Sample size: n = 350 spots from one gel in the probed condition and n = 218 spots from one gel in the immuno-HCR condition. Statistical significance was determined with Mann-Whitney U-Tests, where ** = $p<0.01$

One important caveat to these results is that DNA-conjugated antibodies were used in both the standard immunoprobing condition and the immuno-HCR condition. Our characterization of antibody binding affinity and partitioning revealed that both are negatively impacted by DNA conjugation. While we do not have results that provide a direct comparison between probing with unconjugated or DNA-conjugated antibodies prior to secondary immunoprobing, we have results from an experiment run under slightly different conditions, where we observed that spots probed with the DNA-conjugated anti-turboGFP were ~50% the intensity of spots probed with unconjugated antibody, while the background was ~75% of the intensity, suggesting a negative effect on the SNRs. We posit that much of this difference could be explained by reduced partitioning and/or reduced binding affinity of the DNA-antibody conjugates. Overall, the reduced signal in gels probed with DNA-conjugated primary antibodies suggests that the difference between the performance of immuno-HCR and standard immunoprobing is even greater than indicated in the data presented here, since the labeled secondary probing condition employed DNA-conjugated primary antibodies. Another observation to note about the immuno-HCR protocol is drastically uneven background across the gel such that there was no distinguishable signal and background that was two orders of magnitude lower on one side of the gel. We posit that uneven fluid layer thickness and/or poor mixing during exposure to the HCR hairpin solution could be responsible for the uneven background, analogous to previous results

we have observed with standard immunoprobing[25]. Since HCR results in signal amplification, it is possible that any difference from uneven fluid layer thickness or mixing would have an oversized effect. The cause of the uneven background is a crucial area of further investigation in the future.

Overall, our in-gel results were contrary to our hypothesis of stronger signal in the immuno-HCR condition. As in the well plate assay, standard immunoprobing always outperformed immuno-HCR. Despite the relative difference in performance, immuno-HCR resulted in good assay performance, indicated by strong fluorescence signal compared to background and SNRs>>3. We initially suspected that poor HCR performance was responsible for standard immunoprobing outperforming immuno-HCR. However, further review of the literature revealed that previous studies that employed DNA-based signal amplification and observed amplification of multiple orders of magnitude were comparing to an unamplified case of a single fluorophore labeled probe hybridized to DNA-conjugated antibodies[17,32]. Fluorophore labeled secondary antibodies are conjugated to multiple fluorophores per antibody, and multiple secondary antibodies are capable of binding to a primary antibody, resulting in a modest degree of signal amplification[33]. Saka et al. developed immuno-SABER, an immunoassay with a novel DNA-based signal amplification method[17]. They directly compared the signal from DNA-conjugated antibodies with single labeled DNA probes to linear immuno-SABER, branched versions of immuno-SABER, and immunoprobing with labeled secondary antibodies in fixed cells. Linear immuno-SABER, which would be analogous to linear HCR, resulted in comparable performance to probing with labeled secondary antibodies, while the branched versions resulted in additional signal amplification of another 1-2 orders of magnitude[17]. Additionally, we ran experiments where a single fluorophore labeled DNA strand was hybridized to either immobilized DNA in the gel (see Chapter 4) or a gel probed with DNA-antibody conjugates and observed signal that was indistinguishable from negative controls that did not contain the immobilized DNA or DNA-antibody conjugates. These results suggest that the linear DNA-based signal amplification was not sufficient to result in amplification over immunoprobing with fluorophore-labeled secondary antibodies. We posit that the linear HCR method that we evaluated is likely not resulting in sufficient signal amplification to outperform standard immunoprobing. Branched HCR strategies have been shown to result in orders of magnitude of signal amplification over standard linear HCR[34,35]. Additionally, HCR initiator conjugation to secondary antibodies has been demonstrated and could result in modest signal amplification[14].

Future work involves investigating branched HCR and other strategies to achieve additional signal amplification. We hypothesize that an immuno-HCR assay with additional signal amplification would outperform standard immunoprobing. Additional work includes validating the results presented here in more gels and with more antigen-antibody pairs to ensure that the method is reproducible and broadly applicable to multiple protein targets. Overall, our preliminary results suggest that immuno-HCR is a promising readout strategy for immobilized proteins in dense polyacrylamide hydrogels.

5.4 Conclusions

Here, we (1) characterized the binding affinity and partitioning behavior of DNA-antibody conjugates and (2) compared the performance of immuno-HCR to standard immunoprobing with

fluorophore-labeled secondary antibodies in both a well plate assay and an in-gel assay. First, we found that conjugation of DNA to antibodies results in modest decreases in the both the binding affinity and the partitioning that will impact assay performance but can likely be overcome with sufficient signal amplification and adjustment of the reagent concentrations. Immuno-HCR experiments revealed strong signal in the well plate assay and the in-gel assay that utilized photopatterned protein. However, standard immunoprobing with fluorophore-labeled secondary antibodies outperformed immuno-HCR both in the well plate assay and the in-gel assay We concluded that the amount of signal amplification achieved by immuno-HCR is likely not sufficient to overcome the decreased partitioning and binding affinity of the DNA-antibody conjugates and the inherent signal amplification already present in our standard immunoprobing protocol with labeled secondary antibodies.

While the linear HCR protocol evaluated in our study did not result in improved in-gel protein signal, there are branched HCR methods that can achieve improvements of multiple orders of magnitude over linear HCR. Future work with branched HCR and other strategies that increase the amount of signal amplification have the potential to improve in-gel immunoassay signal and improve the LLOD of single-cell immunoblotting. While we did not demonstrate improved in-gel immunoassay performance with immuno-HCR, our findings are an important tangible step toward applying DNA signal amplification strategies with DNA-conjugated antibodies to single-cell immunoblotting and other in-gel immunoassays. Ultimately, our results suggest that immuno-HCR is a feasible readout strategy for single-cell immunoblotting

5.5 Bibliography

(1) Choi, J.; Love, K. R.; Gong, Y.; Gierahn, T. M.; Love, J. C. Immuno-Hybridization Chain Reaction for Enhancing Detection of Individual Cytokine-Secreting Human Peripheral Mononuclear Cells. *Anal. Chem.* **2011**, *83* (17), 6890–6895. https://doi.org/10.1038/jid.2014.371.

(2) Kage, D.; Hoffmann, K.; Nifontova, G.; Krivenkov, V.; Sukhanova, A.; Nabiev, I.; Resch-Genger, U. Tempo-Spectral Multiplexing in Flow Cytometry with Lifetime Detection Using QD-Encoded Polymer Beads. *Sci. Rep.* **2020**, *10* (1), 1–11. https://doi.org/10.1038/s41598-019-56938-2.

(3) Goltsev, Y.; Samusik, N.; Kennedy-Darling, J.; Vazquez, G.; Black, S.; Correspondence, G. P. N.; Bhate, S.; Hale, M.; Nolan, G. P. Deep Profiling of Mouse Splenic Architecture with CODEX Multiplexed Imaging In Brief A DNA Barcoding-Based Imaging Technique Uses Multiplexed Tissue Antigen Staining to Enable the Characterization of Cell Types and Dynamics in a Model of Autoimmune Diseas. *Cell* **2018**, *174* (4), 1–14. https://doi.org/10.1016/j.cell.2018.07.010.

(4) Stoeckius, M.; Hafemeister, C.; Stephenson, W.; Houck-loomis, B.; Chattopadhyay, P. K.; Swerdlow, H.; Satija, R.; Smibert, P. Large-Scale Simultaneous Measurement of Epitopes and Transcriptomes in Single Cells. *Nat. Methods* **2017**, *14* (9), 865–868. https://doi.org/10.1038/nmeth.4380.Large-scale.

(5) Peterson, V. M.; Zhang, K. X.; Kumar, N.; Wong, J.; Li, L.; Wilson, D. C.; Moore, R.; Mcclanahan, T. K.; Sadekova, S.; Klappenbach, J. A. Multiplexed Quantification of Proteins and Transcripts in Single Cells. *Nat. Biotechnol.* **2017**, *35* (10), 936–939. https://doi.org/10.1038/nbt.3973.

(6) Lin, R.; Feng, Q.; Li, P.; Zhou, P.; Wang, R.; Liu, Z.; Wang, Z.; Qi, X.; Tang, N.; Shao, F.; Luo, M. A Hybridization-Chain-Reaction-Based Method for Amplifying Immunosignals. *Nat. Methods* **2018**, *15* (4), 275–278. https://doi.org/10.1038/nmeth.4611.

(7) Hughes, A. J.; Spelke, D.; Xu, Z.; Kang, C. C.; Schaffer, D.; Herr, A. E. Single-Cell Western Blotting. *Nat. Methods* **2015**, *11* (7), 455–464. https://doi.org/10.1007/978-1-4939-2694-7_46.

(8) Tentori, A. M.; Yamauchi, K. A.; Herr, A. E.; John, L.; Dewar, L.; Distinguished, L. Detection of Isoforms Differing by a Single-Charge Unit in Individual Cells. *Angew. Chemie - Int. Ed.* **2017**, *55* (40), 12431–12435. https://doi.org/10.1002/anie.201606039.

(9) Kang, C.; Ward, T. M.; Bockhorn, J.; Schiffman, C.; Huang, H.; Pegram, M. D.; Herr, A. E. Electrophoretic Cytopathology Resolves ERBB2 Forms with Single-Cell Resolution. *npj Precis. Oncol.* **2018**, No. February, 1–10. https://doi.org/10.1038/s41698-018-0052-3.

(10) Vlassakis, J.; Herr, A. E. Effect of Polymer Hydration State on In-Gel Immunoassays. *Anal. Chem.* **2015**, *87* (21), 11030–11038. https://doi.org/10.1021/acs.analchem.5b03032.

(11) Li, J. J.; Bickel, P. J.; Biggin, M. D. System Wide Analyses Have Underestimated Protein Abundances and the Importance of Transcription in Mammals. *PeerJ* **2014**.

https://doi.org/10.7717/peerj.270.

(12) Shi, M.; Geng, X.; Wang, C.; Guan, Y. Quantification of Low Copy Number Proteins in Single Cells. *Anal. Chem.* **2019**, *91* (18), 11493–11496. https://doi.org/10.1021/acs.analchem.9b02989.

(13) Shah, S.; Lubeck, E.; Schwarzkopf, M.; He, T.-F.; Greenbaum, A.; Sohn, C. H.; Lignell, A.; Choi, H. M. T.; Gradinaru, V.; Pierce, N. A.; Cai, L. Single-Molecule RNA Detection at Depth by Hybridization Chain Reaction and Tissue Hydrogel Embedding and Clearing. *Development* **2016**, *143* (15), 2862–2867. https://doi.org/10.1242/dev.138560.

(14) Schwarzkopf, M.; Liu, M. C.; Schulte, S. J.; Ives, R.; Husain, N.; Choi, H. M. T.; Pierce, N. A. Hybridization Chain Reaction Enables a Unified Approach to Multiplexed, Quantitative, High-Resolution Immunohistochemistry and in Situ Hybridization. *Dev.* **2021**, *148* (22). https://doi.org/10.1242/DEV.199847.

(15) Dirks, R. M.; Pierce, N. A. Triggered Amplification by Hybridization Chain Reaction. *Proc. Natl. Acad. Sci.* **2004**, *101* (43), 15275–15278. https://doi.org/10.1073/pnas.0407024101.

(16) Schweitzer, B.; Wiltshire, S.; Lambert, J.; O'Malley, S.; Kukanskis, K.; Zhu, Z.; Kingsmore, S. F.; Lizardi, P. M.; Ward, D. C. Immunoassays with Rolling Circle DNA Amplification: A Versatile Platform for Ultrasensitive Antigen Detection. *Proc. Natl. Acad. Sci.* **2000**, *97* (18), 10113–10119. https://doi.org/10.1073/pnas.170237197.

(17) Saka, S. K.; Wang, Y.; Kishi, J. Y.; Zhu, A.; Zeng, Y.; Xie, W.; Kirli, K.; Yapp, C.; Cicconet, M.; Beliveau, B. J.; Lapan, S. W.; Yin, S.; Lin, M.; Boyden, E. S.; Kaeser, P. S.; Pihan, G.; Church, G. M.; Yin, P. Immuno-SABER Enables Highly Multiplexed and Amplified Protein Imaging in Tissues. *Nat. Biotechnol.* **2019**, *37* (9), 1080–1090. https://doi.org/10.1038/s41587-019-0207-y.

(18) Su, A.; Smith, B. E.; Herr, A. E. In Situ Measurement of Thermodynamic Partitioning in Open Hydrogels. *Anal. Chem.* **2019**, *92* (2), 875–883. https://doi.org/10.1021/acs.analchem.9b03582.

(19) Moss, A. C.; Herr, A. E. In-Gel Fluorescence Detection by DNA Polymerase Elongation. *APL Bioeng.* **2020**, *4* (4). https://doi.org/10.1063/5.0021149.

(20) Sundah, N. R.; Ho, N. R. Y.; Lim, G. S.; Natalia, A.; Ding, X.; Liu, Y.; Seet, J. E.; Chan, C. W.; Loh, T. P.; Shao, H. Barcoded DNA Nanostructures for the Multiplexed Profiling of Subcellular Protein Distribution. *Nat. Biomed. Eng.* **2019**, *3* (9), 684–694. https://doi.org/10.1038/s41551-019-0417-0.

(21) Maerle, A. V.; Simonova, M. A.; Pivovarov, V. D.; Voronina, D. V.; Drobyazina, P. E.; Trofimov, D. Y.; Alekseev, L. P.; Zavriev, S. K.; Ryazantsev, D. Y. Development of the Covalent Antibody-DNA Conjugates Technology for Detection of IgE and IgM Antibodies by Immuno-PCR. *PLoS One* **2019**, *14* (1), 1–19. https://doi.org/10.1371/journal.pone.0209860.

(22) *Cold Spring Harbor Protocols*; Sever, R., Ed.; Cold Spring Harbor Laboratory Press,

2020.

(23) Gong, H.; Holcomb, I.; Ooi, A.; Wang, X.; Majonis, D.; Unger, M. A. Simple Method To Prepare Oligonucleotide-Conjugated Antibodies and Its Application in Multiplex Protein Detection in Single Cells. **2016**. https://doi.org/10.1021/acs.bioconjchem.5b00613.

(24) Kang, C. C.; Yamauchi, K. A.; Vlassakis, J.; Sinkala, E.; Duncombe, T. A.; Herr, A. E. Single Cell-Resolution Western Blotting. *Nat. Protoc.* **2016**, *11* (8), 1508–1530. https://doi.org/10.1038/nprot.2016.089.

(25) Geldert, A.; Huang, H.; Herr, A. E. Probe-Target Hybridization Depends on Spatial Uniformity of Initial Concentration Condition across Large-Format Chips. *Sci. Rep.* **2020**. https://doi.org/10.1038/s41598-020-65563-3.

(26) Demaree, B.; Delley, C. L.; Vasudevan, H. N.; Peretz, C. A. C.; Ruff, D.; Smith, C. C.; Abate, A. R. Joint Profiling of DNA and Proteins in Single Cells to Dissect Genotype-Phenotype Associations in Leukemia. *Nat. Commun.* **2021**, *12* (1), 1–10. https://doi.org/10.1038/s41467-021-21810-3.

(27) Horta, S.; Neumann, F.; Yeh, S. H.; Langseth, C. M.; Kangro, K.; Breukers, J.; Madaboosi, N.; Geukens, N.; Vanhoorelbeke, K.; Nilsson, M.; Lammertyn, J. Evaluation of Immuno-Rolling Circle Amplification for Multiplex Detection and Profiling of Antigen-Specific Antibody Isotypes. *Anal. Chem.* **2021**, *93* (15), 6169–6177. https://doi.org/10.1021/acs.analchem.1c00172.

(28) Hermanson, G. T. *Bioconjugate Techniques*; 2013.

(29) Goodrich, J. A.; Kugel, J. F. *Binding and Kinetics for Molecular Biologists*; Cold Spring Harbor Laboratory Press, 2006.

(30) Kamat, V.; Ra, A. Designing Binding Kinetic Assay on the Bio-Layer Interferometry (BLI) Biosensor to Characterize Antibody-Antigen Interactions. **2017**, *536*, 16–31. https://doi.org/10.1016/j.ab.2017.08.002.

(31) Tong, J.; Anderson, J. L. Partitioning and Diffusion of Proteins and Linear Polymers in Polyacrylamide Gels. *Biophys. J.* **1996**, *70* (3), 1505–1513. https://doi.org/10.1016/S0006-3495(96)79712-6.

(32) Lin, R.; Feng, Q.; Li, P.; Zhou, P.; Wang, R.; Liu, Z.; Wang, Z.; Qi, X.; Tang, N.; Shao, F.; Luo, M. A Hybridization-Chain-Reaction-Based Method for Amplifying Immunosignals. *Nat. Methods* **2018**, *15* (4), 275–278. https://doi.org/10.1038/nmeth.4611.

(33) Dhawan, S. Signal Amplification Systems in Immunoassays: Implications for Clinical Diagnostics. *Expert Rev. Mol. Diagn.* **2006**, *6* (5), 749–760. https://doi.org/10.1586/14737159.6.5.749.

(34) Bi, S.; Chen, M.; Jia, X.; Dong, Y.; Wang, Z. Hyperbranched Hybridization Chain Reaction for Triggered Signal Amplification and Concatenated Logic Circuits. *Angew. Chemie - Int. Ed.* **2015**. https://doi.org/10.1002/anie.201501457.

(35) Bi, S.; Yue, S.; Zhang, S. Hybridization Chain Reaction: A Versatile Molecular Tool for

Biosensing, Bioimaging, and Biomedicine. *Chem. Soc. Rev.* **2017**, *46* (14), 4281–4298. https://doi.org/10.1039/C7CS00055C.

Chapter 6: A Single-Cell In-Gel Multimodal Electrophoretic Assay for Co-Detection of mRNA and Proteins from the Same Cell

6.1 Introduction

Single-cell multimodal assays are becoming increasingly important to elucidate cellular heterogeneity and explore the relationships between multiple classes of biomolecules in complex signaling pathways[1–3]. Many single-cell assays solely consist of RNA expression measurements[1], which are inherently limited for studying cellular function because proteins are the functional units of the cell, and protein and mRNA expression are often poorly correlated[4–6]. Additionally, protein isoforms and other post-translational modifications that impact cellular functions are common and cannot be measured at the mRNA level[7]. Therefore, there is a need for single-cell multimodal assays that incorporate protein measurements.

Multimodal measurements of protein isoforms and nucleic acid point mutations represent a niche that has been little explored. A specific biological application that would benefit from single-cell co-detection of protein isoforms and nucleic acid point mutations is studying the interplay between truncated HER2 protein isoforms and oncogenic point mutations in conferring resistance to the monoclonal antibody drug trastuzumab. Trastuzumab is the frontline therapy in cancers that exhibit HER2 amplification, which occurs in around 20-30% of breast cancer cases and with lower frequency in other cancers[8–10]. Truncated HER2 protein isoforms are known contributors to trastuzumab resistance in breast cancer[9,11]. Point mutations in the gene PIK3CA have also been implicated in trastuzumab resistance in multiple studies[12,13], and there is evidence that KRAS point mutations may also contribute to trastuzumab resistance[10,14]. Studying these protein isoforms and nucleic acid point mutations together would allow for new questions to be answered related to rare subpopulations of cells that drive trastuzumab resistance and contribute to disease progression.

However, such studies are not possible as current multimodal single-cell assays lack the ability to detect nucleic acid point mutations and protein isoforms from the same single cells. Most multimodal assays that combine nucleic acid measurements with protein measurements simply quantify the number of transcripts by 3’ end sequencing, which is not capable of identifying point mutations or providing other detailed sequence information[1,3,15]. At the protein level, current multimodal assays depend exclusively on antibody specificity for protein detection[2,4], limiting the ability to detect protein isoforms for which specific antibodies do not exist.

The single-cell western blot (scWB) is an assay developed by our group that combines an electrophoretic separation stage with an immunoassay stage to achieve isoform-specific protein detection from single cells without the need for isoform-specific antibodies[16,17]. Our group recently developed snapBlot[18], a multimodal extension of the scWB that incorporates nucleic acid measurements by fractionally lysing cells to leave intact nuclei and laser existing gel pallets that contain the nuclei for off-chip qPCR analysis. While snapBlot is a step forward toward protein isoform and nucleic acid multimodal measurements, it is only capable of detecting

nuclear nucleic acids, it is not optimized for single cells, point mutation detection has not been demonstrated, and it suffers from low throughput[18]. These limitations could be overcome with an in-gel assay that utilizes whole-cell lysis followed by electrophoretic separation of the mRNA from the protein and point mutation-specific in-situ mRNA detection prior to immunoprobing with antibodies.

Here, we introduce Single-Cell Protein and RNA Electrophoresis (scPREP), a multimodal assay that achieves in-gel co-detection of beta-actin mRNA and beta-actin protein from the same single cells. Our assay links single-cell protein polyacrylamide gel electrophoresis (PAGE), demonstrated in the scWB[16,17], with a single nucleotide-specific in-situ hybridization strategy that utilizes rolling circle amplification (RCA) with padlock probes (PLPs)[19,20] to enable high specificity single-cell co-detection of mRNA and proteins. This work represents a major step forward toward single-cell co-detection of nucleic acid point mutations and protein isoforms.

6.2 Materials and Methods

Reagents

DNA oligomers were purchased from IDT (Coralville, IA, USA). M-MuLV Reverse Transcriptase (M0253L), RNaseH (M0297L), and phi29 DNA polymerase (M0269L) were purchased from New England Biolabs (Ipswich, MA). Ampligase DNA ligase (A3202K) was purchased from Epicentre (Madison, WI). dATP (R0141), dGTP (R0161), dTTP (R0171), dCTP (R0151), ribolock RNase Inhibitor (EO0381), sodium chloride (S271), Alexa Fluor 647-labeled donkey anti-rabbit (A31573), trypsin-EDTA 0.05% (25300054), and penicillin–streptomycin (15140-122) were purchased from Thermo Fisher Scientific (Waltham, MA). Bovine serum albumin (BSA, A7030), urea (U5378), sodium dodecyl sulfate (SDS, L3771), sodium deoxycholate (D6750), Triton X-100 (X100), Tween-20 (P1379), formamide (F7503), 30% acrylamide/bis-acrylamide (29:1) solution (A3574), tetramethylethylenediamine (TEMED, T9281), ammonium persulfate (APS, A3678), potassium chloride (P9333), sodium citrate dihydrate (W302600), 3-(trimethoxylsilyl)propyl methacrylate (440159), chlorotrimethylsilane (386529), and nuclease-free water (W4502), were purchased from Sigma-Aldrich (St. Louis, MO, USA). A pan-actin rabbit monoclonal antibody (8456S) was purchased from Cell Signaling Technology (Danvers, MA). RPMI-1640 media (11875-119) and sterile phosphate buffered saline (PBS, 10010049) were purchased from Gibco. Fetal bovine serum (100-106) was purchased from Gemini Bio-Products (West Sacramento, CA). Buffers were prepared according to standard protocols[21].

DNA Sequences

DNA sequences for the human beta-actin primer and probe set were adopted from Larsson et al.[19] and displayed in Table 6-1. The poly(T) mRNA anchor consisted of a 20 nucleotide-long poly(T) sequence terminated with a 5’ acrydite group for co-polymerization in the gel.

Table 6-1: Sequences of DNA oligomers used in scPREP. The '+' indicates locked nucleic acid (LNA) bases.

Function	Sequence
Poly(T) anchor	5'-(acrydite)-TTTTTTTTTTTTTTTTTTTT-3'
Beta-actin LNA primer for RT	5'-A+TC+AT+CC+AT+GG+TG+AGCTGGCGGCGG-3'
Beta-actin PLP	5'-(phosphate)-AGCCTCGCCTTTGCCTTCCTTTTACGACCTCAATGCTGCTG CTGTACTACTCTTCGCCCCGCGAGCACAG-3'
Labeled detector oligo	5'-(Cy3)-CCTCAATGCTGCTGCTGTACTAC-3'

Gel Fabrication

Polyacrylamide gels were fabricated on silicon wafer substrates with 30 µm diameter microposts and 40 µm rails patterned in SU-8, as previously reported[16,22]. Gel precursor solutions containing acrylamide/bis-acrylamide stock solution (30%, 29:1) were prepared to a concentration of 7% T and 3.3% C. BPMAC was added to a concentration of 3mM and acrydite-terminated poly(T) to a concentration of 10 µM, followed by degassing via sonication for 5 min. APS and TEMED were then added to the precursor to a concentration of 0.08% each before pipetting the solution between the SU-8 patterned wafer (rendered hydrophobic by treatment with dichlorodimethylsilane) and a glass microscope slide functionalized with 3-(trimethoxysilyl)propyl methacrylate. After a 20-min chemical polymerization, the slides with the attached gels were lifted from the wafers and washed in 1xPBS for at least 1 h prior to use in experiments. Precautions were taken to prevent RNase contamination, including using solutions prepared with RNase free water and cleaning all surfaces and gel substrates with RNase ZAP.

Cell Culture

MDA-MB-231 cells were obtained from the UC Berkeley Tissue Culture Facility via the American Type Culture Collection and cultured in RPMI-1640 growth medium that was supplemented with 10% fetal bovine serum (FBS) and 1% penicillin/streptomycin. Cells were maintained in an incubator at 37 °C with humidified 5% CO_2 air.

scPREP Assay Workflow

Cell settling, lysis, and electrophoresis followed established protocols[16,22]. Briefly, MDA-MB-231 cells were harvested from tissue culture flasks by treating with 0.05% trypsin-EDTA for 3 min followed by inactivation with medium that contains serum, centrifugation, and resuspension in ice cold PBS at a concentration of 1-1.5x10^6 cells/mL. Cell settling consisted of pipetting 200 µL of cell suspension on top of each half slide gel and incubating for 10 min followed by 2 washes with 1 mL of 1xPBS to remove excess cells on the gel surface. Gels were then placed in an electrophoresis chamber and 12 mL of 55°C 1xRIPA buffer (with or without 6 M urea) was poured into the chamber. Lysis proceeded for 30 s, followed by 15 s electrophoresis at 40 V/cm

and a 45 second photocapture step using a Hamamatsu LC5 Spot Light Source. The gels were then placed back in 1xPBS in a 4-well dish and the buffer exchanged for 1xTBST for a 30 minute wash on an orbital shaker, changing out the TBST halfway through. The reverse transcription (RT) solution was prepared during the wash step, applied to the gels and incubated overnight at 37°C. The gels were then transferred to a 4-well dish with 1xPBST buffer for 15 minutes, the buffer changed, and the gels exposed to UV light for exposed for 300 s at ~20 $mW/cm^{2.}$ Next, the gels were washed for another 15 min in 1xTBST and the PLP hybridization/ligation solution applied. The PLP hybridization/ligation step involved incubating the gels at 37°C for 30 min, followed by 45°C for 45 min. After PLP hybridization and ligation, the gels were washed in 2xSSC buffer for 15 min at 37°C, followed by 15 min at 37°C in 1xPBST. RCA solution was then applied and the gels incubated for 4 h at 37°C. After RCA, the gels were washed for 30 min in 1xPBST, changing out the TBST halfway through. The detector oligo solution was then applied to the gels and incubated for 2 h at 37°C, followed by a 30 min wash in 1xTBST, changing out the buffer halfway through. After the wash step, the gels were briefly rinsed 3x in tap water and dehydrated with a N_2 stream. All reagent incubation steps consisted of pipetting 100 µL of reagent solution onto a glass plate, placing the glass slide with the gel side down on top of the drop of solution, and gently moving the slide with tweezers to ensure an even fluid layer and even mixing of reagents. Incubations were performed in a HybEZ oven manufactured by Advanced Cell Diagnostics. Wash steps were at room temperature, unless otherwise indicated. Reagent solutions were prepared with the same composition as outlined in Larsson et al.[19]

After imaging the RCPs, immunoprobing was carried out following the standard scWB protocol[16,22]. Each half slide gel was probed with 50 µL of antibody solution. The primary antibody (rabbit anti-actin) was diluted 1:10, and the secondary antibody (AF647-labeled donkey anti-rabbit) was diluted 1:20 in 2% BSA in 1xTBST. Gels were incubated for 2 h with the primary antibody, washed for 1 h in 1xTBST, incubated for 1 h with the secondary antibodies, and washed again in 1xTBST.

Imaging and Data Analysis

Imaging of the dehydrated gels was conducted using a GenePix 4300A microarray scanner equipped with 488 nm, 532 nm, 594 nm, and 635 nm lasers. Cy3 stained RCPs were imaged with the 532 nm laser, and immunoprobed beta-actin protein bands were imaged with the 635 nm laser. Imaging settings were chosen for high dynamic range without achieving saturation. Rough quantification of mRNA migration distance was carried out in ImageJ and consisted of drawing a line from the center of each microwell to the midpoint of the 'band' of puncta, which was estimated by eye. Beta-actin protein bands in post-immunoprobing images were analyzed with the scWB analysis pipeline[23] to generate ROIs from each lane of the gel, calculate intensity profiles, fit gaussian peaks to the protein bands, and extract the area-under-the-curve (AUC) integrated fluorescence.

The z-directional RCP distribution profile was measured with aberration-compensated laser scanning confocal microscopy (AC-LSCM), according to previously published methods[24]. Briefly, gels were hydrated in 1xPBS and a number 1.5 coverslip (Fisher Scientific, 12-544-E) was placed on top. Images were then acquired on a Carl Zeiss LSM 710 AxioObserver inverted

laser scanning confocal microscope using a C-Apochromat 40×/1.1 NA water-immersion objective with correction collar. The 561 nm laser line was used to excite Cy3 and to perform reflected light confocal microscopy of the coverslip-sample interface to find the optimal correction collar setting. Fluorescence was imaged using a 488/561/633 nm dichroic filter and a pinhole set to 1.0 Airy units. Reflected light confocal images were acquired using a T80/R20 partial mirror over a 212.55 μm × 212.55 μm field of view with 0.71 μm × 0.71 μm × 0.10 μm cubic voxels.

6.3 Results and Discussion

Assay Overview

scPREP is a novel multimodal assay that enables co-detection of mRNA and proteins from lysed and electrophoresed single cells. The scPREP device design and upstream portion of the assay workflow are largely based on scWB, a well-established electrophoretic assay for high-specificity single-cell protein detection[16,22]. scPREP devices consist of polyacrylamide gels with microwells that are fabricated on chemically treated glass slide supports. A 20-mer poly(T) DNA oligomer at a concentration of 10 μM is co-polymerized into the gels via a 5' acrydite group to facilitate mRNA capture, and benzophenone methacryalmide (BPMA) is included at a concentration of 3 mM to enable UV photocapture of proteins, as demonstrated in scWB[16]. The upstream portion of the assay consists of gravity settling single cells in microwells and performing chemical cell lysis, followed by electrophoresis and UV photocapture. As a result of the BPMA photocapture and poly(T) hybridization, proteins and mRNA are captured in the gel matrix. Devices are subsequently subjected to in situ hybridization to detect the mRNA followed by immunoprobing with fluorescently labeled antibodies to detect the proteins. The scPREP concept and assay workflow is outlined in Fig. 6-1.

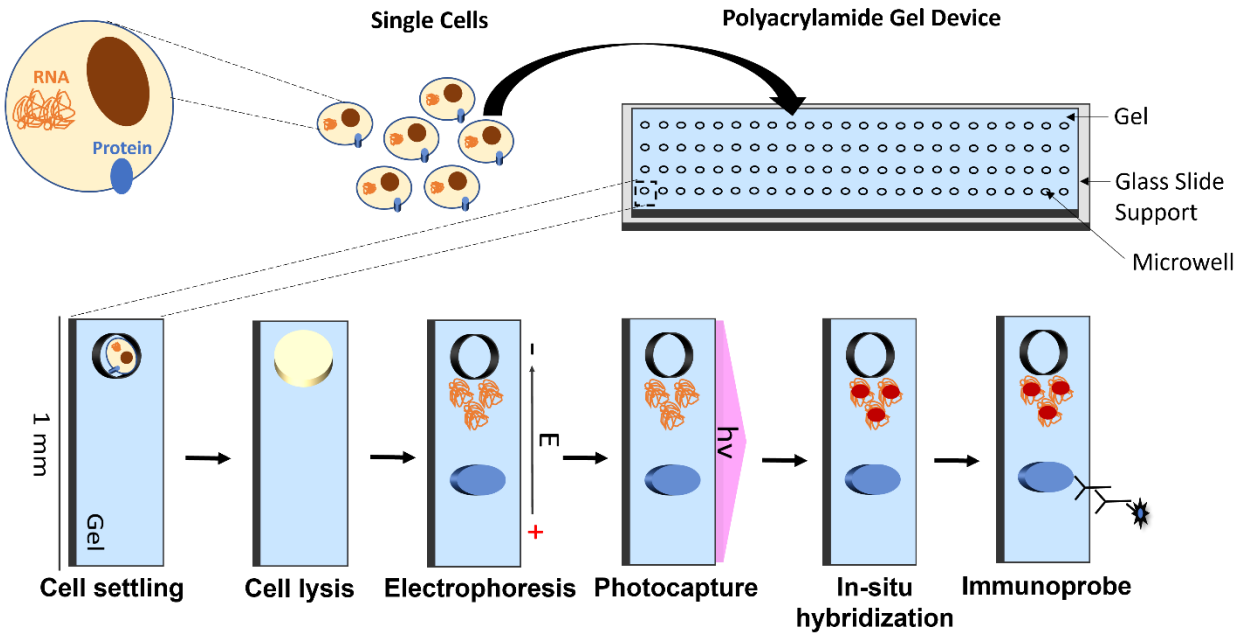

Figure 6-1: Overview of scPREP for co-detection of mRNA and protein from single cells. Single cells are gravity settled into microwells in a polyacrylamide gel followed by chemical cell lysis, electrophoresis, UV photocapture to immobilize the proteins and mRNA, fluorescence in situ hybridization to detect the mRNA, and immunoprobing with fluorescently labeled antibodies to detect the proteins

To enable nucleic acid point mutation detection in the future, rolling circle amplification (RCA) with padlock probes (PLPs) was chosen as the mRNA detection strategy. RCA with PLPs has been well-established in the literature for its high specificity and sensitivity[19,20]. The PLPs confer single-nucleotide specificity during the hybridization and ligation steps. RCA results in signal amplification of several orders of magnitude, generating rolling circle products (RCPs), which arise from single mRNA molecules. RCPs are detected by hybridizing complementary short fluorescently labeled detector oligos, resulting in fluorescent puncta. Prior to scPREP, RCA with PLPs has been limited to detecting mRNA in fixed cells and tissues. Here, we apply RCA with PLPs for in-gel detection of mRNA from lysed and electrophoresed single cells. Fig. 6-2 depicts the scPREP in-gel mRNA detection protocol.

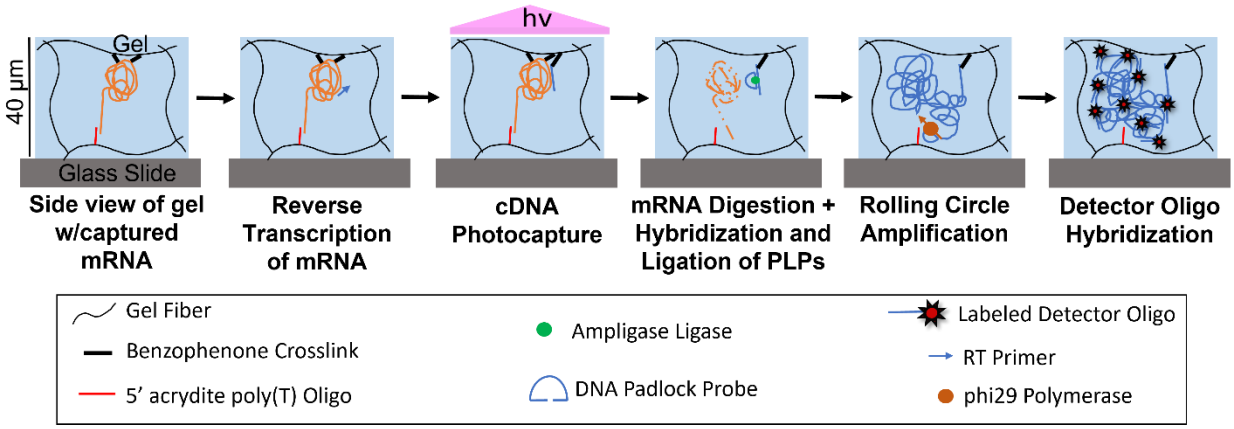

Figure 6-2: Scheme outlining the in situ hybridization protocol for mRNA detection. A mRNA molecule that is captured in the gel via benzophenone photocapture and poly(T) hybridization undergoes reverse transcription of the beta-actin gene, followed by a step that involves simultaneous digestion of the mRNA, hybridization of the padlock probe (PLP) sequence to the cDNA, and ligation to form a circular PLP. PLPs are then subjected to rolling circle amplification (RCA) to generate large concatemers of amplified DNA that are detected by hybridizing fluorescently labeled short detector oligos.

Compared to other single-cell multimodal assays, the scPREP concept presents many advantages. First, scPREP is a high-throughput assay that can analyze thousands of single cells per run. Second, scPREP does not require highly specialized equipment or training, making it accessible to other researchers. Most importantly, scPREP theoretically has the potential to detect co-expression of protein isoforms and nucleic acid point mutations due to the electrophoretic protein separation and the high-specificity nucleic acid detection method.

In-Gel mRNA Detection with RCA and PLPs

We first sought to demonstrate in-gel detection of beta-actin mRNA from lysed and electrophoresed single MDA-MB-231 cells. Beta-actin is a common target during assay development due to its high abundance and universal presence across different cell types such that we were able to harness an established probe set from the literature[19]. For proof-of-concept experiments with MDA-MB-231 cells, we chose 7% T, 3.3% C gels that were 40 µm thick with 30 µm diameter microwells. Device dimensions and gel density can be easily adjusted to accommodate different cell lines and protein targets based on the principles of scWB device design[22]. The assay run conditions consisted of a 30 s lysis step and a 15 s electrophoresis step in 1xRIPA buffer, followed by a 45 s UV photocapture. Gels then underwent the mRNA detection protocol outlined in Fig. 6-2 and were imaged with a microarray scanner.

Fluorescent puncta were initially detected at the microwell interface (Fig. 6-3A), which is not ideal for puncta identification. We hypothesized that poor solubilization and electrophoretic injection of the mRNA into the gel was resulting in the mRNA molecules being captured at the microwell interface. Urea is a chaotropic agent commonly used in the literature to fully denature

RNA prior to and during electrophoresis[25,26]. Addition of 6 M urea to the dual-function lysis and electrophoresis buffer resulted in a two-fold increase in the migration distance of the beta-actin mRNA (Fig. 6-3B and 6-3C), which we attribute to improved solubilization and electrophoretic injection of the mRNA into the gel. Negative controls (not shown) that omitted either the reverse transcriptase enzyme during the RT step or cells during the settling step did not exhibit fluorescent puncta, confirming that beta-actin mRNA was detected.

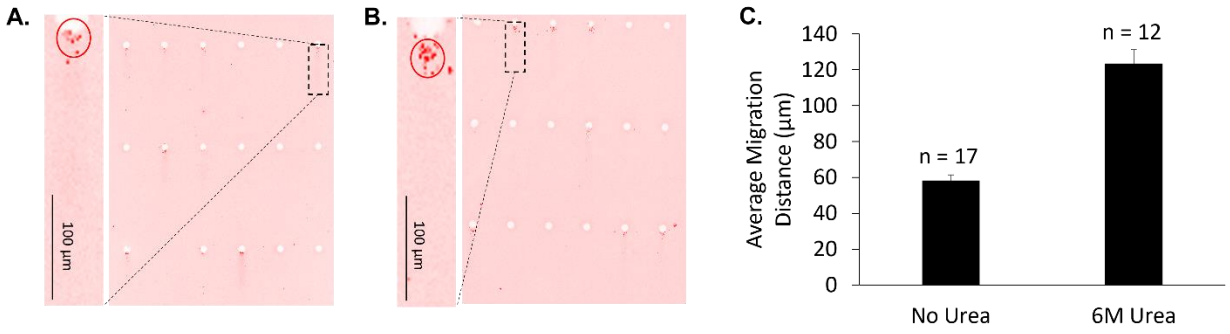

Figure 6-3: Inclusion of 6 M urea during lysis and electrophoresis results in farther migration of beta-actin mRNA into the gel, facilitating in-gel detection. (A) rolling circle products (RCPs) resulting from amplified beta-actin mRNA molecules are localized close to the microwell interface when using standard dual-function lysis and electrophoresis buffer, (B) RCPs are localized farther from the microwell interface when 6 M urea is included in the dual-function lysis and electrophoresis buffer, (C) quantification of the data shown in the micrographs reveals that 6 M urea results in a 2-fold increase in the average mRNA migration distance. Mean migration distance from multiple lanes with standard deviation error bars was reported.

While beta-actin mRNA was detected in the gel, far fewer puncta than anticipated were observed. Beta-actin mRNA expression in mammalian cells is typically on the order of 10^3 copies per cell, and individual puncta in the RCA FISH assay have been previously shown to correspond to single mRNA molecules[19,20]. At most, we were observing up to ~30 puncta per single cell. There are multiple possibilities for this discrepancy, including poor mRNA capture, diffusive and/or convective losses of captured molecules, transport limitations during the enzymatic reactions, poor reaction efficiency, or that each punctum represents multiple amplified mRNA molecules.

Measuring the distribution of RCPs throughout the depth of the gel (in the z-direction) has the potential to shed light into the cause of the discrepancy between the number of beta-actin mRNA molecules per cell and the number of observed puncta. More puncta near the surface of the gel would suggest poor transport of reagents throughout the depth of the gel, potentially due to retarded diffusion[27], while a larger number of puncta deeper in the gel would suggest diffusive loss of captured molecules. We chose to measure the distribution of RCPs throughout the depth of the gel with aberration-compensated laser scanning confocal microscopy (AC-LSCM)[24]. With AC-LSCM, we observed an even distribution of RCPs throughout the depth of the gel (Fig. 6-4).

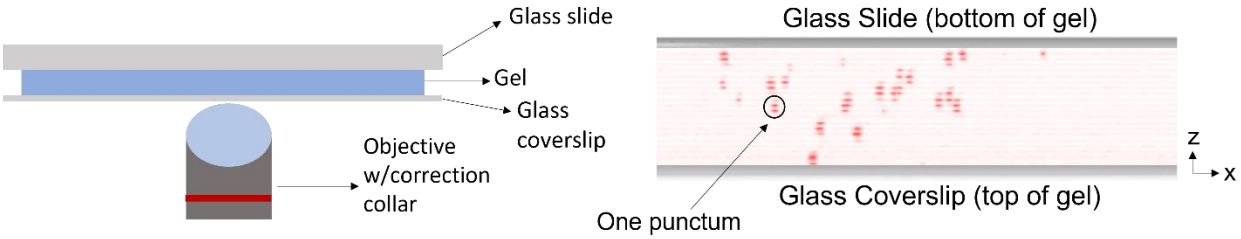

Figure 6-4: Beta-actin rolling circle products (RCPs) are detectable throughout the entire depth of the gel. A gel was imaged with aberration-compensated laser scanning confocal microscopy (AC-LSCM) to evaluate the distribution in the z-direction of the RCPs that arose from beta-actin mRNA molecules. The imaging configuration is depicted on the left, while the gel image is depicted on the right. The appearance of lines is due to the boundaries between individual slices in the image stack.

The even distribution of RCPs in the z-direction suggests that the discrepancy between the number of observed puncta and the number of beta-actin mRNA molecules per cell is not due to diffusive loss of mRNA during the early stages of the assay or transport limitations of the reagents during the enzymatic reaction steps. We currently posit that the discrepancy is due to inefficient in-gel reactions or each punctum arising from multiple mRNA molecules. With confocal microscopy, which has a 10-fold higher resolution than the microarray scanner, we were able to determine that the average punctum size was ~5-8x larger in area than the puncta in fixed cells subjected to the standard protocol from the literature[19,20]. The larger punctum size supports the hypothesis that each RCP arises from multiple mRNA molecules. However, the result is not conclusive because different RCA conditions can affect the RCP size[20]. Overall, further investigation is needed to evaluate the cause of signal loss in the mRNA detection phase of scPREP.

Co-Detection of Beta-Actin mRNA and Protein

We next sought to demonstrate the complete scPREP assay, which consists of co-detection of beta-actin mRNA and protein from the same single cells. mRNA detection was carried out prior to protein detection since mRNA is far more unstable and prone to degradation than proteins. The gels were then immunoprobed according to the scWB immunoprobing protocol with a rabbit anti-beta-actin primary antibody followed by an Alexa Fluor 647-labeled donkey anti-rabbit secondary antibody. After immunoprobing, clear gaussian protein bands were visible in the gel alongside the beta-actin RCPs (Fig. 6-5), with the protein migrating an average distance of 342±21 µm (n = 198 cells) into the gel.

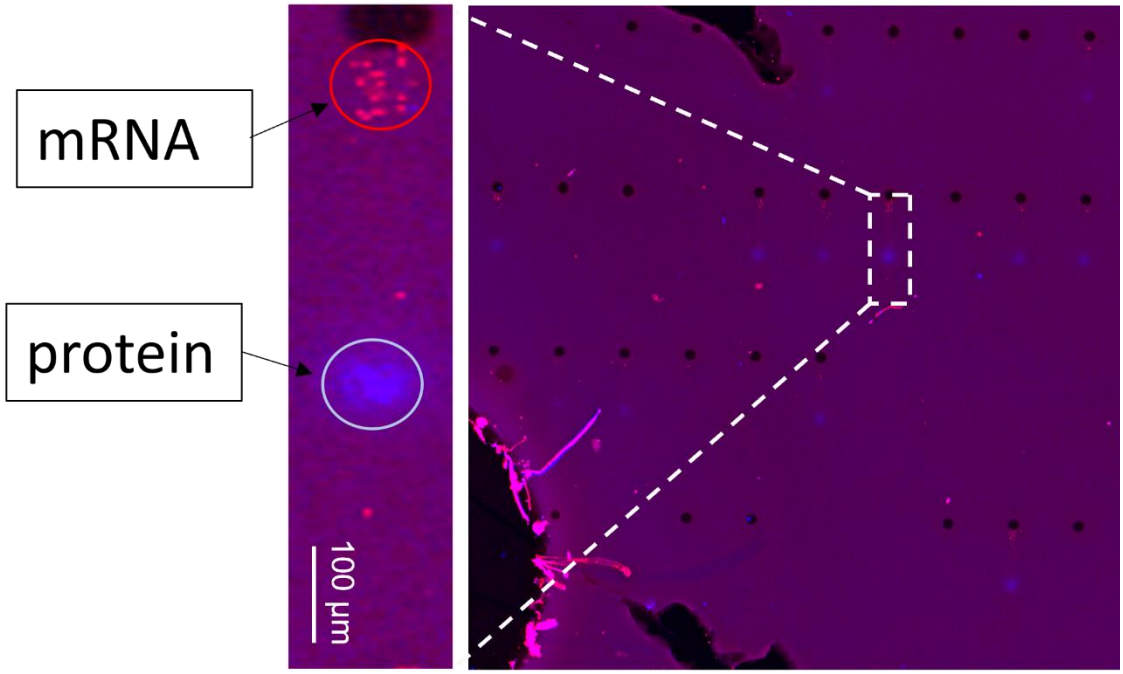

Figure 6-5: Co-detection of beta-actin mRNA and beta-actin protein from single cells demonstrated with scPREP. Fluorescently stained RCPs arising from mRNA molecules and immunoprobed gaussian protein bands are visible in a gel that was subjected to the standard scWB immunoprobing protocol following the mRNA detection protocol. Red represents Cy3 fluorescence and blue represents Alexa Fluor 647 fluorescence.

The result shown in Fig. 6-5 demonstrates that carrying out the mRNA detection protocol prior to the standard scWB immunoprobing protocol does not preclude protein detection. An important observation to note is the large difference between the migration distance of the mRNA and the protein. This difference is consistent with the theory, as there is a large difference between the estimated hydrodynamic radii of the beta-actin mRNA (~10 nm) and the beta-actin protein (~2.6 nm). Our results here suggest that the choice of a 7% T, 3.3% C gel is appropriate for beta-actin mRNA and protein. Different protein and mRNA targets are different sizes and will require different conditions, an important topic of further investigation in the future.

To the best of our knowledge, scPREP is the first demonstration of single-cell gel electrophoresis followed by co-detection of mRNA and protein. Our results serve as a promising starting point for single-cell co-detection of nucleic acid point mutations and protein isoforms, as point mutation detection has been demonstrated with the mRNA detection strategy here,[19] and isoform-specific protein detection has been demonstrated with the scWB[17].

Issues with Reproducibility and RCP Localization

All the results discussed above are preliminary results from a few replicates. As we ran more replicates, we began to notice large differences in the number of puncta detected within different

regions of a gel and from gel-to-gel. The number of puncta detected in the most recent scPREP experimental runs ranges from few to none (Fig. 6-6A). Additionally, we have often observed a drastic difference in the background across a gel. The more recent results present a large caveat to all the results presented so far in this chapter. In an attempt to improve the reproducibility, we evaluated numerous hypotheses.

The three primary hypotheses for the inconsistent results were (1) an uneven fluid layer thickness resulting in different concentrations of reagents from gel-to-gel or between regions of the same gel, (2) convective losses of mRNA during the lysis and electrophoresis phases of the assay, or (3) poor capture of the mRNA and/or the cDNA resulting in loss of molecules throughout the assay. The first hypothesis is based on published work from our group that identified nonuniform fluid layers during immunoprobing[28], and we used the same method to apply the solutions in the mRNA detection protocol. To test the first hypothesis, we affixed a SecureSeal hybridization chamber over the gel to create a fixed volume chamber during the reaction steps. The result was large numbers of non-microwell-localized puncta spread across the gel and trails of puncta originating from some of the microwells that contained cells (Fig. 6-6B).

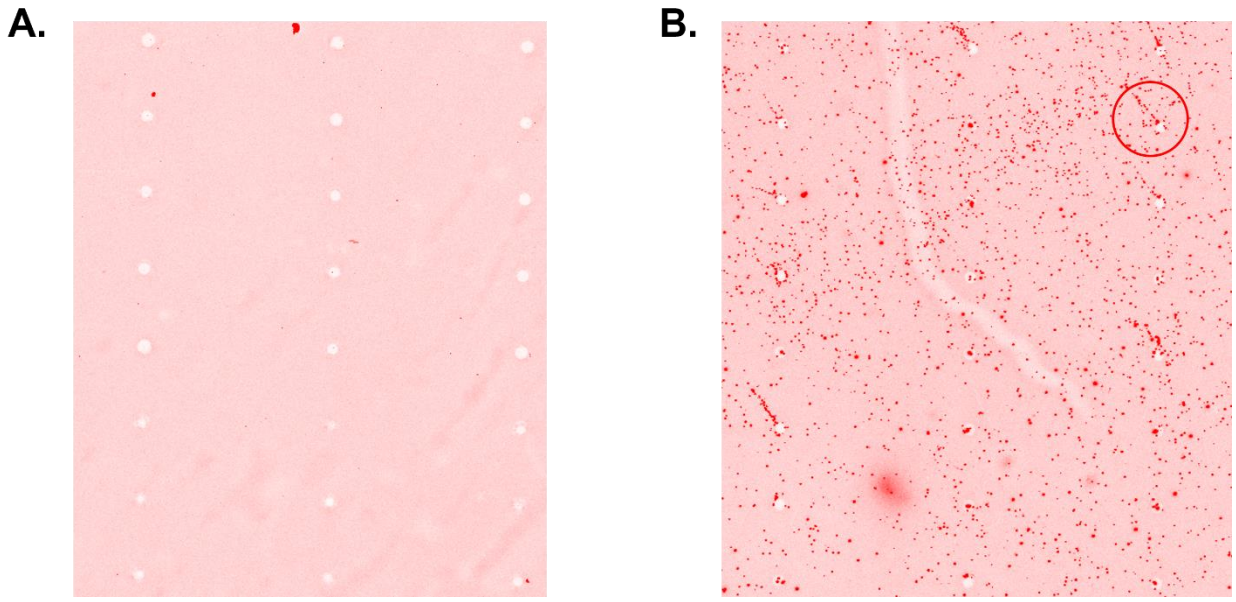

Figure 6-6: Challenges with reproducibility of mRNA detection and RCP localization. (A) most gels subjected to the reported protocol currently exhibit few or no puncta, (B) the use of a SecureSeal gasket to deliver reagents during the mRNA detection protocol results in puncta across the gel surface with trails of puncta adjacent to some microwells that contained cells. An example microwell with a trail of puncta is circled.

We were surprised that the use of a SecureSeal chamber would result in such a drastic change in the result. The observed trails of puncta would be consistent with convection during the lysis and electrophoresis steps, but still would not explain why the result with the SecureSeal was drastically different. To test the second hypothesis of convection during lysis and

electrophoresis, we used lid gels to apply the buffers, as this approach has been previously demonstrated to result in a reduction in convection by two orders of magnitude[29]. After electrophoresis, we performed a buffer exchange via lid gel with a high salt 6xSSC buffer to promote hybridization of the mRNA to the poly(T) oligomer. The high salt buffer exchange was motivated by a post-electrophoresis buffer exchange in a system that involved binding mRNA to a poly(T) oligomer on a surface[30]. Even with the lid gel delivery of the lysis and electrophoresis buffer followed by the high salt buffer exchange, there was no change in the result. No puncta were observed using the original method of reagent delivery, while non-localized puncta across the gel and puncta trails were observed when the reagents were delivered with a SecureSeal.

We made a key observation that certain regions of gels that were fluidically addressed with a SecureSeal had far more puncta than other regions. Specifically, regions downstream in the flow path and outside of the direct flow streams had more puncta. These observations strongly support our third hypothesis of mRNA or cDNA loss at some point during the assay. The drastic difference between the SecureSeal and applying the reagents sandwiched between the gel and a glass plate could also be explained by this hypothesis, as the shear when sandwiching the gels against the glass plate and the increased convection from washing without the SecureSeal could result in displacement of more molecules. A deeper dive into the literature revealed that in situ sequencing protocols that utilize a similar form of RCA all include covalent capture strategies for the cDNA and/or the RCPs[31,32]. The cDNA capture is a weak link in the whole mRNA detection protocol because the cDNA is small and, if not well-anchored, could easily diffuse out of the gel when the mRNA is digested. While we had been including a second photocapture step after reverse transcription, it is possible that the cDNA capture was still insufficient. Thus, we hypothesized that the cDNA was diffusing within and out of the gel, leading to displacement of cDNA molecules. This hypothesis would explain the non-localized puncta and the trails.

To improve the capture of the cDNA, we implemented two different covalent capture strategies from the literature based on incorporation of amine-labeled dUTP into the reverse transcription rection followed by crosslinking. In one experiment, we also included a covalent captures step for the RCPs, since previous studies indicated that RCP capture may also be necessary[31,32]. None of these methods resulted in any change to the results. We currently hypothesize that either the covalent capture was not successful with the approaches we implemented or there is loss of mRNA and/or cDNA further upstream in the assay workflow. Future experiments are planned to further investigate the causes of the irreproducibility and RCP localization issues. We are optimistic that further troubleshooting and optimization of the chemistries will result in interpretable and reproducible mRNA detection, meeting or exceeding the assay performance in our preliminary experiments.

6.4 Conclusions

Here, we presented scPREP, a single-cell multimodal electrophoretic assay for co-detection of mRNA and proteins. We demonstrated in-gel beta-actin mRNA detection from lysed and electrophoresed single MDA-MB-231 cells, where inclusion of 6 M urea in the dual-function lysis and electrophoresis buffer resulted in a two-fold increase in the mRNA migration distance. Far fewer puncta were identified from each cell than anticipated based on the estimated beta-actin mRNA copy number. We observed a uniform distribution of RCPs throughout the depth of

the gel, which suggests that the discrepancy between the number of puncta visible and the number of mRNA copies is not due to diffusion of the mRNA out of the gel during electrophoresis or transport limitations of the reagents during the mRNA detection protocol. Most crucially, we found that beta-actin protein was detectable with the standard scWB immunoprobing protocol after subjecting gels to the mRNA detection protocol, allowing us to demonstrate co-detection of beta-actin mRNA and protein from single cells.

The preliminary scPREP results show a great deal of promise as a single-cell multimodal assay. Future work has the potential to expand the capabilities of scPREP to detect mRNA point mutations and protein isoforms from single cells, presenting a major contribution to the single-cell multimodal -omics field. However, we encountered substantial reproducibility issues that we are currently resolving prior to further expanding the capabilities of scPREP.

6.5 Bibliography

(1) Ogbeide, S.; Giannese, F.; Mincarelli, L.; Macaulay, I. C. Into the Multiverse: Advances in Single-Cell Multiomic Profiling. *Trends Genet.* **2022**, *38* (8), 831–843. https://doi.org/10.1016/j.tig.2022.03.015.

(2) Demaree, B.; Delley, C. L.; Vasudevan, H. N.; Peretz, C. A. C.; Ruff, D.; Smith, C. C.; Abate, A. R. Joint Profiling of DNA and Proteins in Single Cells to Dissect Genotype-Phenotype Associations in Leukemia. *Nat. Commun.* **2021**, *12* (1), 1–10. https://doi.org/10.1038/s41467-021-21810-3.

(3) Stoeckius, M.; Hafemeister, C.; Stephenson, W.; Houck-loomis, B.; Chattopadhyay, P. K.; Swerdlow, H.; Satija, R.; Smibert, P. Large-Scale Simultaneous Measurement of Epitopes and Transcriptomes in Single Cells. *Nat. Methods* **2017**, *14* (9), 865–868. https://doi.org/10.1038/nmeth.4380.Large-scale.

(4) Reimegård, J.; Tarbier, M.; Danielsson, M.; Schuster, J.; Baskaran, S.; Panagiotou, S.; Dahl, N.; Friedländer, M. R.; Gallant, C. J. A Combined Approach for Single-Cell MRNA and Intracellular Protein Expression Analysis. *Commun. Biol.* **2021**, *4* (1), 1–11. https://doi.org/10.1038/s42003-021-02142-w.

(5) Ståhlberg, A.; Thomsen, C.; Ruff, D.; Åman, P. Quantitative PCR Analysis of DNA, RNAs, and Proteins in the Same Single Cell. *Clin. Chem.* **2012**, *58* (12), 1682–1691. https://doi.org/10.1373/clinchem.2012.191445.

(6) Liu, Y.; Beyer, A.; Aebersold, R. On the Dependency of Cellular Protein Levels on MRNA Abundance. *Cell* **2016**, *165* (3), 535–550. https://doi.org/10.1016/j.cell.2016.03.014.

(7) Aebersold, R.; Agar, J. N.; Amster, I. J.; Baker, M. S.; Bertozzi, C. R.; Boja, E. S.; Costello, C. E.; Cravatt, B. F.; Fenselau, C.; Garcia, B. A.; Ge, Y.; Gunawardena, J.; Hendrickson, R. C.; Hergenrother, P. J.; Huber, C. G.; Ivanov, A. R.; Jensen, O. N.; Jewett, M. C.; Kelleher, N. L.; Kiessling, L. L.; Krogan, N. J.; Larsen, M. R.; Loo, J. A.; Ogorzalek Loo, R. R.; Lundberg, E.; Maccoss, M. J.; Mallick, P.; Mootha, V. K.; Mrksich, M.; Muir, T. W.; Patrie, S. M.; Pesavento, J. J.; Pitteri, S. J.; Rodriguez, H.; Saghatelian, A.; Sandoval, W.; Schlüter, H.; Sechi, S.; Slavoff, S. A.; Smith, L. M.; Snyder, M. P.; Thomas, P. M.; Uhlén, M.; Van Eyk, J. E.; Vidal, M.; Walt, D. R.; White, F. M.; Williams, E. R.; Wohlschlager, T.; Wysocki, V. H.; Yates, N. A.; Young, N. L.; Zhang, B. How Many Human Proteoforms Are There? *Nat. Chem. Biol.* **2018**, *14* (3), 206–214. https://doi.org/10.1038/nchembio.2576.

(8) Majumder, A.; Sandhu, M.; Banerji, D.; Steri, V.; Olshen, A.; Moasser, M. M. The Role of HER2 and HER3 in HER2-Amplified Cancers beyond Breast Cancers. *Sci. Rep.* **2021**, *11* (1), 9091. https://doi.org/10.1038/s41598-021-88683-w.

(9) Sáez, R.; Molina, M. A.; Ramsey, E. E.; Rojo, F.; Keenan, E. J.; Albanell, J.; Lluch, A.; Garcia-Conde, J.; Baselga, J.; Clinton, G. M. P95HER-2 Predicts Worse Outcome in Patients with HER-2-Positive Breast Cancer. *Clin. Cancer Res.* **2006**, *12* (2), 424–431. https://doi.org/10.1158/1078-0432.CCR-05-1807.

(10) Meric-Bernstam, F.; Hurwitz, H.; Raghav, K. P. S.; McWilliams, R. R.; Fakih, M.; VanderWalde, A.; Swanton, C.; Kurzrock, R.; Burris, H.; Sweeney, C.; Bose, R.; Spigel, D. R.; Beattie, M. S.; Blotner, S.; Stone, A.; Schulze, K.; Cuchelkar, V.; Hainsworth, J. Pertuzumab plus Trastuzumab for HER2-Amplified Metastatic Colorectal Cancer (MyPathway): An Updated Report from a Multicentre, Open-Label, Phase 2a, Multiple Basket Study. *Lancet Oncol.* **2019**, *20* (4), 518–530. https://doi.org/10.1016/S1470-2045(18)30904-5.

(11) Arribas, J.; Baselga, J.; Pedersen, K.; Parra-Palau, J. L. P95HER2 and Breast Cancer. *Cancer Res.* **2011**, *71* (5), 1515–1519. https://doi.org/10.1158/0008-5472.CAN-10-3795.

(12) Berns, K.; Horlings, H. M.; Hennessy, B. T.; Madiredjo, M.; Hijmans, E. M.; Beelen, K.; Linn, S. C.; Gonzalez-Angulo, A. M.; Stemke-Hale, K.; Hauptmann, M.; Beijersbergen, R. L.; Mills, G. B.; van de Vijver, M. J.; Bernards, R. A Functional Genetic Approach Identifies the PI3K Pathway as a Major Determinant of Trastuzumab Resistance in Breast Cancer. *Cancer Cell* **2007**, *12* (4), 395–402. https://doi.org/10.1016/j.ccr.2007.08.030.

(13) Wong, H.; Leung, R.; Kwong, A.; Chiu, J.; Liang, R.; Swantson, C.; Yau, T. Integrating Molecular Mechanisms and Clinical Evidence in the Management of Trastuzumab Resistant or Refractory HER-2+ Metastatic Breast Cancer. *Oncologist* **2011**, *16* (0), 1051–1062.

(14) Patra, S.; Young, V.; Llewellyn, L.; Senapati, J. N.; Mathew, J. BRAF, KRAS and PIK3CA Mutation and Sensitivity to Trastuzumab in Breast Cancer Cell Line Model. *Asian Pacific J. Cancer Prev.* **2017**, *18* (8), 2209–2213. https://doi.org/10.22034/APJCP.2017.18.8.2209.

(15) Peterson, V. M.; Zhang, K. X.; Kumar, N.; Wong, J.; Li, L.; Wilson, D. C.; Moore, R.; Mcclanahan, T. K.; Sadekova, S.; Klappenbach, J. A. Multiplexed Quantification of Proteins and Transcripts in Single Cells. *Nat. Biotechnol.* **2017**, *35* (10), 936–939. https://doi.org/10.1038/nbt.3973.

(16) Hughes, A. J.; Spelke, D.; Xu, Z.; Kang, C. C.; Schaffer, D.; Herr, A. E. Single-Cell Western Blotting. *Nat. Methods* **2015**, *11* (7), 455–464. https://doi.org/10.1007/978-1-4939-2694-7_46.

(17) Kang, C.; Ward, T. M.; Bockhorn, J.; Schiffman, C.; Huang, H.; Pegram, M. D.; Herr, A. E. Electrophoretic Cytopathology Resolves ERBB2 Forms with Single-Cell Resolution. *npj Precis. Oncol.* **2018**, No. February, 1–10. https://doi.org/10.1038/s41698-018-0052-3.

(18) Rosàs-Canyelles, E.; Modzelewski, A. J.; Geldert, A.; He, L.; Herr, A. E. Multimodal Detection of Protein Isoforms and Nucleic Acids from Mouse Pre-Implantation Embryos. *Nat. Protoc.* **2021**, *16* (2), 1062–1088. https://doi.org/10.1038/s41596-020-00449-2.

(19) Larsson, C.; Grundberg, I.; Söderberg, O.; Nilsson, M. In Situ Detection and Genotyping of Individual MRNA Molecules. *Nat. Methods* **2010**, *7* (5), 395–397. https://doi.org/10.1038/nmeth.1448.

(20) Weibrecht, I.; Lundin, E.; Kiflemariam, S.; Mignardi, M.; Grundberg, I.; Larsson, C.; Koos, B.; Nilsson, M.; Söderberg, O. In Situ Detection of Individual MRNA Molecules

and Protein Complexes or Post-Translational Modifications Using Padlock Probes Combined with the in Situ Proximity Ligation Assay. *Nat. Protoc.* **2013**, *8* (2), 355–372. https://doi.org/10.1038/nprot.2013.006.

(21) *Cold Spring Harbor Protocols*; Sever, R., Ed.; Cold Spring Harbor Laboratory Press, 2020.

(22) Kang, C. C.; Yamauchi, K. A.; Vlassakis, J.; Sinkala, E.; Duncombe, T. A.; Herr, A. E. Single Cell-Resolution Western Blotting. *Nat. Protoc.* **2016**, *11* (8), 1508–1530. https://doi.org/10.1038/nprot.2016.089.

(23) Vlassakis, J.; Yamauchi, K. A.; Herr, A. E. Summit: Automated Analysis of Arrayed Single-Cell Gel Electrophoresis. *SLAS Technol.* **2021**, *26* (6), 637–649. https://doi.org/10.1177/24726303211036869.

(24) Su, A.; Smith, B. E.; Herr, A. E. In Situ Measurement of Thermodynamic Partitioning in Open Hydrogels. *Anal. Chem.* **2019**, *92* (2), 875–883. https://doi.org/10.1021/acs.analchem.9b03582.

(25) Summer, H.; Grämer, R.; Dröge, P. Denaturing Urea Polyacrylamide Gel Electrophoresis (Urea PAGE). *J. Vis. Exp.* **2009**, No. 32. https://doi.org/10.3791/1485.

(26) Kirchdoerfer, R. N.; Huang, J. J.; Isola, M. K.; Cavagnero, S. Fluorescence-Based Analysis of Aminoacyl- and Peptidyl-TRNA by Low-PH SDS PAGE. *Anal. Biochem.* **2007**, *364* (1), 92–94. https://doi.org/10.1016/j.ab.2007.01.019.Fluorescence-Based.

(27) Moss, A. C.; Herr, A. E. In-Gel Fluorescence Detection by DNA Polymerase Elongation. *APL Bioeng.* **2020**, *4* (4). https://doi.org/10.1063/5.0021149.

(28) Geldert, A.; Huang, H.; Herr, A. E. Probe-Target Hybridization Depends on Spatial Uniformity of Initial Concentration Condition across Large-Format Chips. *Sci. Rep.* **2020**. https://doi.org/10.1038/s41598-020-65563-3.

(29) Su, E. J.; Jeeawoody, S.; Herr, A. E. Protein Diffusion from Microwells with Contrasting Hydrogel Domains. *APL Bioeng.* **2020**, *3* (2). https://doi.org/10.1063/1.5078650.

(30) Borm, L. E.; Albiach, A. M.; Mannens, C. C. A.; Janusauskas, J.; Özgün, C.; Fernández-garcía, D.; Hodge, R.; Castillo, F.; Hedin, C. R. H.; Villablanca, E. J.; Uhlén, P.; Lein, E. S.; Codeluppi, S.; Linnarsson, S. Scalable in Situ Single-Cell Profiling by Electrophoretic Capture of MRNA Using EEL FISH. *Nat. Biotechnol.* **2022**. https://doi.org/10.1038/s41587-022-01455-3.

(31) Lee, J. H.; Daugharthy, E. R.; Scheiman, J.; Kalhor, R.; Ferrante, T. C.; Terry, R.; Turczyk, B. M.; Yang, J. L.; Lee, H. S.; Aach, J.; Zhang, K.; Church, G. M. Fluorescent in Situ Sequencing (FISSEQ) of RNA for Gene Expression Profiling in Intact Cells and Tissues. *Nat. Protoc.* **2015**, *10* (3), 442–458. https://doi.org/10.1038/nprot.2014.191.

(32) Wang, X.; Allen, W. E.; Wright, M. A.; Sylwestrak, E. L.; Samusik, N.; Vesuna, S.; Evans, K.; Liu, C.; Ramakrishnan, C.; Liu, J.; Nolan, G. P.; Bava, F.; Deisseroth, K. Three-Dimensional Intact-Tissue Sequencing of Single-Cell Transcriptional States. **2018**, *5691*. https://doi.org/10.1126/science.aat5691.

Chapter 7: Toward a Single-Cell Electrophoretic Assay with a qPCR-Based Readout for Absolute Quantification of Cellular mRNA

Work in collaboration with Yaw O. Ansong Jnr.

7.1 Introduction

As previously introduced in Chapter 6, the single-cell Protein and RNA Electrophoresis (scPREP) assay for in-gel measurements of nucleic acid point mutations and proteoforms from electrophoresed single cells has the potential to open the door to novel areas of biological inquiry. Good assay performance of scPREP depends on the solubilization of mRNA during the cell lysis step, along with complete injection of the mRNA into the polyacrylamide gel, and subsequent capture by the immobilized poly(T) oligo and/or benzophenone-based photocapture. We have multiple questions related to how the lysis/solubilization conditions and the mRNA capture conditions affect the performance of scPREP. Two crucial questions are (1) how lysis buffer composition and lysis time affect mRNA solubilization and subsequent injection into the gel during electrophoresis, and (2) how poly(T) oligomers incorporated into the gel and BMPA photocapture affect the amount of mRNA captured in the gel. It is currently challenging to decouple the effects of the upstream portion of scPREP, which includes mRNA solubilization, electrophoresis, and capture, from the downstream in-gel detection portion of the assay. Additionally, it is generally necessary to better understand the behavior of mRNA electrophoresis in our single-cell electrophoretic assays for future technology development. Therefore, there is a need for an assay specifically designed for the study of mRNA electrophoresis and in-gel mRNA capture.

RT-qPCR is a robust and well-established method to detect mRNA from single cells with high sensitivity and specificity[1–3]. Additionally, RT-qPCR is well-suited to providing absolute quantification of mRNA molecules, even at the single-cell level[2,3]. Our group has previously developed a multimodal nucleic acid and protein assays termed snapBlot that relies on a qPCR-based readout to detect nucleic acids[1]. The snapBlot protocol involves settling cells in microwells in a polyacrylamide gel and performing a fractional lysis of the cytoplasm prior to electrophoresis of the cytoplasmic proteins, laser excision of gel pallets containing the intact nuclei in the microwells, and subsequent qPCR analysis of the nuclear contents[1]. While a powerful assay, there are many limitations of snapBlot that preclude its utility for our characterization studies. First, due to the fractional lysis protocol, snapBlot is inherently limited to detecting only nuclear mRNA via qPCR, while the majority of cellular mRNA resides in the cytoplasm. Additionally, the detected mRNA is from intact nuclei rather than captured in the gel, as in scPREP. Quantifying total cellular mRNA that has been electrophoresed and captured in the gel matrix is crucial for our application of characterizing mRNA solubilization, electrophoresis, and capture. An assay that is similar to snapBlot yet incorporates whole-cell lysis and a mechanism for mRNA release from the gel pallets after electrophoresis has the

potential to assist us in answering our questions about mRNA solubilization, electrophoresis, and capture from single cells. In addition to enabling characterization studies, a modified version of snapBlot that enables the detection of cytoplasmic mRNA has the potential to expand the capabilities of the original assay. Here, we present our approach to designing an assay based on snapBlot that will enable absolute quantification of single-cell total mRNA extracted from gel pallets.

7.2 Materials and Methods

Reagents

A 20 nucleotide-long poly(T) sequence terminated with a 5' acrydite group was purchased from IDT (Coralville, IA, USA). Quick-DNA/RNA Microprep Plus Kit (D7005T) was purchased from Zymo Research (Irvine, CA). QIAquick Gel Extraction Kit (28704) was purchased from Qiagen (Hilden, Germany). High-Capacity cDNA Reverse Transcription Kit (4368814), TaqMan Universal PCR Master Mix (4324018), TaqMan Gene Expression Assay (human beta-actin Hs99999903_m1), TaqMan PreAmp Master Mix (4391128), SYBR Green I nucleic acid stain (S7563), 50 bp DNA ladder (10416014), UltraPure Agarose (16500500), trypsin-EDTA 0.05% (25300054), and penicillin–streptomycin (15140-122) were purchased from Thermo Fisher Scientific (Waltham, MA). Bovine serum albumin (BSA, A7030), urea (U5378), sodium dodecyl sulfate (SDS, L3771), sodium deoxycholate (D6750), Triton X-100 (X100), acrylamide (A3553), N,N'-Bis(acryloyl)cystamine (BAC, A4929), tetramethylethylenediamine (TEMED, T9281), ammonium persulfate (APS, A3678), 3-(trimethoxylsilyl)propyl methacrylate (440159), chlorotrimethylsilane (386529), and nuclease-free water (W4502), were purchased from Sigma-Aldrich (St. Louis, MO, USA). RPMI-1640 media (11875-119) and sterile phosphate buffered saline (PBS, 10010049) were purchased from Gibco. Fetal bovine serum (100-106) was purchased from Gemini Bio-Products (West Sacramento, CA). Buffers were prepared according to standard protocols[4].

Device Fabrication

Polyacrylamide gels were fabricated on silicon wafer substrates with 40 µm tall rails patterned in SU-8, as previously reported[5,6]. After photolithography, wafer substrates were subjected to oxygen plasma treatment for 5 min and subsequently treated for >30 min with chlorotrimethylsilane vapor in vacuum desiccator. Wafers were then rinsed briefly with isopropanol and baked at 110°C for 10 min. After the baking step, the wafers were rinsed with toluene, acetone, isopropanol, and water in series to remove excess silane residue. Prior to casting each gel, wafer substrates were treated with Gel Slick solution.

A stock solution containing acrylamide and BAC (30% acrylamide, 29:1 acrylamide:BAC ratio) was prepared. Gel precursors were then prepared from the stock solution to a concentration of 7% T. Acrydite-terminated poly(T) was added to a final concentration of 10 µM, followed by degassing via sonication for 5 min. APS and TEMED were then added to the precursor to final concentrations of 0.08% and 1%, respectively, before pipetting 150 µL of the solution between the treated SU-8 silicon wafer substrate and a piece of GelBond (Lonza) cut to ~25 mm x 75

mm. The GelBond was weighed down with a glass slide during polymerization. After a 20-min chemical polymerization, the GelBond was lifted from the wafer and washed in 1xPBS for at least 1 h prior to use in experiments.

Cell Culture

MDA-MB-231 cells were obtained from the UC Berkeley Tissue Culture Facility via the American Type Culture Collection and cultured in RPMI-1640 growth medium that was supplemented with 10% fetal bovine serum (FBS) and 1% penicillin/streptomycin. Cells were maintained in an incubator at 37 °C with humidified 5% CO_2 air.

RT-qPCR

RNA extraction followed the Zymo Quick-DNA/RNA Microprep Plus Kit protocol and was performed on either 500,000 cells (bulk) or from one dissolved gel pallet per extraction. DNase treatment was included, and each sample was eluted in either 15 µL of nuclease free water for bulk extractions or 6 µL for gel pallet extractions. After RNA extraction, cDNA synthesis was performed according to the High-Capacity cDNA Reverse Transcription Kit protocol, and pre-amplification was performed according to the protocol included with the pre-amplification master mix (10 cycle pre-amplification option was chosen). RT, pre-amplification, and qPCR reactions were all 20 µL. All qPCR reactions were run in triplicate with -RT controls and no template controls (NTCs) included in each run. qPCR reactions were prepared according to the TaqMan Universal Master Mix protocol. cDNA synthesis and pre-amplification were run on a Bio Rad T100 thermal cycler. qPCR experiments were run on a Bio Rad CFX Connect instrument in Hard-Shell 96-Well PCR Plates (Bio Rad, HSP9601) with Microseal 'B' PCR Plate Sealing Film (Bio Rad, MSB1001) and data were analyzed in Bio Rad Maestro software.

Beta-Actin mRNA Standard Curve Development

Two standard curves were developed, one based on the number of cell equivalents of total RNA extracted in bulk (Cell Standard Curve), and one based on the copy number of beta-actin cDNA amplicons (PCR Standard Curve). For the Cell Standard Curve, bulk extracted RNA from MDA-MB-231 cells was serially diluted in nuclease free water to concentrations ranging from 0.5-5,000 single cell equivalents per reaction before being subjected to cDNA synthesis, pre-amplification, and qPCR. The standard curve equation and plot were generated in Bio Rad Maestro software. For the PCR Standard Curve, a 20 µL cDNA synthesis reaction containing 100,000 single cell equivalents of bulk extracted MDA-MB-231 was prepared. A bulk PCR reaction was prepared with 4.8 µL of the cDNA reaction included in a 20 µL reaction with the TaqMan PreAmp Master Mix and 0.05x concentration of the beta-actin TaqMan Gene Expression Assay. The bulk PCR amplification step followed the cycling protocol recommended in the pre-amplification master mix protocol except that the reaction was run for 30 cycles rather than the 10-14 cycles normally recommended for pre-amplification. Beta-actin amplicons were then run on a 3% agarose gel cast with SYBR Green I dye at a 1x concentration alongside a 50 bp DNA ladder. Electrophoresis was run in 1xTAE buffer for 70 min at 50 V. After confirmation

of the correct PCR product by gel electrophoresis, the band was excised with a razor blade and the amplicons extracted with the QIAquick Gel Extraction kit. Beta-actin amplicons were quantified by UV-vis spectrophotometry on a NanoDrop 2000 and diluted to concentrations ranging from 10^1-10^6 copies before undergoing pre-amplification and qPCR. The standard curve equation and plot were generated in Bio Rad Maestro software.

Single-Cell Assay Protocol

Cell settling, lysis, and electrophoresis followed established protocols[1,5,6] Briefly, MDA-MB-231 cells were harvested from tissue culture flasks by treating with 0.05% trypsin-EDTA for 3 min followed by inactivation with medium that contains serum, centrifugation, and resuspension in ice cold PBS at a concentration of 1-1.5x10^6 cells/mL. Cell settling consisted of pipetting 400 µL of cell suspension on top of a gel and incubating for 10 min followed by 2-4 washes with 1xPBS to remove excess cells on the gel surface. The gel was then aligned with the alignment grid, the wells inspected in brightfield to determine which wells contained cells, and the number of cells in each well recorded on a piece of paper with a printed grid. Gels were then placed in an electrophoresis chamber and the cells lysed for 30 s followed by 15 s electrophoresis at 40 V/cm. Lysis and electrophoresis were carried out in 1xRIPA buffer, as previously described[5], with the addition of 6 M urea. After electrophoresis, gels were washed in 1xTBST for 30 min, aligned with the alignment grid, and the desired gel pallets excised. Gel pallets were individually placed in 0.6 mL microcentrifuge tubes containing 50 µL of 20 mM DTT in 1xPBS and incubated at 60°C for 30 min, vortexing periodically. The dissolved gel pallets were then mixed with 150 µL of DNA/RNA Lysis Buffer from the Zymo Quick-DNA/RNA Microprep Plus Kit. RNA extraction, including DNase treatment, was then carried out according to the kit protocol, and the final purified RNA was eluted in 6 µl of nuclease free water. Each sample was then split in half to create one complete reaction and one -RT control per sample. Finally, the previously described cDNA synthesis, pre-amplification, and qPCR protocols were carried out.

Laser Cutting and Etching

The alignment grid for gel pallet excision was laser etched onto a sheet of acrylic using a Muse Core Desktop CO_2 Laser Cutting and Engraving Machine (Full Spectrum Laser) with settings of 50% speed, 5% power, and 50% current. Prior to gel fabrication, the cut GelBond substrate was placed on the alignment grid and the alignment markers cut with the laser cutter using settings of 20% speed, 3% power, and 40% current. After electrophoresis, the alignment markers on the GelBond substrate were aligned with the markers on the alignment grid and the laser positioned in the top left corner of the top left rectangular region on the grid. Gel pallets of interest were then selected in the software from a pallet array and excised using settings of 20% speed, 3% power, and 40% current.

7.3 Results and Discussion

Assay Overview

We present the concept of a single-cell electrophoretic assay for the detection of both nuclear and cytoplasmic mRNA (Fig. 7-1). Briefly, single cells are gravity settled into microwells in a polyacrylamide gel that contains cleavable crosslinks, subjected to whole-cell lysis to release the contents of both the cytoplasm and the nucleus, and exposed to an electric field to electrophoretically inject the mRNA into the gel. mRNA is captured in the gel by poly(T) oligonucleotides that were co-polymerized into the gel via 5' acrydite groups. After electrophoresis, gel pallets are excised with a CO_2 laser and transferred to a solution containing a reducing agent to dissolve the disulfide crosslinks of the gel and liberate the mRNA for RT-qPCR analysis.

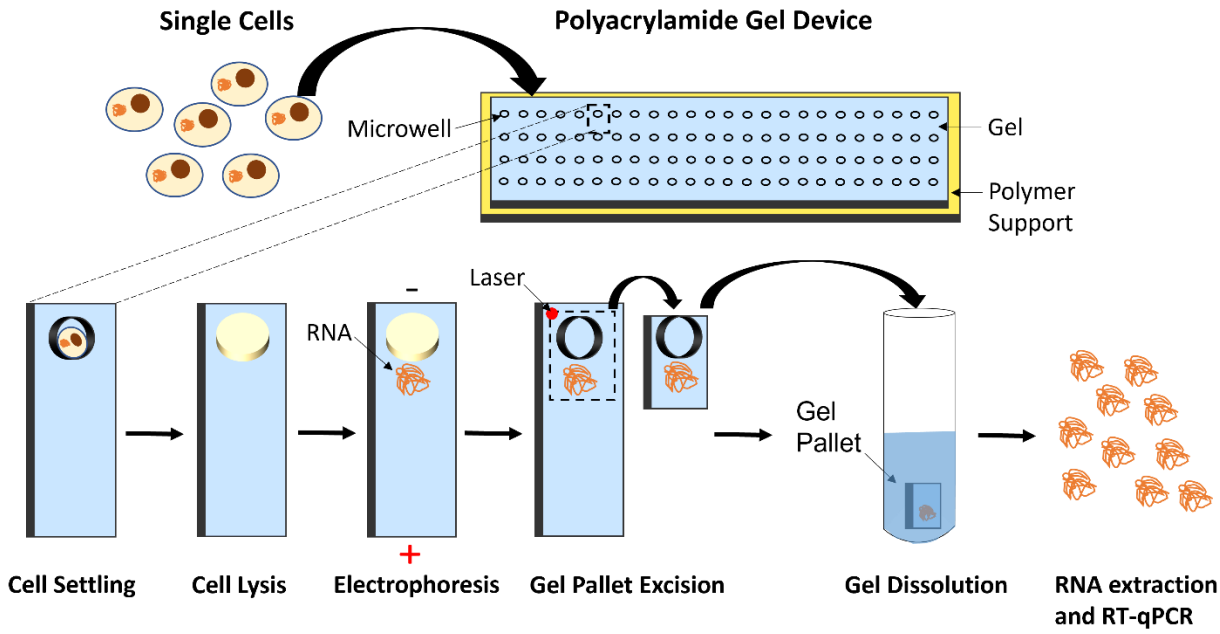

Figure 7-1: A single-cell electrophoretic assay for whole-cell mRNA detection by qPCR of liberated mRNA from dissolved gel pallets. Single cells are settled in a polyacrylamide gel crosslinked with N,N'-bis(acryloyl)cystamine (BAC), lysed, and the mRNA is electrophoresed into the gel. After electrophoresis, gel pallets are excised with a CO_2 laser and transferred to a microcentrifuge tube with DTT solution, which cleaves the disulfide bonds of the BAC crosslinks and dissolves the gel, liberating the mRNA for subsequent RT-qPCR analysis.

At a high level, the workflow is similar to the snapBlot assay as both rely on laser excision of gel pallets and an RT-qPCR readout for mRNA detection and analysis[1]. However, there are several design modifications to snapBlot (Table 7-1) that enable total mRNA detection, enable absolute quantification, and generally improve the assay workflow. The overarching objective of the assay presented here is to enable characterization of mRNA solubilization, electrophoresis, and capture in polyacrylamide gels. Future iterations of this assay also have the potential to expand the capabilities of snapBlot to detect cytoplasmic RNA along with proteins.

Table 7-1: Comparison of the original snapBlot assay to our modified assay. The new assay incorporates many modifications that enable highly specific absolute quantification of mRNA from single cells and improve the assay workflow. Design modifications and different capabilities of the assays are outlined in the table.

	Original snapBlot[1]	**Modified System**
Gel type	Acrylamide/Bis	Acrylamide/BAC (dissolvable)
Well size	200 µm	30 µm (single-cell optimized)
Well selection/inspection	Nuclear stain	Brightfield well inspection (simpler)
Laser excision	Manual one-by-one pallet excision	Multiple pallet extraction + alignment grid (higher throughput)
RNA extraction	Intact nuclei lysed from pallet and RNA extracted via silica-based kit	Gel dissolved with DTT and RNA extracted via silica-based kit
Location of Detected RNA	Only nuclear mRNA	Nuclear and cytoplasmic mRNA
qPCR Detection method	SybrGreen	Taqman Probes (higher specificity)
Level of Quantification	Relative quantification	Absolute quantification down to single cell level

The first major modification to the snapBlot workflow is the choice of gel crosslinker. N,N'-methylenebisacrylamide (bis) is the standard crosslinker used in polyacrylamide gels, including in previous work by our group[1,5]. N,N'-bis(acryloyl)cystamine (BAC) is an alternative crosslinker that contains disulfide bonds that can be cleaved in the presence of a reducing agent, such as dithiothreitol (DTT), resulting in gel dissolution[7]. Dissolution of a polyacrylamide gel crosslinked with BAC represents a simple method to achieve release of biomolecules from a polyacrylamide gel, as liberation of proteins from polyacrylamide gels crosslinked with BAC upon gel dissolution has been demonstrated in the literature[8,9]. We anticipate the need for such a chemical release mechanism. The currently depicted assay does not include the BPMA photocapture step that is included in snapBlot and in the single-cell western blot (scWB)[5], but we anticipate evaluating the effect of benzophenone photocatpure in our characterization experiments. We posit that gel dissolution will be especially necessary in the case of BPMA photocaptured mRNA. For these reasons, BAC was chosen as the crosslinker in place of bis to enable gel dissolution and liberation of captured mRNA molecules from the gel upon exposure to DTT. Inclusion of the in-gel mRNA capture and release mechanism will ultimately enable the detection of both cytoplasmic and nuclear mRNA, expanding the capabilities of snapBlot, which is only capable of detecting nuclear mRNA.

Other changes to the snapBlot device design and assay workflow include changes to the microwell dimensions, microwell selection process, and gel pallet excision protocols. snapBlot was optimized for detecting mRNA and proteins from mouse embryos consisting of multiple cells. Therefore, the original snapBlot assay includes 200 µm diameter microwells in 200 µm

thick polyacrylamide gels, which encourages settling of multiple cells per well. Meanwhile, scWB gels that are optimized for single-cell settling are ~40 µm thick and contain ~30 µm diameter wells[5]. Here, we incorporate 30 µm diameter microwells in 40 µm thick gels to promote single-cell settling. The use of smaller microwells requires other modifications to the device design, as small wells are challenging to locate under the microscope during the imaging step prior to lysis and electrophoresis, and during the gel pallet excision step. Imaging prior to lysis and electrophoresis is necessary to determine which wells contain cells, subsequently enabling selection of gel pallets to excise after electrophoresis. To improve the identification of microwells, alignment markers were included on the silicon wafer mold, and a grid with alignment markers was laser etched in acrylic. Alignment of the gel to the grid after cell settling results in a simple method to locate the microwells. The use of small microwells that are similar in size to a single cell also allows us to visualize the cells in the wells in brightfield, eliminating the nuclear staining step, which can affect the cell yield and viability. Another key benefit of the alignment markers and the etched grid is simpler, faster alignment of the gel to the grid prior to gel pallet excision. Such a reduction in the time and the amount of manipulation of the gel reduces the risks of mRNA degradation or contamination. The grid with alignment markers also enables laser excision of multiple pallets in one run of the laser cutter rather than needing to re-align and manually adjust the laser cutter prior to excising each pallet of interest, also reducing the assay time. Overall, our modifications to the snapBlot device, well selection process, and laser excision protocol will result in a more streamlined, simpler assay optimized for single cell mRNA detection with less risks of RNA loss or contamination.

In addition to modifying the gel chemistry and the device design, we chose a different qPCR chemistry and mRNA target. TaqMan qPCR chemistry was chosen in place of SYBR Green qPCR chemistry due to its consistently high specificity and the commercial availability of many primer + probe sets that can be used for both pre-amplification and qPCR, eliminating the need for in-house primer design. We chose to detect beta-actin rather than GFP as our mRNA target for assay validation to eliminate the need for GFP transfected cell lines. Beta-actin is a particularly advantageous target due to its high abundance, presence in all mammalian cells, and absolute quantification previously documented in the literature[10]. We are currently focused solely on mRNA detection but could expand to protein detection in the future for a multimodal assay capable of detecting total cellular mRNA and proteins.

Device Design and Fabrication

Silicon wafer molds are fabricated by patterning a 3x15 array of 30 µm diameter SU-8 microposts that are spaced 5 mm apart in the x-direction and 8 mm apart in the y-direction (Fig. 7-2A). The large spacing between wells enables laser excision of gel pallets. SU-8 rails to control the gel height during polymerization and alignment markers are patterned along with the micropost array. A feature height of 40 µm was chosen for the well aspect ratio to be within the optimal range for single cell settling[6]. Polyacrylamide gels are fabricated on a treated polyester film substrate (GelBond) with the patterned silicon wafer serving as a positive mold, resulting in a gel patterned with a microwell array.

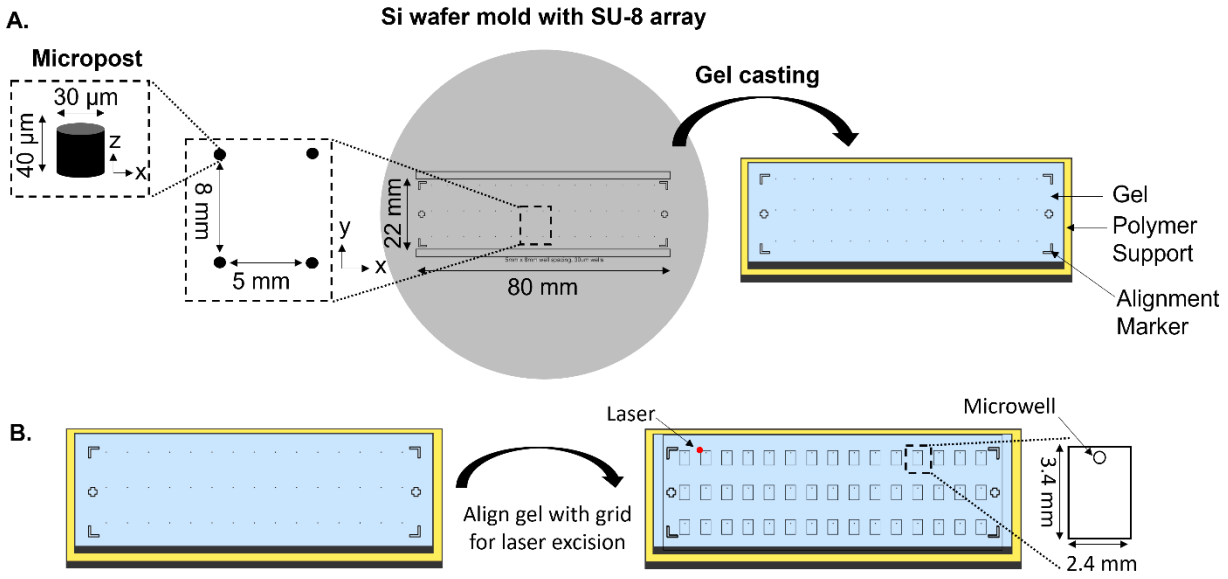

Figure 7-2: Devices are designed for single-cell settling and efficient, simple gel pallet excision. (A) Devices are fabricated by polymerizing a 40 µm-thick layer of polyacrylamide gel between a silicon wafer patterned with a 15 x 3 array of 30 µm diameter SU-8 microposts and a piece of treated polyester film (GelBond), (B) After electrophoresis, gels are aligned via alignment markers with a grid that was laser etched in acrylic to facilitate efficient laser excision of 3.4 x 2.4 mm gel pallets.

The device design allows for simple gel pallet excision through the alignment of the gel to a laser etched grid patterned with the alignment markers and rectangular boxes to demarcate each gel pallet (Fig. 7-2B). Gel pallet dimensions are 2.4 mm x 3.4 mm with the microwell located near the top of the gel pallet to allow maximum space along the direction of electrophoresis to excise the region where electrophoresed mRNA is captured. This gel pallet configuration is in contrast to the pallet configuration in snapBlot, where the microwell is located in the center of each pallet because the intact nuclei are contained within the microwells. The use of alignment markers eliminates the need to search for the small microwells under the microscope and align based on the well position, which is a tedious and time-consuming process in snapBlot that limits the assay to larger microwells. Another benefit of the grid design is the ability to program the laser cutter to excise multiple pallets of interest in one run without the need to individually align each pallet. The excision protocol involves aligning the alignment markers in the GelBond substrate to the alignment markers on the grid and positioning the laser in the top left corner of the first rectangular box corresponding to the position of the first gel pallet. An array consisting of the gel pallet positions of interest is then created in the laser cutter software and all the selected pallets excised.

Upon execution of the gel fabrication and pallet excision protocols, various challenges and observations led to specific improvements. First, we noticed that polyacrylamide gels crosslinked with BAC were sticking to the silicon wafer molds rather than adhering to the GelBond substrate. The gel residue on the silicon wafers was far more challenging to remove than residue

from standard polyacrylamide gels. We hypothesized that the issue was due to the dichlorodimethylsilane surface treatment that is applied to all our silicon wafer molds to render the surface hydrophobic and promote adhesion to the substrate rather than the mold. A literature search revealed that thiol groups can replace residual chlorines on dichlorodimethylsilane to form covalent bonds[11]. Chlorotrimethylsilane is chemically similar to dichlorodimethylsilane yet lacks a second chlorine that could react with free thiols and is also used as a common hydrophobic surface treatments[12], which led us to try surface treatment with chlorotrimethylsilane. Less adhesion of the gel to the silicon wafer mold was observed when the mold was treated with chlorotrimethylsilane than with dichlorodimethylsilane, but the issue was not completely solved. Successful gel fabrication was achieved with a combination of a tricholortrimethylsilane treatment after mold fabrication together with the application of Gel Slick prior to fabricating each gel. Difficulty seeing the alignment markers in the gel was another challenge that arose during the alignment and gel pallet excision steps. We found that laser excising the alignment markers in the GelBond substrate prior to gel fabrication results in more consistent alignment of the substrate with the silicon wafer mold and improved visibility of the alignment markers during the alignment with the laser etched grid prior to gel pallet excision. With the described modifications to the gel fabrication and pallet excision protocols, we are able to achieve reliable gel fabrication, alignment, and gel pallet excision.

Development of qPCR Standard Curves for Absolute mRNA Quantification

One of our essential assay design requirements is absolute quantification of mRNA. The relative mRNA quantification in the snapBlot assay does not meet our needs because we need to make precise comparisons between the amount of mRNA captured by the assay to the amount of mRNA contained in a single cell. Absolute mRNA quantification in RT-qPCR is achieved by comparing the quantification cycle (C_q) of an unknown sample to a standard curve that relates C_q values to known quantities of nucleic acids[2,3]. Standard curves can be generated from serial dilutions of a known quantity of total RNA extracted from a bulk cell population or from serial dilutions with known copy numbers of amplicons of the gene of interest. We chose to generate two standard curves, one based on the number of cell equivalents of total RNA (‘Cell Standard Curve’) and one based on known quantities of beta-actin amplicons (‘PCR Standard Curve’). Standard curves were generated following best practices for qPCR standard curve development[2,3] with the workflows for generating both standard curves outlined in Fig. 7-3. Performing the bulk PCR to generate beta-actin amplicons for the PCR Standard Curve initially proved challenging due to the high GC content (>75%) of the portion of the beta-actin gene that needed to be amplified to allow for detection with the commercial qPCR primer + probe set. Since the pre-amplification step of our protocol that takes place prior to qPCR utilizes the same primer + probe set as the qPCR, we were able to modify the pre-amplification protocol to serve as a bulk PCR step for beta-actin amplicon generation. The reaction composition of the bulk PCR was the same as in a standard pre-amplification reaction and the cycling protocol was the same except that 30 amplification cycles were run instead of the standard 10-14 cycles recommended for pre-amplification. The PCR reaction with the pre-amplification mix resulted in concentrated beta-actin amplicons of the correct size, verified by UV-vis spectrophotometry and gel electrophoresis, and were detectable with qPCR.

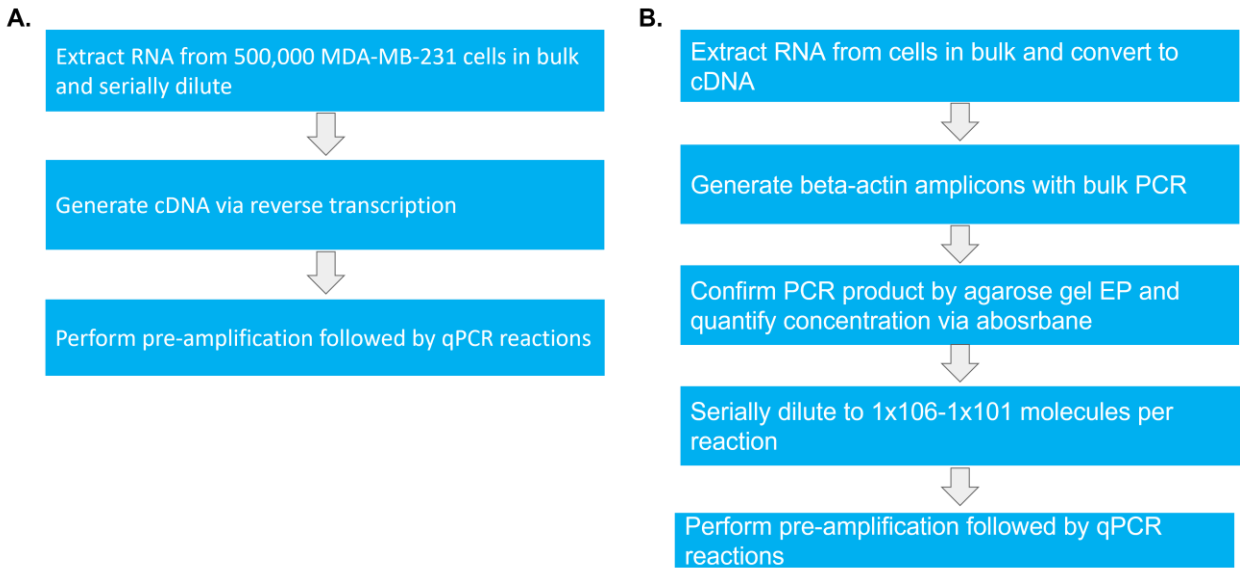

Figure 7-3: Workflows for standard curve generation of (A) the Cell Standard Curve, and (B) the PCR Standard Curve.

Both standard curves exhibited the anticipated trends of decreasing C_q values with increasing concentrations of nucleic acids and exhibited R^2 values of 0.999, indicating a strong linear trend (Fig. 7-4). With the PCR Standard Curve, we were able to estimate the beta-actin mRNA copy number in a single MDA-MB-231 cell. An estimated beta-actin mRNA copy number of ~10^3 molecules per single MDA-MB-231 cell was obtained by applying the PCR Standard Curve equation to the C_q value corresponding to a 10^0 cell equivalent dilution of bulk RNA. Our result is consistent with results in the literature that estimate a beta-actin mRNA copy number on the order of 10^3 molecules per single mammalian cell[10]. While both standard curves allow for forms of absolute quantification, we chose to move forward primarily with the PCR Standard Curve, as we prefer being able to quantify the number of beta-actin mRNA molecules directly.

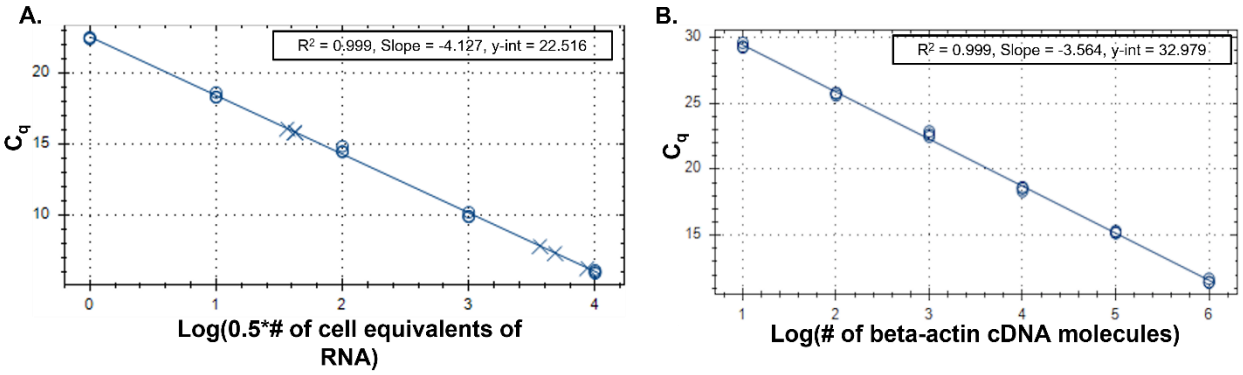

Figure 7-4: Two standard curves were developed to enable absolute quantification of beta-actin mRNA. (A) The Cell Standard Curve relates the qPCR C_q values to the number of cell

equivalents of total RNA included in a reaction, (B) The PCR Standard Curve relates the qPCR C_q values to the number of beta-actin cDNA molecules per reaction. All qPCR measurements were taken in triplicate, with all data points displayed on each plot. Controls (-RT and NTC) were included in each run and did not exhibit any amplification.

Preliminary Results and Challenges to Running the Full Assay

We attempted to run the full assay twice to detect beta-actin mRNA from single cells that were lysed and electrophoresed in a 7% T, 3.3% C BAC gel. Positive and negative controls were included to match best practices when designing single-cell qPCR assays[2,3]. One negative control consisted of blank gel pallets encompassing wells that did not contain cells to identify potential contamination from cell debris on the surface of the gel after cell settling or from mRNA diffusion. Additional negative controls included no template controls (NTCs) to identify the presence of contamination in the qPCR reaction, and -RT controls where the reverse transcriptase was omitted to evaluate for the presence of contaminating genomic DNA. The extracted RNA sample from each pallet was split in half to allow for a -RT control for each pallet. A positive control consisting of 10^4 copies of beta-actin amplicons was also included. Precautions were taken to minimize RNase contamination included the use of RNase free reagents and wiping down all surfaces with RNase ZAP prior to running experiments.

We encountered multiple challenges during our preliminary runs of the assay that will require modifications to the protocol to correct. First, we observed many deformed microwells that cells would not settle in and found that deformed microwellsare far more common in BAC gels than standard gels crosslinked with bis. The increased prevalence of deformed microwells in gels crosslinked with BAC is likely due to different mechanical properties of BAC gels and related to issues of gels sticking to the silicon wafer mold. Weighing down the gel during polymerization and using a sufficient amount of precursor resulted in fewer deformed wells. Additionally, it was difficult to see the wells when under a microscope, even when using the alignment markers. We selected wells that we thought contained cells but did not observe qPCR amplification. We hypothesize that we may have selected different wells than we thought due to the challenges of identifying the wells under the microscope. Future work will involve (1) fabricating thicker gels with larger microwells to evaluate our assay performance under conditions similar to the original snapBlot and (2) developing better methods for identifying small microwells to enable the use of microwells optimized for single cell settling. In the longer term, we plan to combine protein measurements with the mRNA measurements, which will result in an assay that is applicable for answering novel biological questions.

Characterization of BAC Gel Pallet Dissolution and mRNA Recovery from BAC Gels

We hypothesize that mRNA captured in polyacrylamide gels crosslinked with BAC can be retrieved through gel dissolution with DTT. A scheme demonstrating the mechanism of gel dissolution and the proposed mRNA release mechanism is outlined in Fig. 7-5. Here, we propose experiments to study mRNA capture and release from polyacrylamide gels crosslinked with BAC.

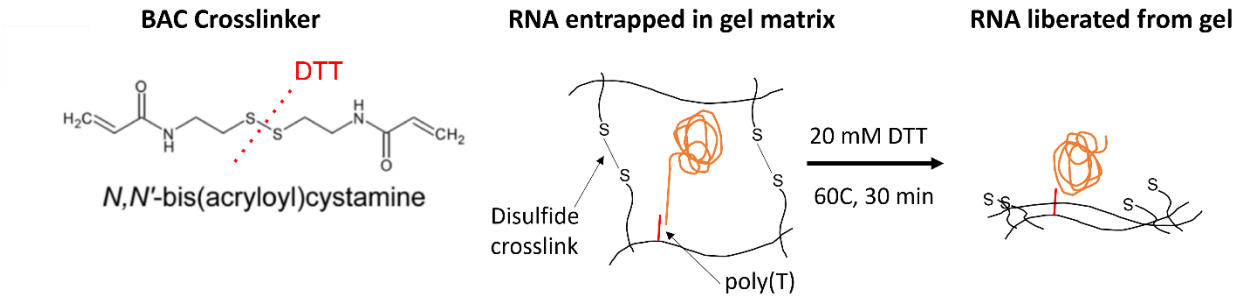

Figure 7-5: BAC crosslinker allows for release of mRNA upon treatment of the polyacrylamide gel with a reducing agent. The chemical structure of BAC, shown on the left, contains a disulfide bond that can be cleaved with the reducing agent DTT. On the right is a schematic depicting mRNA in a polyacrylamide gel pore that is released upon treatment with DTT. Note: chemical structure adopted from Sigma Aldrich.

The first step toward mRNA release studies from gels crosslinked with BAC is optimization of the gel pallet dissolution conditions. Dissolution of polyacrylamide gels crosslinked with BAC is dependent on the gel polymerization conditions and the molar ratio of reducing agent to BAC[7,9]. High concentrations of TEMED are necessary to form shorter chains during polymerization. Otherwise, the gels will be insoluble regardless of reducing agent concentration and reaction time. The most crucial factor to ensure gel dissolution is including a molar excess of reducing agent. Our calculations indicate that 50 µL of 1 mM DTT solution provides a sufficient excess to dissolve a gel pallet. However, an open question is whether visible gel dissolution is sufficient for RNA release, or whether the reaction must continue for longer to ensure complete molecular cleavage of the BAC crosslinks. When gels crosslinked with BAC are dissolved for a standard time of 15 min, the resultant solution is highly viscous, suggesting incomplete decrosslinking at the molecular level. For this reason, it is important to study the effect of gel dissolution conditions on mRNA release. In preliminary experiments to qualitatively evaluate gel dissolution, gel pallets were excised from a 7% T, 3.3% C polyacrylamide gel crosslinked with BAC and subjected to dissolution in 20 mM DTT for 20 min at 60ºC with periodic vortexing. The gel dissolution starting conditions were chosen because they were found in a previous study to result in RNase inactivation and keep mRNA stable[13], a coincidental additional benefit as RNase degradation of mRNA during our protocol is a concern. A negative control of a gel pallet incubated in PBS was evaluated alongside the pallets exposed to DTT. After the incubation, the pallets were removed from the microcentrifuge tubes and the GelBond scraped with tweezers to identify undissolved gel residue on the surface. No gel residue was observed on the gel pallets incubated in DTT solution upon scraping with tweezers, while gel was clearly still present on the pallet incubated in PBS, suggesting complete gel dissolution under the conditions evaluated.

After qualitative confirmation of gel dissolution under the selected conditions, we seek to evaluate recovery of mRNA released from dissolved gel pallets. We propose a workflow where a set quantity of bulk extracted RNA is included in the gel precursor prior to polymerization. This approach of including mRNA and acrydite-terminated poly(T) in a polyacrylamide gel precursor prior to polymerization has been successfully demonstrated in the literature[14]. Such a workflow eliminates the variability introduced from single-cell lysis and electrophoresis, simplifying the

assay to answer specific questions of interest. We plan to evaluate different incubation times and DTT concentrations to optimize the mRNA recovery with this system. Ultimately, we wish to apply the optimized conditions to experiments evaluating the effect of different mRNA capture mechanisms (e.g. BPMA and poly(T)), and study these phenomena from electrophoresed single cells.

7.4 Conclusions

In this chapter, we introduce the concept of a single-cell electrophoretic assay for absolute quantification of both cytoplasmic and nuclear mRNA. While our novel assay shares many similarities with the snapBlot assay, there are key modifications to the device design, fabrication, and operation to enable detection of both cytoplasmic and nuclear mRNA from single cells. The most substantial modification is the use of a polyacrylamide gel crosslinked with BAC, which enables whole cell lysis and electrophoreses followed by gel dissolution and retrieval of electrophoresed mRNA from the gel for qPCR analysis. Additional modifications include the addition of alignment markers to enable inspection of small microwells and streamline the gel pallet laser excision protocol. To improve the release of gels crosslinked with BAC from the silicon wafer molds, we developed a new surface treatment protocol with chlorotrimethylsilane and Gel Slick. We also report on the generation of standard curves for beta-actin mRNA quantification to meet the essential design requirement of absolute mRNA quantification. While preliminary experiments with the complete assay indicate the need for further modifications to the well selection and alignment processes, we were able to demonstrate successful gel pallet dissolution with DTT. Future work includes improving the well selection and alignment processes to accommodate single cell settling and evaluating mRNA capture and release in a simplified system that involves direct incorporation of bulk mRNA into the gels.

The primary objective of the assay presented here is to serve as a tool for characterization of mRNA solubilization, electrophoresis, and capture in polyacrylamide gel electrophoretic assays. We seek to apply this assay to answer fundamental questions about factors that affect the performance of the scPREP assay and other fundamental questions about mRNA behavior in our electrophoretic assays. In the future, we also plan to incorporate single-cell protein measurements into the assay workflow for a multimodal assay that expands on the capabilities of snapBlot. Such a multimodal assay has the potential to open the door to new areas of biological inquiry.

7.5 Bibliography

(1) Rosàs-Canyelles, E.; Modzelewski, A. J.; Geldert, A.; He, L.; Herr, A. E. Multimodal Detection of Protein Isoforms and Nucleic Acids from Mouse Pre-Implantation Embryos. *Nat. Protoc.* **2021**, *16* (2), 1062–1088. https://doi.org/10.1038/s41596-020-00449-2.

(2) Stahlberg, A.; Kubista, M. The Workflow of Single-Cell Expression Profiling Using Quantitative Real-Time PCR. *Expert Rev. Mol. Diagn.* **2014**, *14* (3), 323–331.

(3) Zucha, D.; Kubista, M.; Valihrach, L. Tutorial : Guidelines for Single-Cell RT-QPCR. *Cells* **2021**, *10* (2607).

(4) *Cold Spring Harbor Protocols*; Sever, R., Ed.; Cold Spring Harbor Laboratory Press, 2020.

(5) Hughes, A. J.; Spelke, D.; Xu, Z.; Kang, C. C.; Schaffer, D.; Herr, A. E. Single-Cell Western Blotting. *Nat. Methods* **2015**, *11* (7), 455–464. https://doi.org/10.1007/978-1-4939-2694-7_46.

(6) Kang, C. C.; Yamauchi, K. A.; Vlassakis, J.; Sinkala, E.; Duncombe, T. A.; Herr, A. E. Single Cell-Resolution Western Blotting. *Nat. Protoc.* **2016**, *11* (8), 1508–1530. https://doi.org/10.1038/nprot.2016.089.

(7) Hansen, J. N.; Pfeiffer, B. H.; Boehnert, J. A. Chemical and Electrophoretic Solubilizable Disulfide Properties Gels Of. *Anal. Biochem.* **1980**, *105*, 192–201.

(8) Bode, J.; Schroter, H.; Maas, K. Dissolvable Disulphide-Polyacrylamide Gels for the Electrophoretic Analysis of Chromosomal Proteins and for Affino-Electrophoresis of Thiol-Proteins. *J. Chromatogr.* **1980**, *190*, 437–444.

(9) Takemori, N.; Takemori, A.; Wongkongkathep, P.; Nshanian, M.; Loo, R. R. O.; Lermyte, F.; Loo, J. A. Top-down/Bottom-up Mass Spectrometry Work Fl Ow Using Dissolvable Polyacrylamide Gels. **2017**. https://doi.org/10.1021/acs.analchem.7b00357.

(10) Larsson, C.; Grundberg, I.; Söderberg, O.; Nilsson, M. In Situ Detection and Genotyping of Individual MRNA Molecules. *Nat. Methods* **2010**, *7* (5), 395–397. https://doi.org/10.1038/nmeth.1448.

(11) Matsuura, S.; Kurita, H.; Nakano, M.; Komatsu, J.; Takashima, K.; Katsura, S.; Mizuno, A. One-End Immobilization of Individual DNA Molecules on a Functional Hydrophobic Glass Surface One-End Immobilization of Individual DNA Molecules. *J. Biomol. Struct. Dyn.* **2012**, *20* (3), 429–436. https://doi.org/10.1080/07391102.2002.10506861.

(12) Szkop, M.; Kliszcz, B.; Kasprzak, A. A. A Simple and Reproducible Protocol of Glass Surface Silanization for TIRF Microscopy Imaging. *Anal. Biochem.* **2018**, *549*, 119–123. https://doi.org/10.1016/j.ab.2018.03.020.

(13) Pasloske, B. L.; Wu, W. METHOD AND REAGENTS FOR INACTIVATING RIBONUCLEASES RNASE A, RNASE I AND RNASE T1. USOO677721OB1, 2004.

(14) Li, S.; Kendall, J.; Park, S.; Wang, Z.; Alexander, J.; Moffitt, A.; Ranade, N.; Danyko, C.; Gegenhuber, B.; Fischer, S.; Robinson, B. D.; Lepor, H.; Tollkuhn, J.; Gillis, J.; Brouzes,

E.; Krasnitz, A.; Levy, D.; Wigler, M. Copolymerization of Single-Cell Nucleic Acids into Balls of Acrylamide Gel. *Genome Res.* **2020**, *30*, 49–61. https://doi.org/10.1101/gr.253047.119.Freely.

Chapter 8: Conclusions and Future Directions

In this dissertation, we sought to address some of the major limitations of current single-cell in-gel assays. In the first portion of this dissertation, we evaluated various approaches aimed at improving the multiplexing capability and sensitivity of in-gel immunoassays. Toward improved multiplexing of in-gel immunoassays with fluorescence readouts, we studied the quenching behavior of common fluorophores when exposed to H_2O_2, observing complete in-gel quenching of antibody conjugated fluorophores. Toward improved sensitivity of in-gel assays, we characterized in-gel DNA signal amplification reactions. We first scrutinized polymerase elongation of gel-immobilized single-stranded DNA overhangs with fluorescently labeled nucleotides, reporting retarded diffusion of the DNA polymerase, a novel observation. The in-gel polymerase elongation system also allowed us to develop DNA sequence design rules for signal amplification based on the number of incorporated labeled nucleotides per strand and the spacing between labeled nucleotides. Next, we characterized hybridization chain reaction (HCR) as a signal amplification strategy in dense polyacrylamide gels, observing that HCR resulted in three orders of magnitude of signal amplification in an 8% T gel and followed pseudo first-order DNA hybridization kinetics. Finally, we evaluated immuno-HCR as a protein signal amplification strategy for in-gel immunoassays. Since immuno-HCR relies on DNA-antibody conjugates, we characterized the binding affinity and thermodynamic partitioning behavior of DNA-antibody conjugates, observing substantial yet not insurmountable decreases in the binding affinity and partition coefficients. Protein detection in dense polyacrylamide gels was achieved with immuno-HCR in preliminary experiments, yet further signal amplification is necessary to result in an improvement over standard antibody immunoprobing.

The characterization studies presented in this dissertation contribute to an improved understanding of in-gel enzymatic and DNA hybridization reactions that will benefit future assay design endeavors. Here, we report retarded diffusion of DNA polymerase for the first time. It is possible that retarded diffusion phenomena due to intermolecular interactions are even more widespread in enzymatic and biomolecular binding reactions. Therefore, there is a need to develop systems to make direct measurements of retarded diffusion and subsequently further study these retarded diffusion phenomena. Our observations of in-gel HCR behavior suggest that HCR signal amplification is applicable across different gel densities and that in-gel HCR kinetics can be modeled by standard pseudo first-order DNA hybridization kinetics. This knowledge will lead to optimization and broader applicability of in-gel HCR assays. Future work is needed to evaluate in-gel HCR under additional gel density and reaction conditions. There is also a need to run more replicates of the in-gel HCR kinetics experiments to demonstrate reproducibility. Our study of in-gel immuno-HCR provides the first quantitative characterization of the binding affinity and thermodynamic partitioning behavior of DNA-antibody conjugates, albeit under a limited set of conditions. There is a large parameter space of different antibody-antigen pairs and gel densities that still need to be explored. Additionally, the effect of the degree of labeling on the binding affinity and partitioning behavior of DNA-antibody conjugates needs to be further studied. While our preliminary immuno-HCR results did not demonstrate an improvement over standard immunoprobing with fluorescently labeled secondary antibodies, we nonetheless see potential for immuno-HCR signal amplification to improve the sensitivity of in-gel

immunoassays with the use of branched HCR systems that provide additional signal amplification. In totality, our characterization studies begin to address many of the knowledge gaps that plague in-gel assays.

In the second portion of this dissertation, we presented two novel assays that represent a step forward toward the development of single-cell multimodal assays for co-detection of nucleic acid point mutations and protein isoforms. We first introduced Single-Cell Protein and RNA Electrophoresis (scPREP), an electrophoretic assay that harnesses the power of the single-cell western blot (scWB) for isoform-specific protein detection and incorporates a single nucleotide-specific in-gel mRNA measurement via rolling circle amplification (RCA) with padlock probes (PLPs). As a proof-of-concept, we demonstrated in-gel co-detection of beta-actin mRNA and beta-actin protein from single cells with scPREP. While detection of protein isoforms and mRNA point mutations is theoretically possible with the chosen detection methods, more work is needed to move the assay forward from the preliminary concept. Additionally, we encountered substantial issues with reproducibility that will need to be resolved. Future work will focus on three primary areas: (1) improving the reproducibility of in-gel mRNA detection, (2) developing an automated image analysis pipeline to enable improved identification and quantification of mRNA, and (3) optimizing the assay for co-detection of point mutations and protein isoforms. In the long run, we would like to see future iterations of scPREP applied to a set of clinically relevant biological targets.

Alongside scPREP, we introduced another assay concept aimed at detecting electrophoresed mRNA from single cells via a qPCR readout. The device design and assay workflow drew on snapBlot, another assay developed by our group, with key modifications to enable absolute quantification of beta-actin mRNA from lysed and electrophoresed single cells. Currently, this assay exists as a concept, as we have not yet completed a successful run. Optimizing the device dimensions and various aspects of the assay workflow are underway. While the initial motivation behind the development of this assay was to serve as a characterization tool to study mRNA capture under different lysis, electrophoresis, and capture conditions, there is potential to employ the assay in a standalone manner to enable novel biological measurements.

The single-cell multimodal assays presented here seek to fill the gap in currently available technologies that precludes co-detection of protein isoforms and nucleic acid point mutations in single cells. Overall, improvements in the sensitivity and specificity of in-gel assays and novel single-cell multimodal assays will usher in new frontiers in biological inquiry. Ultimately, the work presented in this dissertation will help unravel the unsolved mysteries surrounding the Central Dogma of Biology.

Appendix A

```
%This function calculates SNRs from good indices (index_dev_to_analyze), determined by the
%fitPeaks function. It can be used for determining SNRs from the initial
%image that was analyzed, and from an image that may have minimal signal
%(i.e. post-quenching)

%input arguments
%data_struct: the data structure being analyzed
%peak_bounds: the peak bounds selected during fitPeaks in the initial image
%good_indices: the indices in the initial structure, which were determined as good from the first
image
%fit_coefficients: the fit coefficients from the initial image

%outputs
%SNRs: signal-to-noise ratios, defined as the ratio maximum signal within the
%peak bounds selected in the first image to the standard deviation of the
%background

function [SNR]=SNRcalc(data_struct,fit_coefficients,good_indices);

%get good devices
devices=data_struct.int_prof(:,:,good_indices);
num_good_indices=numel(good_indices);

%calculate noise
for i=1:num_good_indices
   device=devices(:,:,i);
   fits=fit_coefficients(:,:,i);
   loci=round((round(fits(2))/5)+1);

   xval=device(:,1);
   yval=device(:,2);
   yvalsmooth=smooth(yval);

   noise(i)=std(yval(end-5:end));
   signal(i)=yvalsmooth(loci);
   SNR(i)=(signal(i)./noise(i))';
end
```

Appendix B

```
%this script fits a PDE unsteady state diffusion model to image
%data of polymerase diffusion in a polyacrylamide gel

clear; clc; close all;

%load timelapse tiff image series (add name into script each time running)
img=ReadTiffStack('121719_timelapese_500ms_noDNA(3).tif');
summed=zeros(1040,7);

%threshold for 0.462 partition coefficient
thres=0.462*(mean(img(1040,500:800,1))-mean(img(1,500:800,1)))+mean(img(1,500:800,1));
for i=1:7
   frame=squeeze(img(:,:,i)); %isolate each frame of the timelapse
   region=frame(1:1040,500:800); %select 300 pixels in center of image
   region(region > thres) = 0; %select only pixels with values >threshold
   summed(:,i)=sum(region,2); %sum together all the pixels in the region
end

%process data by subtracting the t=0 timepoint and normalizing
summed_0=summed(:,1);
summed=minus(summed(:,2:7),summed_0);
[M,I]=max(summed(:,1));
summed=summed(1:I,:);
Cnorm=bsxfun(@rdivide,summed,max(summed,[],1)); %normalize
Cnorm=transpose(flip(Cnorm,1)); %flip values in each column and transpose
Cnorm=([[1,zeros(1,I-1)]; Cnorm]); %add in initial condition

%_____________________________________________________________________%
%define diffusion coefficient guess in cm^2/s for fitting the PDE
Dg = 0.000000139;
D=zeros(1); %define the variable D

%enter x and t values
data.t = [0,5*60,10*60,15*60,20*60,25*60,30*60];
data.x = [(1/3125):(1/3125):(I/3125)]; %adjusted for number of pixels after processing
%use lsqcurvefit to fit the data to the PDE model
[D resnorm residual, exitflag]=lsqcurvefit(@pset,Dg,data,Cnorm);

Csol=pset(D,data);

%plot the data and fitted model
figure(1)
mesh(data.x,data.t,Csol,'edgecolor','b')
hold on
```

```
mesh(data.x,data.t,Cnorm,'edgecolor','g')
xlabel('Distance in cm')
ylabel('Time in s')
zlabel('Normalized Fluor Intensity')

%calculate R2 value
SST=sum(((Cnorm-mean2(Cnorm)).^2),'all'); %SST for R^2 calculation
R2=1-(resnorm/SST); %calculate R^2=SSE/SST

%_____________________________________________________________________%
%function that solves the PDE
function sol=pset(D,data)

m = 0; %cartesian coordinates
x=data.x; %distance in units of cm (based on pixel size)
t=data.t; %time in s
options=[]; %default options

%solve PDE with pdepe function
sol = pdepe(m,@pdefun,@pdeic,@pdebc,x,t,options);

    %function to specify 1D PDE for diffusion
    function [c,f,s] = pdefun(x,t,Cnorm,DCDz)
    c = 1;
    f = D*DCDz;
    s = 0;
    end

    %IC function that specifies initial conditions for the PDE in time
    function u0 = pdeic(x)
    u0 = 0;
    end

    %function with the boundary conditions for the diffusion PDE

    function [pl,ql,pr,qr] = pdebc(xl,Cl,xr,Cr,t)
    Cp = 1; %normalized concentration of polymerase
    pl = Cl-Cp;
    ql = 0;
    pr = 0;
    qr = 1;
    end
end
```

Appendix C

```
%this script fits an exponential curve based on first-order DNA hybridization
%kinetics outlined in Wetmur et al. 1991 to HCR data in gel

clear; clc; close all;

%input data
t=[0.167,0.5,1,2,4,8,24]; %time in hr
f=input('Input fluorescence intensity data '); %input fluorescence data
err=input('Input STDEV of fluorescence data '); %input standard deviation

%constants
x0=[1,5]; %guess value for the hybridization rate constant and proportionality constant
C=5*10^-5; %0.5 uM of each HCR hairpin

%compute model prediction of fluorescence
fun=@(x,t)x(1)*(1-exp(-x(2)*C*t));

%least squares curve fit with varying k
[x,resnorm,residual,exitflag,output,lambda,jacobian]=lsqcurvefit(fun,x0,t,f);

%R^2 estimate
SST=sum(((f-mean(f)).^2),'all'); %SST for R^2 calculation
R2=1-(resnorm/SST); %calculate R^2=SSE/SST

%obtain 95% confidence interval around fit parameter
conf = nlparci(x,residual,'jacobian',jacobian);

%plot data and fitted curve
times = linspace(t(1),t(end));
errorbar(t,f,err,'.','MarkerSize',20)
hold on
plot(times,fun(x,times),'b-','LineWidth',1.5)
xlabel('Time (h)')
ylabel('Fluorescence Intensity')
set(gca,'fontsize', 18)
```